A theoretical framework for waveguide quantum electrodynamics and its application to resonance energy transfer

Dissertation

zur Erlangung des akademischen Grades

doctor rerum naturalium

(Dr. rer. nat.)

im Fach Physik

Spezialisierung: Theoretische Physik

eingereicht an der

Mathematisch-Naturwissenschaftlichen Fakultät

der Humboldt-Universität zu Berlin

von

Diplom-Physiker Tobias Sproll

Präsidentin der Humboldt-Universität zu Berlin

Prof. Dr. Jan-Hendrik Olbertz Kunst

Dekan der Mathematisch-Naturwissenschaftlichen Fakultät

Prof. Dr. Elmar Kulke

Gutachter/innen:

1. Prof. Dr. Kurt Busch
2. Prof. Dr. Jörg Schamlian
3. Prof. Dr. Wolfgang Nolting

Tag der mündlichen Prüfung: 20.07.2016

Ich erkläre, dass ich die Dissertation selbständig und nur unter Verwendung der von mir gemäß § 7 Abs. 3 der Promotionsordnung der Mathematisch-Naturwissenschaftlichen Fakultät, veröffentlicht im Amtlichen Mitteilungsblatt der Humboldt-Universität zu Berlin Nr. 126/2014 am 18.11.2014 angegebenen Hilfsmittel angefertigt habe.

Berlin, den 31. März 2015

To my parents

Introduction & Outline

In 1965, Gordon Moore formulated a law [1], which turned out to be of fundamental importance to make computers one of the irreplaceable tools for our modern world. It is stated as follows (in its weaker form of 1975): " The number of transistors per area in integrated circuits doubles roughly every two years " As it turned out this was not only true in this technical environment for which is was originally developed but also for example for data rates in communication technology. For many years there was an impressive agreement between predictions and the technological progress in real world. Unfortunately, due to fundamental physical principles, deviations started to become significant in recent years especially in high end applications. On the fabricational side the technical requirements to perform necessary lithographic processes on the 10nm scale get incredibly sophisticated. For example, for the fabrication of state-of-the-art chips one needs mirrors which have a numerical aperture as small as this number which poses major technical problems if one wants to reach even smaller scales. On a more fundamental level we have the problem that if the transistors become even smaller they reach the size of just a few atoms which means that there are non-vanishing tunnel currents between them even if the transistor is switched off. Also the heat production in small electronic junctions starts to become significant which can eventually lead to destruction in integrated circuits. There are different approaches to overcome this fundamental problems:
One promising candidate is based on spintronics, where instead of the electronic degrees of freedom the spin degrees of freedom of solid state systems are manipulated [2]. Techniques for transporting spin polarized currents as well as basic logic elements like spin field effect transistors have already been successfully build and theoretically understood [2, 3]. Nevertheless, there are still problems, for example, due to spin coherence and gate-induced Rashba coupling which have to be resolved before industrial applications become a realistic possibility [4, 3].
Another maybe more straightforward approach would be to essentially keep the electronic based approach, but looking for new materials with more favorable electronical properties. An example for this direction of research is the replacement of silicon based transistors by counterparts based on graphene [5] or MoS_2 (Molybdenumsulfid) [6], both with their own problems and advantages (for example graphene transistors are already working at frequencies of 10^5 GHz but on the other hand the missing gap of natural graphene causes profound fabricational problems).
A third possible direction for future computer technology is based on optics, which has the advantage of higher switching times because the speed of light is much faster then the typical velocity of electrons (and of spinwaves). Furthermore, the power consumption is much less because of the missing charging of transmission lines (this is the main source of power loss in conventional computers). It is also worth noting that because of the lack of direct photon-photon coupling at low energies there is always need for an operating medium which is capable of inducing interactions because they are crucial to perform actual computations [7]. There

are already several possible realizations of optical interconnections to transport information between different logical elements for example on the basis of silicon which has the great advantage that the required technologies are already well developed because they are also used in conventional chip production [8]. There are also promising steps forward in the construction of optical transistors relying on nanoantennas or nanoresonators coupled to single molecules or quantumn dots,just to name a few possibilities [7]. Whereas the mass production of computers based on this technology may still be a matter of decades, integrated chips based on a mixture of optical interconnections and electronic transistor are already much closer to enter real life products as was recently demonstrated [9].

Everything we where talking about above was, regardless of its novel physical and technological aspects, dealing with possible new directions in the construction of usual computers by which we mean they are based in principle on well-known Boolean operations. One can now make a step back and ask the question:
Is this sufficient? Or would it be nice to have a computer which can do something more? The answer is affirmative. For example, if we want to simulate a quantum system consisting of N particles we know that the corresponding general quantum state will contain $\mathcal{O}(2^N)$ independent variables and even if N is just of $\mathcal{O}(10^3)$ which is way smaller then Avogadros constant, this number is bigger than everything we can expect to be handled by an ordinary computer. To overcome this problem Richard Feynman proposed in 1981 to build a so called quantum computer which makes use of the laws of quantum mechanics to perform calculations in a very different way then we know from a classical computers [10]. The key idea is to use a system of N qubits to simulate a system of N particles (this works at least for local quantum systems [11]). One of the main advantages of this approach is that we can use the principle of superposition, a quantum computer features many (classical) states at the same time which allows us to perform a huge amount of parallel computations. This phenomenon is called quantum parallelism. If not only computations are performed by the help of quantum mechanical effects but also information transport and storage we are doing quantum information processing. There are many proposals how to realize this in experiments. Majorana fermion based approaches [12], spintronics [13] or systems predicated on superconductivity [14] are possible (but by no means all) candidates to complete this formidable task, each with its own problems and advantages. For example Majoranas are not even detected in nature at the time this thesis is written, but on the other hand they are predicted to be quite robust to environmental influences due to their topological protection. For spintronics the situation is reversed, relatively well understood techniques to produce the underlying (pseudo) particles are countered by great problems due to quantum decoherence induced by coupling to external degrees of freedom. Another promising and quite old (rough ideas already show up in [10]) route to quantum computing and quantum information processing is making use of quantum optics.
Whereas the 2001 proposal for a scalable linear optical quantum computer consisting only of linear elements like single photon sources, beam splitters or single photon detectors [15] offers the conceptually easiest way to realize optical quantum computation, problems with the experimental implementation of scalability still remain to be solved. For this reasons schemes based on non-linear optical effects (for example the Kerr effect) are still a valid alternative [16].

It is clear that because both, the linear as well as the non-linear, optical schemes discussed above are based on a very controlled interaction between light and matter degrees of freedom, it is essential to understand the underlying physical processes in detail.
The purpose of this thesis is to make a contribution to reach this objective in the area of waveguide quantum electrodynamics which is also a valid candidate for the practical implementation of quantum information processing where the transmission lines are 1-D waveguides and the qubits are realized through two-level-systems which could be suitable atoms or NV centers in diamond, for example [17][18][19].

Outline

We now outline the content of the different chapters of this thesis
In chapter one we discuss the quantization of the electro-magnetic (EM) field with a special emphasis on the correct implementation and interpretation of gauge constraints. We go in some details through the specific example of the Coulomb gauge, because it will be used for all the applications we discuss later on. The second part of this chapter is devoted to light-matter interaction. This includes the discussion of the two most common approximations in the field of waveguide quantum electrodynamics (WQED) the dipole approximation and the rotating wave approximation. Related to this, we will investigate under which specific assumptions we may substitute a particle interacting with an EM field by a simple two level system (TLS). In the last section we introduce WQED. We give an overview of the experimental state of the art in this field and finally construct and motivate the most simple model Hamiltonian emphasizing especially the role of different dispersion relations which will be a key aspect for the rest of the thesis.
The topic of the second chapter is an introduction of quantum field theory (QFT) which is the backbone of the formalism we develop in later chapters for tackling WQED problems. We start with a short overview of how one can include time dependence in quantum mechanics. We then give a proof of the Gell-Mann Low theorem which is of fundamental importance for developing the perturbative schemes present in most QFT calculations. After a discussion of Wick's theorem we are ready to develop many concepts by help of an important physical model, the ϕ^4 theory, namely self energies, S-Matrices and the linked cluster theorem. We especially emphasize how many calculations can be made transparent and physically understandable by introducing Feynman diagrams.
In the third chapter, we develop a Feynman diagram approach to WQED for a toy model a 1-D waveguide with arbitrary dispersion relation and a two level system. We consider the one excitation as well as the two excitation sub-sector. We then reproduce results obtained by other authors in a much more transparent and compact manner then before. Especially we classify different processes like photon-photon interaction or interaction-induced radiation trapping according to a corresponding classes of Feynman diagrams. Furthermore, we discuss how Fano resonances can be interpreted as a signature of a photon-photon non-linearity. We also discuss in great detail how different choices of dispersion relations give rise to totally different physical results. Especially we show that the usual linearization of the photon dispersion relation isn't a very good approximation under many circumstances.

In the fourth and last chapter of this thesis we are going to generalize the model systems by adding an additional TLS. We exactly solve the associated perturbation series discussing again the differences which occur for different kind of dispersion relations. We give an in-depth discussion of the particular families of eigenmodes occurring in this system. This is done numerically as well as by a big amount of asymptotic calculations. Afterwards, we give a short overview about fluctuating forces in general but focusing on a specific type, which is related to the so called Förster energy. We then show under which circumstances it might appear in our model system and how it can be tuned by the choice of the initial state. Last but not least, we discuss the bound states in continuum also present in our system. We give general conditions for their existence and we show that they have a profound impact on the time dynamics of the TLS. We end this thesis with an conclusion, where we summarize our results and discuss some possible further areas of application for the tools we developed.

Acknowledgments

First of all, I want to thank Professor Kurt Busch for the hospitality, help, money and continuous support over the last years. Especially I want to highlight the big patience which was necessary to make me finish this work, I know this must be hard from time to time.
Furthermore I want to thank Professor Jörg Schmalian and Professor Wolfgang Nolting to be the external- and second assessor of my PhD thesis, respectively.
Without the help of the other member of the TOP group at MBI and HU I would never have been able to finish this thesis. Even in the darkest times there was always something to laugh about, thank you for that (and many other things)!
A special thanks goes also to Euler-Lagrange who were always a source of great pleasure and inspiration.
Last but not least I want to thank everyone from my family, I owe all of them so much.

Contents

List of Figures

1 QUANTIZATION OF THE EM-FIELD AND LIGHT-MATTER INTERACTION

We discuss the quantization of the electromagnetic field and light matter interaction

1.1 Introduction

We begin with a short overview of the history of quantum field theory (QFT). Then we discuss the quantisation of the electromagnetic field and especially the role of the $U(1)$-Gauge symmetry. Later on we will introduce light matter coupling and justify the approximations leading to the standard effective Hamiltonian used in Quantum optics. In the last section we give a brief introduction to the status of experiments in wavequide QED as well as to its theoretical foundations. We thereby obtain the Hamiltonian used throughout the main part of this thesis.

1.2 A broad perspective on QFT

The roots of QFT lie in the realm of particle phyiscs, beginning with works of Heisenberg, Pauli,Jordan and Dirac in the second half of the 1920s [20]. Its first important application was the description of β-decay by Fermi 1934 [21], where the formalism showed its ability to make physically important predictions which are not easily obtained by using standard quantum mechanics. A period of slow progress followed because of a lack of tools to interpret (infrared and ultraviolett) divergences which are a quite generic feature of QFT. Those problems remained unsolved until the late 1940's when a new generation of physicists (Schwinger, Dyson, Feynman and others) found a solution to this problem by a proper interpretation of the physical constants (mass, electron charge,...), appearing in quantum electrodynamics (QED) as effective parameters which are renormalized by vacuum fluctuations and self energy corrections [22, 23]. A further boost to the field was induced by the ingenious observation of Feynman that one can assign pictorial representations to the complicated mathematical expressions which appear in perturbation theory, the so called Feynman Diagrams [24]. They opened the door for an intuitive interpretation of QFT and will be one of the main tools of this PhD thesis and will be the

topic of the next chapter. Since that time, QFT was the main driving force in the understanding of the fundamental forces of nature, culminating in the unification of electroweak, electrostrong and electromagnetic interactions by Glashow, Weinberg, Salam and others [25, 26] which is now known as the standard model. Furhtermore QFT has found its way in may areas of theoretical physics, like condensed matter theory [27], statistical physics [28] and also quantum optics [29], partly unifying the theoretical foundations of all these fields.

1.3 Quantization of the EM Field

In this section we mainly follow the script of Tong [30]. We use the following conventions: Quantities with a lower index, like $t_{\mu_1,\dots,\mu_n}$, transform as rank-n covariant tensors, objects with an upper index $t^{\mu_1,\dots,\mu_n}$ transform as rank-n contravariant tensors . The metric tensor is defined as $g = \mathrm{diag}(-1, 1, 1, 1)$. Space-time indices are labeled by Greek letters, whereas usual space indices are labeled by Latin letters. Furthermore, Einstein summation convention is imposed.

1.3.1 Covariant formulation and Gauge Symmetry

We start from the classical Lagrangian density of the EM field (we set the source terms to zero)

$$\mathcal{L} = \frac{1}{2} F_{\mu\nu} F^{\mu\nu} \tag{1.1}$$

where the covariant field strength tensor is given by $F_{\mu\nu} = \partial_\mu A_\nu - \partial_\nu A_\mu$ (A_μ is the four vector potential). Its contravariant counterpart might be obtained by the usual contractions with metric tensors $g^{\mu\nu}$. Two of Maxwell's equations are given by the Euler-Lagarange equations:

$$-\partial_\mu F^{\mu\nu} = 0 \Leftrightarrow \nabla \cdot \vec{E} = 0, \quad \partial_t \vec{E} = \nabla \times \vec{B} \tag{1.2}$$

It turns out that the second pair of Maxwell's equation follows from the Bianchi identiy

$$\partial_\lambda F_{\mu\nu} + \partial_\mu F_{\nu\lambda} + \partial_\nu F_{\lambda\mu} = 0 \tag{1.3}$$

which can be proven by applying Jacobi's identity which can be stated for this particular case as $[\partial_\lambda, [\partial_\nu, A_\mu]] = 0$,where $[,]$ denotes the Lie bracket. Plugging in the components of the field strength tensor we obtain:

$$\nabla \cdot \vec{B} = 0, \quad -\partial_t \vec{B} = \nabla \times \vec{E} \tag{1.4}$$

Even at this general level, an obvious but profound problem shows up:
A_μ has four components but the photon should only have two degrees of freedom (the two polarisation directions).
How can we resolve this issue?
The first degree of freedom can be eliminated by the fact that A_0 is static (this follows directly from the anti-symmetry of $F_{\mu\nu}$). Applying ∂^i to $F_{i0} = E_i$ we might conclude that

$$\nabla^2 A_0 = -\nabla \partial_t \vec{A} \tag{1.5}$$

so the time component of the vector potential is uniquely fixed by the three space components. The second degree of freedom can be eliminated by the inherent $U(1)$ (local) gauge symmetry of electromagnetism. We recall that this means that $F_{\mu\nu}$ is invariant under a transformation of the connection having the form $A_\mu \to A_\mu + \partial_\mu \alpha(x)$.
We interpret a gauge transformation in the following way:
In contrast to global symmetry, which implies a conserved charge by Nöther's theorem, the (infinite dimensional and space-time dependent) gauge transformation is a redundancy of the system, or in other words, just a simple relabeling of its physical states.
We can see that this interpretation is useful by looking at the wave equation

$$\left(g_{\mu\nu}\partial^2 - \partial_{\mu\nu}\right) A^\nu = 0 \tag{1.6}$$

We might observe that the special choice $A^\nu = \partial^\nu \alpha(x)$ is a zero mode of the operator and therefore the equation above is non-invertible. This is a problem because that would mean that we can't distinguish between the solutions A_ν and $A_\nu + \partial_\nu \alpha(x)$. Fortunately this problem can naturally solved by just identifying $A_\nu \equiv A_\nu + \partial_\nu \alpha(x)$, because this is just of the relabelings of physical states allowed by gauge symmetry. This additional possibility of relabeling the vector potential eliminates another degree of freedom (we fix a gauge by choosing a particular representative for A_ν).

We now have a quick look at two different gauge conditions:

- Lorenz gauge: $\partial_\mu A^\mu = 0$

This choice has the particular advantage that it preserves the Lorentz invariance of the theory. It is therefore the preferred choice in high energy physics. It's drawback is the quite difficult quantization procedure (see [30],[31]) .

- Coulomb gauge: $\nabla \vec{A} = 0$

This choice has as an obvious drawback of breaking of the Lorentzian invariance. On the other hand it turns out that its quantization is quite straightforward. Furthermore because we will work at quite low energies, we don't have to take into account relativistic effects and therefore we will work in this gauge throughout this thesis.

1.3.2 Quantization in Coulomb Gauge

In Coulomb gauge the wave equation (1.6) has the simpler form ($A_0 = 0$ see (1.5))

$$\partial^2 \vec{A} = 0 \tag{1.7}$$

using a plane wave decomposition $\vec{A}(x) = \int \frac{d^3\vec{k}}{(2\pi)^2} \vec{q}(\vec{k}) e^{i\vec{k}\cdot\vec{x}}$ we see that the Coulomb condtion turns into

$$\vec{q} \cdot \vec{k} = 0 \tag{1.8}$$

which means that the polarizations $\vec{q}$ are perpendicular to the direction of motion given by $\vec{k}$. Furthermore we observe that due to the vanishing mass of the photons and the on-shell

condition we may fix $E = k_0 = \epsilon(k)$ where $\epsilon(k)$ denotes the photon dispersion relation. As a side-remark we might note that photons in free space field theory have a dispersion relation $\epsilon(k) = k$ but later on we will also deal with photons which travel trough more structured environments, so we include this possibility already at this point. Condition (1.8) suggests that we can decompose $\vec{q}$ as

$$\vec{q}(\vec{k}) = c_1\vec{\zeta_1}\cdot(\vec{k}) + c_2\vec{\zeta_2}\cdot(\vec{k}) \tag{1.9}$$

where $\vec{\zeta_l}\cdot\vec{\zeta_m} = \delta_{lm}, \quad \vec{\zeta_l}\cdot\vec{k} = 0$. This vectors also obey the completeness relation

$$\sum_l \zeta_l^i \zeta_l^j = \delta^{ij} - \frac{k^i k^j}{\vec{k}^2} \tag{1.10}$$

To show this we observe that the above quantity can be also seen as the projection matrix onto the directions perpendicular to $\vec{k}$. The most general form of this projection matrix which respects rotational symmetry is given by $P^{ij} = a\delta^{ij} + bk^i k^j$. The relation $P^{ij}k_j = 0$ fixes the constants.
No we are ready to start with the quantisation procedure. We will try to use E_i and A_i as conjugate variables because they are the two conjugate variables in classical field theory($\frac{\partial\mathcal{L}}{\partial(\partial_t A)_i} = E_i$).
Note that from here on A_i, E_i are always understood as operators until stated otherwise. Straightforwardly replacing Poisson brackets by commutators yields

$$\begin{aligned}[E_i, E_j] &= [A_i, A_j] = 0\\ [E_i, A_j] &= -i\delta_{ij}\delta(\vec{x}-\vec{y})\end{aligned} \tag{1.11}$$

but this would imply (go to momentum space to see that)

$$[\nabla\cdot\vec{E}, \nabla\cdot\vec{A}] = i\nabla^2\delta(\vec{x}-\vec{y}) \tag{1.12}$$

which is clearly not consistent with our constraints
$\nabla\cdot\vec{E} = \nabla\cdot\vec{A} = 0$.

We therefore see that our naive quantization procedure is clearly wrong. We don't go into the details how one does quantization under constraints, which is a very deep and broad field [31]. We choose rather an ad-hoc method, replacing $\delta_{ij} \to \delta_{ij} - (\nabla^2)^{-1}\nabla_i\nabla_j$ in (1.11).

$$\begin{aligned}[\vec{E}_i, \vec{E}_j] &= [\vec{A}_i, \vec{A}_j] = 0\\ [\vec{E}_i, \vec{A}_j] &= -i\left(\delta_{ij} - (\nabla^2)^{-1}\nabla_i\nabla_j\right)\delta(\vec{x}-\vec{y})\end{aligned} \tag{1.13}$$

Going to momentum space, we may now check that the constraints are correctly implemented. It is furthermore worth noting that this are exactly the projection operator on the transverse and therefore physical degrees of freedom (1.10).

We now again apply a plane wave decomposition

$$\vec{A} = \int \frac{d^3k}{(2\pi)^3} \frac{1}{\sqrt{2\epsilon(\vec{k})}} \sum_{l=1,2} \vec{\zeta}_l(\vec{k}) \left(a_{\vec{k},l} e^{ikx} + a^\dagger_{\vec{k},l} e^{-ikx} \right) \tag{1.14}$$

where the operators $a_{\vec{k},l}$ fulfill the usual Heisenberg algebra

$$\begin{aligned} [a_{\vec{k},l}, a_{\vec{k}',s}] = [a^\dagger_{\vec{k}',l}, a^\dagger_{\vec{k},s}] = 0 \\ [a_{\vec{k},l}, a^\dagger_{\vec{k}',s}] = (2\pi)^3 \delta_{rs} \delta(\vec{k} - \vec{k}') \end{aligned} \tag{1.15}$$

which induces ($E = -\partial_t A$)

$$\vec{E} = -i \int \frac{d^3k}{(2\pi)^3} \frac{\sqrt{\epsilon(\vec{k})}}{\sqrt{2}} \sum_{l=1,2} \vec{\zeta}_l(\vec{k}) \left(a_{\vec{k},l} e^{i\vec{k}\cdot\vec{x}} - a^\dagger_{\vec{k},l} e^{-i\vec{k}\cdot\vec{x}} \right) \tag{1.16}$$

With this expressions at hand, we may calculate the Legendre transform of $\mathcal{L}$ and find (using the Coulomb condition and setting $c = 1$)

$$\begin{aligned} H = \int d^3x (E_i \partial_t A_i - \mathcal{L}) = \\ \frac{1}{2} \int d^3x \left(\vec{E}^2 + \vec{B}^2 \right) \end{aligned} \tag{1.17}$$

Using (1.16) it follows that

$$H = \sum_{l=1,2} \int \frac{d^3k}{(2\pi)^3} \omega(k) a^\dagger_{\vec{k},l} a_{\vec{k},l} \tag{1.18}$$

Note that we already have thrown away an infinite constant $\int \frac{d^3\vec{k}\omega(k)}{(2\pi)^3}$ which doesn't affect the dynamics of the system (or normal ordered the Hamiltonian to speak in more technical terms).

We therefore showed that the EM Hamiltonian is equivalent to an ensemble of harmonic oscillators. This allows for the useful interpretation that the quanta created and destroyed by $a^\dagger_{\vec{k},l}$ and $a_{\vec{k},l}$ are exactly the photons.

1.4 Light Matter coupling

1.4.1 The Dipole Approximation

In this section, we want to couple the degrees of freedom of the quantized EM field to matter degrees of freedom. To understand the fundamental principles let's have a look at a single,

charged particle in an $SO(3)$ symmetric potential coupled to the EM field. We neglect the free field part in what follows because it will not be of any further concern. We rely loosely on [32] generalizing the arguments for a quantized light field. Note,that for the sake of clarity we don't write out constants of proportionality here, which is indicated by $\sim$.

The Hamiltonian can be obtained by the principle of minimal substitution $\vec{p} \to \vec{p} - e\vec{A}$,

$$H = \frac{1}{2m}\left(\vec{p} - e\vec{A}\right)^2 + \phi(|\vec{x}|) \tag{1.19}$$

Where $\phi(|\vec{x}|)$ is the potential. Next we omit the diamagnetic term $\sim \vec{A}^2$ which is legal in many situations because it is suppressed by a factor of $1/c$ (in Gaussian units). Additionally it doesn't affect light matter coupling so it is of no concern to us anyways (This term induces also the so called ponderomotive force, important in strong field theory). Furthermore employing the Coulomb condition we get

$$H = \frac{1}{2m}\vec{p}^2 - \frac{e}{m}\vec{A}\vec{p} + \phi(|\vec{x}|) \tag{1.20}$$

using (1.16) and defining $|i/f\rangle \equiv |n_{i/f}, \psi_{i/f}\rangle = |n_{i/f}\rangle|\psi_{i/f}\rangle$, the initial/final states composed of a light part $|n_{i/f}\rangle$ and a matter part$|\psi_{i/f}\rangle$, we see that the overlap matrix element $O_{fi} \sim \langle f|\vec{A}\vec{p}|i\rangle$ may be written as

$$O_{fi} \sim \int d^3k \sum_{l=1,2} \langle f|\vec{\zeta}_l(\vec{k}) a_{\vec{k},l} e^{ikx}\vec{p}|i\rangle + h.c \tag{1.21}$$

If the size of the particle x_0 is now much smaller then the typical wavelength of our electromagnetic field we might perform a Taylor expansion $e^{ikx} \approx 1 + \mathcal{O}(ikr)$ to get

$$O_{fi} \sim \int d^3k \sum_{l=1,2} \langle f|\vec{\zeta}_l(\vec{k}) a_{\vec{k},l}\vec{p}|i\rangle + h.c = \tag{1.22}$$

$$\int d^3k \sum_{l=1,2} \vec{\zeta}_l(\vec{k}) \langle f|a_{\vec{k},l}\vec{p}|i\rangle + h.c \tag{1.23}$$

Note that the argument above is not completely rigorous because we formally integrate over all photon momenta so the Taylor expansion seems questionable. This can be cured by remembering that a real photon has a momentum distribution $g(k)$ which is peaked around some value $k = k_0$ for which we assume that $x_0 k_0 \ll 1$ (in real world system this factor is of $10^{-4} - 10^{-5}$ most of the time).

Now remembering that $[\frac{p^2}{m} + \phi(|\vec{x}|), x] = \frac{p}{m}$ we may rewrite (1.22) as

$$O_{fi} \sim \int d^3k \sum_{l=1,2} \vec{\zeta}_l(\vec{k}) \langle n_f|a_{\vec{k},l}|n_i\rangle \langle \psi_f|\vec{d}|\psi_i\rangle - h.c \tag{1.24}$$

Here we have introduced the dipole operator $\vec{d} \equiv e\vec{x}$, Now after reintroducing the constants of proportionality and using again (1.16) we see can show that

$$O_{fi} = -\langle\psi_f|\vec{d}|\psi_i\rangle\langle n_f|\vec{E}|n_i\rangle \tag{1.25}$$

Now, without loss of generality, let's choose $\vec{\zeta}(\vec{k}) = (0, 0, \zeta_z(\vec{k}))^T$ so the position dependent part of the matrix element simplifies to

$$\langle\psi_f|\vec{d}|\psi_i\rangle = e\langle\psi_f|z|\psi_i\rangle \tag{1.26}$$

Notice that because our potential is radially symmetric we can decompose our final and initial states as $|\psi\rangle = |\psi\rangle_{lmn} = |R(r)_{nl}\rangle|\Psi_{lm}(\phi, \Theta\rangle)$ into a radial and an angular part. According to the general theory of selection rules [32] we can fix $l = l' \pm 1, m = m'$. Furthermore we find that $\langle n_f|a|n_i\rangle = \sqrt{n_i + 1}\sqrt{n_f + 1}\delta_{n_{f+1},n_i}$. Putting everything together, our Hamiltonian can be now written in the form

$$\begin{aligned} H =& \frac{p^2}{2m^2} + \phi(|\vec{x}|) - \\ & \sum_{n_k,n,n',m,l} O^{n_k}_{n,n',m,l}|R_{n,l+1}\rangle|\Psi_{l+1,m}\rangle|n_k\rangle\langle n_{k+1}|\langle\Psi_{l,m}|\langle R_{n'l}| \\ & + h.c. \end{aligned} \tag{1.27}$$

where have absorbed some constants into the matrix element and we have the usual constraints on the ranges of summation for l and m [32].
Let's discuss this Hamiltonian shortly. Because of the dipole approximation there are only processes allowed which contain one photon. These are absorption of a photon by the atom, as well as the more exotic creation of an excited state and a photon, which are accompanied by their time reversed counterparts. Due to the conservation of angular momentum all the processes allowed involve the transfer of one quantum of angular momentum (this can be motivated by the fact that a photon is a spin 1 particle).

To make our model even simpler, let's assume that our photon is sharply peaked around some frequency ω_0 Furthermore we demand that the atomic transition energies at this frequency are well separated so that we have only one transition which is on resonance with the photon field $\omega_0 \approx \Omega_{lmn} \equiv \Omega$. If these conditions are fullfiled it is sufficent to replace our particle by a simple two level system with energy Ω and states $|e\rangle$ (the excited state) and $|g\rangle$ (the ground state). A real world example for atoms where this might be a good approximation are the heavy alkaline earth metals caesium and rubidium or nitrogen vacancy (NV) centers in diamond [33]. We get, neglecting irrelevant constants

$$\begin{aligned} H = & \frac{\Omega}{2}\sigma_z + \int \frac{d^3k}{(2\pi)^3}\epsilon(k)a^\dagger_k a_k + \\ & \int \frac{d^3k}{(2\pi)^3}O_k(a_k - a^\dagger_k)(\sigma_+ - \sigma_-) \end{aligned} \tag{1.28}$$

with $\sigma_z = |e\rangle\langle e| + |g\rangle\langle g|$ and $\sigma_+ = |e\rangle\langle g|, \sigma_- = |g\rangle\langle e|$ We also used the fact that $|n_k\rangle\langle n_{k+1}| \sim a_k$ and we restored the field part of the Hamiltonian. We note that the overlap element can be chosen to be real, a consequence of the $U(1)$ symmetry of the EM field (a simple phase can be "gauged out").

1.4.2 The Rotating Wave Approximation

The purpose of this subsection is to motivate another common approximation, the rotating wave approximation (RWA). Its effect is the replacement

$$(a_k - a_k^\dagger)(\sigma_+ + \sigma_-) \to a_k\sigma_+ + a_k^\dagger\sigma_- \tag{1.29}$$

in (1.28). A first heuristic argument would be that the neglected terms $a_k^\dagger\sigma_+$and $a_k\sigma_-$ violate the conservation of energy because they create or destroy two excitations (an excited atom and an photon). But as we know this argument is not entirely safe because in quantum mechanics energy conservation is washed out on small time scales. Therefore we need a bit of more rigor. To do so, we perform a unitary transformation $U = e^{-iH_0t}$ at our Hamiltonian, where $H_0 = H_{0,field} + H_{0,atom}$. This might be also interpreted as change from Schroedinger to Heisenberg picture. We furthermore need the following relations $e^{-iH_0t}\sigma_\pm e^{iH_0t} = \sigma_\pm e^{\pm i\Omega t}$. and $e^{-iH_0t}a_k^{(\dagger)}e^{iH_0t} = e^{\mp i\epsilon(k)}a_k^{(\dagger)}$. The left side of (1.29) now reads:

$$\begin{aligned} &a_k\sigma_+e^{-i(\epsilon(k)-\Omega)t} + a_k^\dagger\sigma_-e^{i(\epsilon(k)-\Omega)t} - \\ &a_k\sigma_-e^{-i(\epsilon(k)+\Omega)t} - a_k^\dagger\sigma_+e^{i(\epsilon(k)+\Omega)t} \end{aligned} \tag{1.30}$$

we see now, that the phase of the terms in the first line are close to zero if our photon is close to resonance, and therefore they will survive a temporal average. On the other side $\epsilon(k) + \Omega \approx 2\Omega$ and this terms will tend to cancel out during an averaging procedure. Therefore the approximation (1.29) is a valid one as long as the coupling is not too strong . Another way to see this is by using Fermi's Golden rule. We will come to this later, when we have introduced perturbation theory.

1.5 Waveguide Quantum Electrodynamics

1.5.1 Experimental Overview

Waveguide quantum electrodynamics (WQED) describes a special case of QED where light propagates in a confined geometry. In contrast to cavitiy quantum electrodynamics (CQED) where the light is confined to a certain region of space, WQED supports the propagation of light over large distances in one dimension. It should be mentioned, that many of the systems one can think about can be thought of as coupled cavities where light can tunnel from one cavitiy into the other. In this sense WQED is a generalization of CQED. On the other hand, there are other possibilities to realize WQED. Line defects in photonic crystals [34], ultra-thin glass fibers [35] and coupled ring resonators (The coupling is due to evanescent fields) [36] for example. One of the points which makes WQED interesting is the fact that the employed boundary

conditions induce very special properties on the propagating photons. The most important one are dispersion relations which can be bounded and curved. This fact can be interpreted that the photons acquire an effective mass, which follows from $\frac{1}{m^*} = \partial_k^2 \epsilon(\vec{k})$ (Remember that this relation only holds around the extrema of the dispersion relation) which also opens up the possibility of a reduced photon group velocity, so we can have a slow light regime [34] and photonic band gaps, even in the presence of disorder [37]. As described in the introduction, WQED has a growing importance in fields like quantum information processing , quantum computing and pump-probe spectroscopy . To obtain an efficient device in this fields it is very important to have quite strong light matter coupling. Possible realizations which offer this feature are ultracold atoms coupled to line defect waveguides as well as well as to nanofibers [38].

Furthermore we want to work with only a few photons to observe quantum mechanical effects such as photon entanglement. Therefore we need single photon sources. This was a great field of experimental research in the past decade, resulting in very different kinds of now available sources including NV centers [39], silicon carbide, which even works at room temperature [40], or silcion quantum dots [41]

1.5.2 Modelling WQED

In this section we want to discuss how to set up the basic model we use together with some slight genralization in the rest of the thesis.

We have discussed light matter coupling as well as quantisation of EM fields ,in quiet some depth, in the last section, so what is left is to specify how exactly we can apply the results we obtained there.

One aspect we want to discuss is, how one can think about a one-dimensional waveguide from a theoretical point of view. We therefore want to discuss two different ways how to realize them. First, a ultra-thin glasfiber. For this purpose let's assume that we have cylindrical (lossless) waveguide with radius r. From the theory of classical radiation transport [42] we know as a consequence of the boundary conditions that the allowed modes are quantized in r-direction but have a continuous spectrum in z direction. Furthermore we might observe that the dispersion relation looks like $k_{mn,z} = \sqrt{k^2 - k_{mn,r}^2}$ where mn labels the different allowed modes. It holds that $k_{mn,r} = \frac{\alpha_{mn}}{r}$ where α_{mn} is a zero of a Bessel function $J_n(x)$ or its derivative $J_n'(x)$. Therefore if r gets smaller and smaller we might reach a point where only one of the radial modes are allowed to propagate because for all other modes the square root gets imaginary. This kind of reasoning takes over to the quantum level and that is the way how one should think about one-dimensionality in these systems.

As mentioned in the subsection before, another type of one-dimensional waveguides is built up of coupled ring resonators. We can think of this system as a one-dimensional linear chain with one resonator on each site. If the coupling between neighboring resonators is small, this

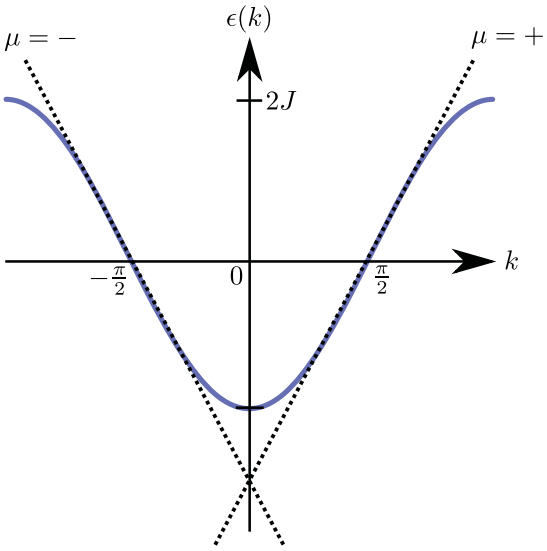

Figure 1.1: *The two different dispersion relations discussed in the text: A cosine dispersion with width $4J$ and the two branches or its linearized approximation around $k = \pm\pi/2$*

can be modeled as a tight-binding chain with dispersion relation $\epsilon(k) = 2J\cos(k)$ where J is a measure for the bandwidth of the waveguide (this shape of the dispersion relation can be observed very well in some experiments, see [43]).

The dispersions in both kinds of systems share the main key features, a linear regime as well as a slow light regime and it turns out that this holds also for the other experimental realizations discussed above. Because we are mainly interested in generic features rather than a specific realistic system, it is sufficient to work with the tight binding model discussed above. It has the advantage that it is quite well known (at least in the condensed matter (CM) community) and it is relatively easy to handle from a mathematical point of view. Our field- or photon Hamiltonian therefore reads:

$$H_{ph} = 2J \int \frac{dk}{2\pi} \cos(k) a_k^\dagger a_k \tag{1.31}$$

where we have performed a field limit, which means that we have dropped an internal length scale given by the lattice constant a. For the purpose of investigating the linear regime we may also occasionally deal with the Hamiltonian

$$H_{ph} = v \sum_{\mu=\pm} \mu \int \frac{dk}{2\pi} |k| a_k^\dagger a_k \tag{1.32}$$

where μ is the chirality and v the group velocity. A plot of both dispersions is given below (Fig. 1.1)

We are now ready too write down a complete model Hamiltonian

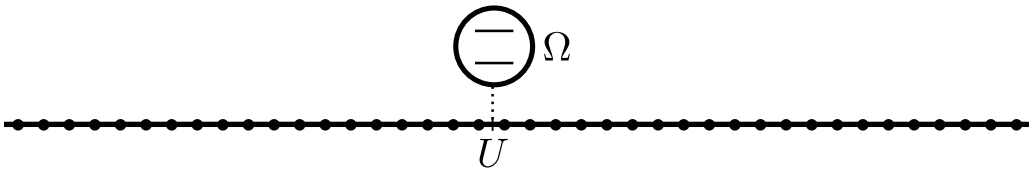

Figure 1.2: *The model system, consisting of a one dimensionl waveguide and a two level system*

$$H = H_{ph} + H_a + H_{int} = \tag{1.33}$$

$$\int \frac{dk}{2\pi}\epsilon(k)a_k^\dagger a_k + \frac{\Omega}{2}\sigma_z + U\int \frac{dk}{2\pi}a_k\sigma_+ + a_k^\dagger\sigma_- \tag{1.34}$$

where have chosen a uniform coupling in momentum space ($O_k \equiv U$) and $\epsilon(k)$ is one of the dispersion relations discussed above. For pictorial representation see (Fig. 1.2)

A first interesting feature of (1.33) is the fact that it supports an additional conserved quantity, the particle number

$$N = \int \frac{dk}{2\pi}\epsilon(k)a_k^\dagger a_k + \frac{1}{2}\left(\sigma_z + 1\right) \tag{1.35}$$

which can be readily seen by showing that $[H, N] = 0$ using the commutation relations of the different involved operators. The appearance of this additional quantum number is a consequence of RWA which neglects processes that increase or decrease the number of particles in the system.

It follows that we can write the Hilbert space $\mathcal{H}$ as a direct sum of Hilbert spaces with distinct particle number n. $\mathcal{H} = {}_0\mathcal{H} \oplus {}_1\mathcal{H} \oplus {}_2\mathcal{H} ... \oplus {}_n\mathcal{H} \oplus ...$ which simplifies many calculations.

2 QUANTUM FIELD THEORY AND DIAGRAMMATICS

We discuss basics of Quantum Field Theory and diagrammtics

2.1 Introduction

In this chapter we discuss the basic techniques of QFT We start with an overview of how the time evolution of a physical system can be described by the time evolution operator. Then we give a prove of the Gell Mann Low theorem (GMT) which is essential to connect states of an interacting Hamiltonian operator to the states of the corresponding non-interacting system. This theorem is quite important because it gives the rigorous justification for a perturbative treatment of QFT. We continue by introducing Wick's theorem which is a necessary tool to perform many QFT calculations, because it allows us to calculate the fundamental objects of any field theory, the correlation functions, in terms of two point correlation functions which is a tremendous simplification. We are then ready to discuss an example of an quantum field theory, namely the ϕ^4 model, and show how perturbative calculations work in principle and how they can be simplified and made more intuitive by introducing Feynman diagrams and the corresponding Feynman rules. Along the way we discuss important physical quantities such as the self-energy and the S-matrix which play a major role during the actual research done in this thesis. Furthermore we discuss, within this framework, the so called linked-cluster-theorem which on the one hand reduces the number of relevant diagrams in a given QFT and also gets rid of some of the divergencies which are an intrinsic problem of quantum field theories.

2.2 Pertubation theory in QFT

2.2.1 The time evolution operator

As already suggested by its name, the time evolution operator $U(t_f, t_i)$ is defined to take a Schroedinger state of our quantum system at time $t = t_i$ and evolve it according to the

principles of Quantum mechanics into a later time $t = t_f > t_i$

$$|\psi(t_f)\rangle = U(t_f, t_i)|\psi(t_i)\rangle \tag{2.1}$$

employing the normaization condition $\langle\psi|\psi\rangle = 1$ we observe that

$$U^\dagger(t_f, t_i)U(t_f, t_i) = U^{-1}(t_f, t_i)U(t_f, t_i)) = 1 \tag{2.2}$$

therefore U is a unitary operator. Furthermore, by repeated application of (2.1) we find that (setting $t_f > t' > t_i$)

$$U(t_f, t_i) = U(t_f, t')U(t', t_i) \tag{2.3}$$

We note that (2.2) and (2.3) induce a group structure on U. This holds as long as we are dealing with closed quantum systems. For open systems, the inverse no longer exists and we only have a semi-group structure.
On the other hand we know that the dynamics of the state ψ is also governed by the Schroedinger equation

$$\partial_t|\psi(t)\rangle = -iH(t)|\psi\rangle \tag{2.4}$$

Integrating recursivly (for a detailed derivation see [48]) we find that

$$|\psi(t)\rangle = Te^{-i\int_0^t dt' H(t')}|\psi(0)\rangle \tag{2.5}$$

where T is the time ordered product defined as

$$T[A(t)B(t')] = \begin{cases} A(t)B(t') & \text{if } t > t' \\ \pm B(t')A(t) & \text{if } t' > t \end{cases} \tag{2.6}$$

for time dependent operators A, B. Here the different signs are for bosons $(+)$ and fermions $(-)$. Comparing (2.5) with (2.1) we conclude that

$$U(t, 0) = Te^{-i\int_0^t dt' H(t')} \tag{2.7}$$

which can be generalized to arbitrary time arguments by properties (2.2,2.3).

$$\begin{aligned} &U(t_f, t_i) = U(t_f, 0)U^{-1}(t_i, 0) = \\ &Te^{-i\int_0^{t_f} dt' H(t')}Te^{i\int_0^{t_i} dt' H(t')} = Te^{-i\int_{t_i}^{t_f} dt' H(t')} \end{aligned} \tag{2.8}$$

In QFT one deals nearly exclusively with Hamiltonians of the form $H = H_0 + V(t)$. This suggests to work in the interaction picture, using $|\psi_I(t)\rangle = e^{iH_0 t}|\psi(t)\rangle$ [48] we obtain

$$|\psi_I(t_f)\rangle = U_I(t_f, t_i)|\psi_I(t_i)\rangle = Te^{-i\int_{t_i}^{t_f} dt' V_I(t')}|\psi_I(t_i)\rangle \tag{2.9}$$

where the subscript I stands for "interaction picture" and $V_I(t) = e^{-iH_0 t}V(t)e^{iH_0 t}$.

2.3 Gell-Mann Low Theorem

In this section we summarize the corresponding section in the book of Fetter and Walecka [44]. The original work can be found in [45]. The Gell-Mann Low theorem relates states of a non-interacting system with those of an interacting system. From this, one can also derive relations between the two (ground) state energies and many more fundamental connections between easily solvable free systems their interacting counterparts.
The fundamental idea is to assume that we can switch on and off our interaction adiabatically which means in our context just infinitely slow (in more physical terms one would say that the amount of interaction energy generated in the system per time is always smaller then the distance between neighboring energy levels). This can be simulated by introducing an auxiliary parameter λ and writing the Hamiltonian as

$$H(t) = H_0 + e^{-\lambda|t|}V \tag{2.10}$$

which means that we have $H(\pm\infty) = H_0$ and $H(0) = H$ is the full Hamiltonian. Now if the adiabatic hypothesis is true, any meaningful computation should be in the limit $\lambda \to 0$. Recalling the definition of the time evolution operator in the interaction picture (2.9), we may write

$$|\psi_I(t_f)\rangle = U_\lambda(t_f, t_i)|\psi_I(t_i)\rangle \tag{2.11}$$

with

$$U_\lambda(t_f, t_i) = \sum_{n=0}^{\infty} \frac{(-i)^n}{n!} \int_{t_i}^{t_f} dt_1 ... \int_{t_i}^{t_f} dt_n e^{-\lambda \sum_{j=1}^{n} |t_j|} T[V(t_1) \cdot ... \cdot V(t_n)] \tag{2.12}$$

As long as λ is finite, the hypothesis of an adiabatic process is valid, because the rate of change of the perturbation is small for all times and we can write

$$|\psi_H\rangle = |\psi_I(0)\rangle = U_\lambda(0, -\infty)|\phi_0\rangle \tag{2.13}$$

which means that the we can express an interacting (Heisenberg) state by an unperturbed state $|\phi_0\rangle$. Note that this is the same relation as the one for a non-interacting system. For the further analysis it is crucial that this state is non-degenerate. The complications which can arise by a degenerate ground state are mainly due to the fact that it is a non-trivial task to choose the correct representative out of the ground state manifold. For a nice summary of these issues and their (partly) resolution, we refer to [46].
The question now is what happens if we let the artificial parameter λ vanish? Are the results sensible? The answer to this questions is affirmative and given by the GML theorem. It is stated as follows :

If

$$\lim_{\lambda\to 0}\frac{U_\lambda(0,-\infty)|\phi_0\rangle}{\langle\phi_0|U_\lambda(0,-\infty)|\phi_0\rangle}\equiv|\tilde{\psi}\rangle \tag{2.14}$$

exists, then $|\tilde{\psi}\rangle$ is an exact eigenstate of the full Hamiltonian H.

Let us apply the full Hamiltonian to to this quantity. We get $(H_0+V)|\tilde{\psi}\rangle = E|\tilde{\psi}\rangle$. Multiplying by $\langle\phi_0|$ from the left and using $\langle\phi_0|H_0 = E_0\langle\phi_0|$ we obtain the following equivalent statement

$$E-E_0=\frac{\langle\phi_0|V|\psi_I(0)\rangle}{\langle\phi_0|\psi_I(0)\rangle} \tag{2.15}$$

It is important to emphasize that the numerator and denominator don't have to exist separately. In most cases only their ratio remains finite. Furthermore the eigenstate (2.14) might not be the interacting ground state, but this only happens in rather exotic cases [44].
Because this theorem lies at the heart of the perturbative treatment of QFT we want to sketch a proof in Appendix D. For the full technical details we refer to [44].

We want to conclude this section with the statement that the above considerations stay valid if we start in the far future $t\to\infty$ and approach zero from that direction. This follows from the fact that our switching on procedure is invariant under time reversal and that we are dealing with non-degenerate states. We obtain that

$$\lim_{\lambda\to 0}\frac{U_\lambda(0,\infty)|\phi_0\rangle}{\langle\phi_0|U_\lambda(0,\infty)|\phi_0\rangle}=\lim_{\lambda\to 0}\frac{U_\lambda(0,-\infty)|\phi_0\rangle}{\langle\phi_0|U_\lambda(0,-\infty)|\phi_0\rangle}\equiv|\tilde{\psi}\rangle \tag{2.16}$$

2.4 Wick theorem

From here on we straighten up our notation a little and denote the non-interacting ground state by $|0\rangle$ which we assume to be adiabatically connected to a generic interacting ground state $|GS\rangle$ by the GMT

The Wick theorem is an important tool in QFT because it allows us to write a correlation function of an arbitrary number of creation and annihilation operators as a sum over two point correlation functions. The operators have to be part of a non-interacting field theory and the theorem is therefore most conveniently formulated in the interaction picture. The correspondence between interacting and non-interacting fields is mediated by the GMT formulated in the last section. It is worth mentioning that this is very similar to the calculation of arbitrary moments of a Gaussian distribution in statistics. To formulate Wicks theorem, it is important to recall the definition of normal ordering because this concept will be used a lot. The normal order of an operator and its adjoint is defined as

$$:\phi^\dagger\phi:=\phi^\dagger\phi,\quad :\phi\phi^\dagger:=\pm\phi^\dagger\phi \tag{2.17}$$

Therefore normal ordering puts the annihilation operators to the left and the $\pm$ sign refers to bosons/fermions. The generalization to the case of n operators is obvious. Note also that $\langle 0| : \phi_1\phi_2 : |0\rangle = 0$ for generic operators of a QFT if $|0\rangle$ is the ground state of the theory.

Another important definition is that of a contraction of two operators. For the case of time ordered operators, it can be defined in the following way

$$\phi_1\underbrace{\phi_2} = T(\phi_1\phi_2) - : \phi_1\phi_2 := \langle 0|T(\phi_1\phi_2)|0\rangle \tag{2.18}$$

and therefore gives the vacuum expectation value of two time ordered operators, a quantity we will later identify with a particular kind of Green's function.
We may now state Wick's theorem:
Let $\phi_i \equiv \phi(t_i, x_i)$ a set of n (bosonic) quantum fields. Then

$$\begin{aligned} &T(\phi_1....\phi_n) = \\ &: \phi_1....\phi_n + \text{all possible contractions} : \end{aligned} \tag{2.19}$$

A full contraction means, that no non-contracted operators are left. To make this general statement a bit clearer let's look at the example of three fields

$$\begin{aligned} &T(\phi_1\phi_2\phi_3) =: \phi_1\phi_2\phi_3 : + : \text{all possible contractions} := \\ &: \phi_1\phi_2\phi_3 : + : \phi_1\underbrace{\phi_2\phi_3} + \phi_1\underbrace{\phi_2\phi_3} + \underbrace{\phi_1\phi_2}\phi_3 := \\ &: \phi_1\phi_2\phi_3 : + \underbrace{\phi_1\phi_2} : \phi_3 : + \underbrace{\phi_1\phi_3} : \phi_2 : + \underbrace{\phi_2\phi_3} : \phi_1 : \end{aligned} \tag{2.20}$$

The proof of the theorem can be done by induction, which we will omit here because it is quite technical but gives no deeper physical insight. Squeezing (2.19) between two ground states we can draw the following important conclusion

$$\langle 0|T(\phi_1....\phi_n)|0\rangle = \text{all possible full contractions} \tag{2.21}$$

which follows from the fact that the expectation value of every normal ordered operator is zero with respect to the ground state. We immediately find that $\langle 0|T(\phi_1\phi_2\phi_3)|0\rangle = 0$ because it is not possible to construct full contractions out of an odd number of operators. A more non trivial example would be

$$\begin{aligned} &\langle 0|T(\phi_1\phi_2\phi_3\phi_4)|0\rangle = \\ &\underbrace{\phi_1\phi_2}\underbrace{\phi_3\phi_4} + \underbrace{\phi_1\phi_3}\underbrace{\phi_2\phi_4} + \underbrace{\phi_1\phi_4}\underbrace{\phi_2\phi_3} \end{aligned} \tag{2.22}$$

2.5 Green's functions

We drop all vector arrows in this section for convenience

2.5.1 Types of Green's functions and connections to perturbation theory

In this subsection we want to discuss different kind of Green's functions corresponding to different physical processes and argue that only one of them will be important for our further analysis. We define the Green's function as $G^{\mathcal{T}_i} = i\langle GS|\mathcal{T}\phi_H(x,t)\phi_H^\dagger(x',t')|GS\rangle$. This expression is given in the Heisenberg picture, $|GS\rangle$ is the ground state of the theory and $\mathcal{T}$ is some time ordering procedure. Note that this can also interpreted as a propagator, giving the probability amplitude of creating a particle at x',t' and destroying it at x,t. We define the time-ordered Green's function to be

$$\begin{aligned} G^T =&\Theta(t-t')\langle GS|\phi_H(x,t)\phi_H^\dagger(x',t')|GS\rangle + \\ &\Theta(t'-t)\langle GS|\phi_H(x',t')\phi_H^\dagger(x,t)|GS\rangle \end{aligned} \tag{2.23}$$

It is important to note the close connection to $\langle 0|T\phi_I(x,t)\phi_I^\dagger(x',t')|0\rangle$ which are on the one hand the time ordered Green's functions of a non-interacting system, and also, according to Wicks theorem, the fundamental building blocks for the calculation of arbitrary n-point correlation function. We can define two new types of Greens functions

$$G^T(t,t') = G^r(t,t') + G^a(t,t') \tag{2.24}$$

where the index a refers to "advanced", which means that propagation goes backward in time and index r stands for "retarded" which means that propagation goes forward in time. It is clear that if we use the free Green's function $V_I = 1$ and choose the vacuum as a ground state (no particles) that G^a is zero and $G^r = G^T$. It will turn out that in the models we actually want to consider it is indeed possible to make this simplification, but this is not always possible, for example in condensed matter theory the most common choice for a ground state is the Fermi sea and G^a becomes non zero (it corresponds to the creation of holes with positive charge). We remark that there are other kinds of Green's functions like the anti-time ordered ("earlier times to the left") one $G^{\tilde{T}}$ and greater and lesser Green's functions $G^{\lessgtr}$ which play a major role in the Keldysh formalism of non-equilibrium many body theory [47] but this will not be of any concern in this work, so we will not discuss them any further.

To calculate the full Green's functions perturbativly in terms of its non-interacting counterparts we can make use of the GMT. We use the normalization of the ground state to write

$$\langle GS|T\phi_H(x,t)\phi_H(x',t')|GS\rangle = \frac{\langle GS|T\phi_H(x,t)\phi_H^\dagger(x',t')|GS\rangle}{\langle GS|GS\rangle} \tag{2.25}$$

We assume that $|GS\rangle$ is adiabatically connected to $|0\rangle$ by the GMT. Using (2.14), we then have that

$$\langle GS|GS\rangle = C\langle 0|U(\infty,-\infty)|0\rangle \tag{2.26}$$

where $C = \langle GS|U(\infty,0)|0\rangle^*\langle GS|U(0,-\infty)|0\rangle$. Making the same manipulations with the numerator one obtains that

$$\langle GS|T\phi_H(x,t)\phi_H^\dagger(x',t')|GS\rangle = \\ C\langle 0|U(\infty,0)T[U(0,t)\phi_I(x,t)U(t,t')\phi_I^\dagger(x',t')U(t,0)]U(0,-\infty)|0\rangle \tag{2.27}$$

Remembering that U is already time ordered (2.9) and using the properties of the time evolution operators we rewrite this as

$$\langle GS|T\phi_I(x,t)\phi_I^\dagger(x',t')|GS\rangle = \\ C\langle 0|T[U(\infty,t)\phi_I(x,t)U(t,t')\phi_I^\dagger(x',t')U(t',-\infty)]|0\rangle = \\ C\langle 0|T[\phi_I(x,t)\phi_I^\dagger(x',t')U(\infty,-\infty)]|0\rangle \tag{2.28}$$

which means that

$$G^T = \frac{\langle 0|T[\phi_I(x,t)\phi_I^\dagger(x',t')U(\infty,-\infty)]|0\rangle}{\langle 0|U(\infty,-\infty)|0\rangle} \tag{2.29}$$

it is clear that if $V = 0$ and we have no interaction, so $U = 1$ and we obtain

$$G_0^T = \langle 0|T[\phi_I(x,t)\phi_I^\dagger(x',t')]|0\rangle \tag{2.30}$$

so we see that these are exactly the objects (2.18) which occur when we Wick contract n-particle correlation functions. Keeping in mind that in general $V = V(\phi, \phi^\dagger)$ and looking at the general equation for the time evolution operator ($\lambda \to 0$) given in (2.12) it is obvious that G^T can be expanded in terms of G_0^T by virtue of Wick's theorem.

2.6 The ϕ^4 model as a case study

To make the statements in the above subsection more clear let's explore G^T for the case of an local interaction of the form

$$V = \frac{g}{4!}\int d^3x\phi^4(x) \tag{2.31}$$

(it is worth noting that this not just some abstract toy model but describes important physical systems for specific sets of parameters. Most importantly maybe, many quantum many body systems in the vicinity of a (quantum-)phase transition [27] or the self interaction of the Higgs boson [48]).
To this end let us define

$$G^T = \frac{\sum_{n=0} g^n N^{(n)}}{\sum_{n=1} g^n D^{(n)}} \tag{2.32}$$

where $N^{(n)}/D^{(n)}$ stands for the contribution of $n-th$ order in the numerator/denominator in (2.29). We now will proceed order by order starting with contributions $\mathcal{O}(g^0)$. We obtain

$$
\begin{aligned}
N^{(0)} &= G_0^T \\
D^{(0)} &= 1
\end{aligned}
\tag{2.33}
$$

So far nothing new. Going to order g^1 we see two contributions which have a quite different meaning. We employ translational invariance in space and time to simplify the arguments of the Green's functions. Starting with the numerator we find

$$
\begin{aligned}
&N^{(1)} = \\
&\frac{3}{4!} G_0^T(x_1 - x_2) \int d^3x G_0^T(x - x)^2 \\
&+ \frac{12}{4!} \int d^3\vec{x} G^T(x_1 - x) G_0^T(x - x) G^T(x - x_2)
\end{aligned}
\tag{2.34}
$$

It is clear that the first contribution is divergent, because we integrate a constant ($G(0)$) over an infinite volume. Furthermore the external coordinates are completely decoupled from the internal ones. We call this contribution a vacuum contribution because there is no interaction with the real particle created at x_1 and destroyed at x_2. The second contribution is of different nature, here internal and external variables are coupled and we might be tempted to interpret this as a kind of self interaction of the particle with itself. We also note that the factors 12 and 4 are due to the different ways of how one can contract the operators during the application of Wick's theorem. Now we have a look at the denominator

$$
\begin{aligned}
&D^{(1)} = \\
&\frac{3}{4!} \int d^3x G_0^T(x - x)^2
\end{aligned}
\tag{2.35}
$$

We make the observation that is the same (divergent) contribution as the first term in the numerator up to a multiplication with a free Green's function.
Let's go further and look at the next order g^2. We don't give any details on the calculation but refer to [49] for more information, giving justification for some of the contributions later on when we have developed our formalism a bit further.

$$N^{(2)} =$$

$$\frac{192}{2!(4!)^2}\int d^3x'd^3xG_0(x_1-x)G_0^T(x-x')^3G_0^T(x'-x_2) \tag{2.36}$$

$$+\frac{288}{2!(4!)^2}\int d^3x\int d^3x'G_0(x_1-x)G_0^T(x-x')G_0^T(x'-x')G_0^T(x'-x)G_0^T(x-x_2) \tag{2.37}$$

$$+\frac{288}{2!(4!)^2}\int d^3x\int d^3x'G_0(x_1-x)G_0^T(x-x)G_0^T(x-x')G_0^T(x'-x')G_0^T(x'-x_2) \tag{2.38}$$

$$+\frac{72}{2!(4!)^2}\int d^3xG^T(x_1-x)G_0^T(x-x)G^T(x-x_2)\int d^3x'G_0^T(x'-x')^2 \tag{2.39}$$

$$+\frac{72}{2!(4!)^2}G_0^T(x_1-x_2)\int d^3x\int d^3x'G_0^T(x-x)G_0^T(x-x')G_0^T(x'-x')G_0^T(x'-x) \tag{2.40}$$

$$+\frac{9}{2!(4!)^2}G_0^T(x_1-x_2)\int d^3xG_0^T(x-x)^2\int d^3x'G_0^T(x'-x')^2 \tag{2.41}$$

$$+\frac{48}{2!(4!)^2}G_0^T(x_1-x_2)\int d^3xG_0^T(x-x')^4 \tag{2.42}$$

and

$$D^{(2)} =$$

$$+\frac{72}{2!(4!)^2}\int d^3x\int d^3x'G_0^T(x-x)G_0^T(x-x')G_0^T(x'-x')G_0^T(x'-x) \tag{2.43}$$

$$+\frac{9}{2!(4!)^2}\int d^3xG_0^T(x-x)^2\int d^3x'G_0^T(x'-x')^2 \tag{2.44}$$

$$+\frac{48}{2!(4!)^2}\int d^3xG_0^T(x-x')^4 \tag{2.45}$$

What can we learn from these expression? There are two main aspects. Firstly, things get really complicated when we try to perform higher-order perturbation theory. The number of terms grows rapidly and individual contributions become so complex that it is not particularly simple to read off their physical properties. It is also very tedious to pick up the correct numerical prefactors which again occur because some of the integrals give equivalent contributions.
To give a glimpse on how this works, lets look at the last diagram in $D^{(2)}$. The starting expression is

$$\int dxdx'\phi(x)\phi(x)\phi(x)\phi(x)\phi(x')\phi(x')\phi(x')\phi(x') \tag{2.46}$$

Now we want to contract every of the $\phi(x)$ with a $\phi(x')$. For the first $\phi(x)$ there are 4 possibilities. for the second one there are 3 and for the third 2 choices. The last contraction is fixed. This yields us a factor of $4! = 24$. Furthermore we can also exchange $\phi \leftrightarrow \phi'$ which gives another factor of 2. Putting everything together we get a total of $2 \cdot 24 = 48$ equivalent

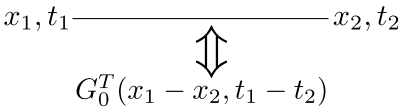

Figure 2.1: *The free Green's function and its diagrammatic representation*

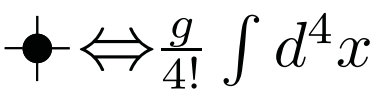

Figure 2.2: *The four point vertex and its diagrammatic representation*

integrals. We also might note that this is the same number as in the last term of the numerator. The reason for that is clear, we only have one choice to contact ϕ_1 with ϕ_2 On the other hand we see that there is definitively some kind of pattern arising. We again find that the terms of the denominator again show up in the numerator (multiplied by G_0^T). Furthermore some of the contributions are just copies of what we have already found in first order perturbation theory. We have to say a lot more about these patterns, but first let's try to give the single terms some clear physical interpretations. And this is where Mr. Feynman comes into play.

2.6.1 Feynman diagrams in the ϕ^4-theory

The invention of a diagrammatic representation of QFT is a major step if one wants to get an intuitive understanding of the different physical processes taking place during an interacting particle makes his path makes his way through space-time. We remember that one can interpret the free Green's function $G_0^T(x - x')$as a propagator, giving the probability amplitude for a particle being created at x, t and destroyed at x', t'. The key idea now is to represent this process by a line as shown in FIG. 2.1

The other fundamental object of our perturbation theory is $\frac{g}{4!}\phi^4(x)$. We can interpret this as the emergence of four particles at a point in four dimensional space x, t, as shown in FIG. 2.2. It is important to keep in mind that this is not an actual space-time trajectory but just a way of representing the propagation of a particle from some point to another. The actual shape of the path is not specified.

First of all let's agree on the following: We interpret the integral d^4x as an averaging over all internal times and positions, which means we only care about the number of interaction events happening between x_1 and x_2 and not at what point exactly they occur.
Now we need to set up up a few rules to make the correspondence between formulas and pictures a true isomorphism (one to one).

- Every leg on a vertex has to be connected to another leg on a vertex or to an external point
- Every external point has to be connected to another external point or to the leg of a vertex

- To avoid overcounting every diagram has to be multiplied by an appropriate symmetry factor S taking into account that there are many equivalent ways of applying the connection rules above to obtain a certain diagram.

The most difficult step of the above procedure in the ϕ^4 model is indeed to find the appropriate symmetry factor of each diagram. Because of reasons which become clear later, it happens that this step is nearly trivial for the actual models we are looking at, so we don't go in much details here. Instead we just state that $S = \frac{1}{|\mathrm{aut(g)}|}$, which means that S is the inverse of the rank of the automorphism group aut(g) of a given diagram g (therefore the rank of the group which takes a diagram into itself preserving its structure aut(g) $\to g$). This allows us to just read of the symmetry factor of many diagrams just by inspection if they aren't too large (For details see [50]). So let's see how all this works by looking at the two terms which contribute to first order in perturbation theory. The first term is given by connecting x_1 by a line with one of the legs at x, perform a "loop" back to another leg of x and finally reach the endpoint x_2 from the last remaining free place at the vertex. We obtain something like FIG. 2.3.

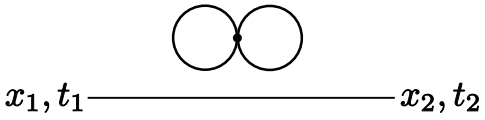

Figure 2.3: *The first diagram in first order perturbation theory*

To obtain the symmetry factor we observe that this object has exactly one symmetry: We can flip the bubble by π around an axis going perpendicular through the diagram at the point of the vertex. This is equivalent to connecting one leg of vertex to another in two possible, indistinguishable ways $1 \to 2$ or $2 \to 1$ for example. The underlying symmetry group is obviously Z_2 and therefore $S = 1/|\mathrm{aut}(g)| = 1/|Z_2| = 1/2$. For the second diagram, we connect the two external points directly. The only thing what is left to connect the legs of the vertex yielding an object looking like the figure eight (See FIG. 2.4).

Here S becomes a litte bit more difficult. The "eight" has two symmetries: Mirroring the two bubbles at the origin gives us a Z_2. The possibility of flipping bubbles as described for the first diagram gives us an additional Z_2 symmetry for every bubble, which makes the altogether symmetry group of the diagram $Z_2 \times Z_2 \times Z_2$ giving us $S = 1/|\mathrm{aut}(g)| = 1/|Z_2 \times Z_2 \times Z_2| = 1/(2 \cdot 2 \cdot 2) = 1/8$.
After we have done the rules right we want to take some more care in the interpretation of the two diagrams: The first one corresponds to a situation where a particle propagates freely from x_1 to x_2. Independent of this we see that another particle is created and destroyed at the same place. Because this process isn't related to the propagation of the real particle we call this a

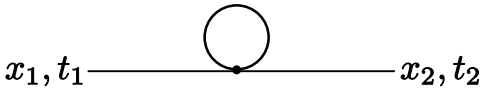

Figure 2.4: *The second diagram in first order perturbation theory*

vacuum bubble.
In contrast, in the second diagram we see that the real particle interacts with itself on some point of its journey. This corresponds to a visible modification of the particles properties (This statement isn't actually completely true for massless theories this "tadpole"-diagrams can be eliminated in dimensional regularization [49]) and can be interpreted as an interaction of the particle with itself. To complete our analysis up to g^1 we need also a diagrammatic representation of the denominator. Applying the Feynman rules we find FIG. 2.5

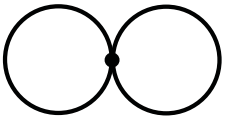

Figure 2.5: *The vacuum diagram in first order perturbation theory*

where the symmetry factor is again $S = 1/8$. This contribution is the same vacuum bubble that we encountered above. We note that this kind of processes is a purely quantum feature which is allowed due to Heisenberg uncertainly which allows for the creation of particles on very short timescales ($\delta t \delta E \sim \hbar$, so if δt is very short there might be enough energy to create a particle)
We can now proceed with the term which are of second order in g and obtain FIG. 2.6. The pattern we mentioned in connection with equation (2.36) and (2.43), becomes clear now. The diagrams can be cast into different classes. The ones which are contained in the numerator (up to multiplication with $G_0^T(x_1 - x_2)$) as well as in the denominator. We call them vacuum

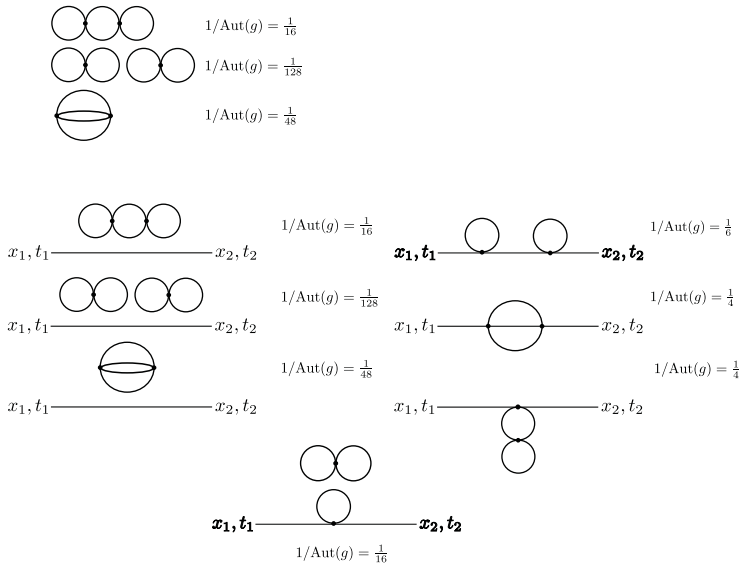

Figure 2.6: *All diagrams in second order perturbation theory. The three in the top row are the vacuum contributions. Additonally the corresponding symmetry factors are shown*

contributions. Furthermore we observe, that there is at least one other diagram (the one in the very bottom of Fig. 2.6) which consists of the product of the two first order contributions. This is called a disconnected diagram (this set of diagrams obviously contains the vacuum diagrams as a subset) All other diagrams are connected. The second pattern allows us to decompose some of the diagrams into subdiagrams which can be traced back to first order contributions by cutting exactly one propagator which is not a bubble. This diagrams are called reducible. Diagrams for which this is not the case are called irreducible.

In a next step lets define (suppressing arguments for brevity) $N_c^{(n)}$ as the set of all connected diagrams in the corresponding order of pertubation theory. Going back to (2.32) it is easy to show that up to g^2

$$\begin{aligned}&\frac{\sum_{n=0} g^n N^{(n)}}{\sum_{n=1} g^n D^{(n)}} = \\ &G_0^T + gN_c^{(1)} + g^2 N_c^{(2)} + \mathcal{O}(g^3)\end{aligned} \tag{2.47}$$

The pictorial proof is based on the identity which is obtained by factoring out the vacuum contributions in the denominator as shown in FIG. 2.7

Using this (informal) diagrammatic calculation, we can cancel the denominator and the theorem in equation (2.47)is proven up to $\mathcal{O}(g^2)$ It is possible to show that this holds in every order of perturbation theory but we will omit the proof here (essentially one has to show that the sum of all diagrams equals the sum of all connected diagrams multiplied with the exponential of all vacuum diagrams) and rather guide the interested reader to the following nice exposition [48]. The corresponding theorem is the linked cluster theorem, which states in our notation as follows

$$G^T = \sum_{n=0}^{\infty} g^n N_c^{(n)} \tag{2.48}$$

We point out, that this kind of theorems are no particularity of this toy model but might be found for all field theories we are aware of. Furthermore we where able to at least eliminate some of divergencies of the theory (there are a lot more which become visible if one starts to calculate

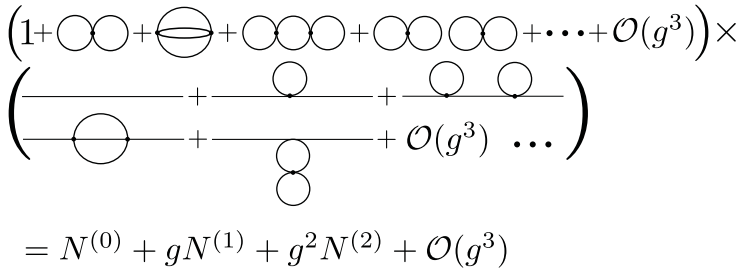

Figure 2.7: *Diagramatic visualization of the linked cluster theorem*

diagrams explicitly a matter we will not discuss here, [48] yields also a good introduction to this topic).

2.7 The self-energy

Looking at the structure of the Green's function G^T it is tempting to amputate the two outer legs (the remainder is called an amputated diagram) and and write $G^T = G_0^T \Sigma G_0^T + ...$, summarizing all the effects of interaction into the object Σ which is called the self-energy (the meaning of this name will become clear later). Note that it consists only of the amputated one-particle irreducible diagrams, therefore, the ones which can not reduced to a combination of lower order contributions by cutting a single line (equivalently one could say the contributions with have no internal free Green's functions). Switching to momentum space via a Fourier transform we might rewrite this as

$$G^T(p,\omega) = G_0^T(p,\omega)\Sigma(p,\omega)G^T(p,\omega) \tag{2.49}$$

or

$$G^T(p,\omega) = \frac{1}{G_0^T(p,\omega)^{-1} - \Sigma(p,\omega)}. \tag{2.50}$$

For simplicity we assume that we are only interested in the retarded sector of the theory (We identify $G^T = G^r$), which might not be physically useful in the context of ϕ^4 theory but serves well for our purpose of explaining some general concepts. We might have a short break here and calculate the free Green's function in momentum space because it is essential for developing any further intuition. Let's start with a Fourier decomposition of the field (Heisenberg) operators: $\phi(x,t) = \int \frac{d^3k}{(2\pi)^3} e^{ikx} a_k(t)$. Let's choose the vacuum as our ground state, we get

$$\begin{aligned} &G_0^r(t,t';x,x') = \\ &\Theta(t-t') \int\int \frac{d^3k}{(2\pi)^3}\frac{d^3k'}{(2\pi)^3} e^{ikx-ik'x'} \langle 0|a_k^\dagger(t)a_{k'}(t)|0\rangle \end{aligned} \tag{2.51}$$

Furthermore using $a_k(t) = e^{-i\omega(k)t}a_k$ and recognizing the number operator we might replace the bracket by $(2\pi)^3\delta(k-k')$ and get

$$\begin{aligned} &G_0^r(t-t';x-x') = \\ &\Theta(t-t') \int \frac{d^3k}{(2\pi)^3} e^{ik(x-x')-i\epsilon(p)(t-t')} \end{aligned} \tag{2.52}$$

now we perform the Fourier transform w.r.t $x - x' \equiv \Delta x$ to obtain

$$\begin{aligned} &G_0^r(t-t';p) = \\ &\Theta(t-t') e^{-i\epsilon(p)(t-t')} \end{aligned} \tag{2.53}$$

where p denotes the momentum. Adding an infinitesimal $+i\delta$ (the choice of sign guarantees causality) to the energy and FT also with respect to $t - t' \equiv \Delta t$ we get

$$G_0^r(\omega; p) = \int_0^\infty d\Delta t e^{i\Delta t - i\epsilon(p)\Delta t - \delta\Delta t} = \frac{i}{\omega - \epsilon(p) + i\delta} \tag{2.54}$$

Here ω denotes the energy. We are now in a position to rewrite the full Green's function of our problem in a more enlightening form

$$G^r(p, \omega) = \frac{1}{(\omega - \Re\Sigma(p, \omega)) - \epsilon(p) - i\Im\Sigma(p, \omega)} \tag{2.55}$$

which gives us a clear interpretation of the effects caused by the self-energy. The first one is a renormalization of the (resonance) energy by the real part.In the literature [48] this effect is known as Lamb shift. The second, in most cases more interesting effect is the spectral broadening implied by the imaginary part. It means that due to interactions our particle has now a finite lifetime given by $\tau = \Im\Sigma^{-1}$. This is also the time scale on which we can speak of a well defined single particle excitation. Because in many metals it is quite large compared to other time scales, the concept of quasi particles is so successful in CMT. Another nice interpretation of the self-energy can be found if we assume that the location of the pole is given by a function $\omega_1(p) = \Re\omega_1(p) + i\Im\omega_1(p)$. We then can expand [48, 51]

$$G^T(\omega, p) = \frac{Z(p)}{\omega - \omega_1(p)} + G_{reg}(p, \omega) \tag{2.56}$$

where G^{reg} is the regular or background part without any poles and $Z(p)^{-1} = 1 - \partial_\omega \Sigma|_{\omega=\omega_1(p)}$ is the quasi particle weight and gives us a measure how good the we can describe our system through well defined quasi particles (for a system without interaction $Z = 1$). For example in electronic systems in 2- or 3d for sufficently small interactions and/or temperatures $Z \approx 1$ so the concept (Landau-Fermi theory) is quite useful, but in one dimension one can show [52] that $Z \to 0$ for arbitrary small interactions so totally different techniques are needed and the system has to be described in terms of collective charge density excitations (Bosonisation [47, 52]).

2.7.1 The scattering matrix

Most physics experiments are scattering experiments. We prepare our system in some initial state $|i\rangle$ let our system of interest evolve in time into a final state $|f\rangle$ what we then eventually measure are the overlap amplitudes $\langle f|i\rangle$. We may interpret this as elements of an operator S which acts as $|f\rangle = S_{fi}|i\rangle$ on a initial state and is called the scattering matrix (SM). Then

$$S_{fi} = \langle f|i\rangle = \langle i|S|i\rangle \tag{2.57}$$

are the scattering matrix elements. We know from our previous discussions that for doing actual computations in the framework of perturbation theory it is convenient to assume that the prepared states of the system are asymptotically free or non-interacting. It is then clear that we can identify $S = U(\infty, -\infty)$ at least for one particle scattering. Going again through some perturbative calculations as in the previous sections we can show that in momentum space

$$S_{fi}^{(1)} = \delta(\epsilon(p_f) - \epsilon(p_i))\delta_{p_i,p_f} + G_0(p_i)^{-1}G(p_i - p_f)G_0(p_f)^{-1}\delta(\epsilon(p_f) - \epsilon(p_i)) \tag{2.58}$$

where the superscript (1) stands for one particle and the delta function enforces energy conservation (putting anything on-shell because external measurable states have to fulfill energy momentum conservation). We will not prove this result because besides of some very technical aspects (for example, we have to take some care in splitting the time domain integrals in appropriate intervals and checking every single one of them if and how poles in energy space can be created there) but instead we try to make sense out of it in an heuristic way. A first observation is that the above formula yields upon comparing with (2.49), the relation $S_{if} = \Sigma_{os}$ so at this level it is just another way of interpreting the self-energy (The subscript *os* (OS) stands again for on-shell). Furthermore one might argue that the transition amplitude should be (except of conservation laws) independent of how the particle reaches the region of interaction which makes it reasonable to divide out the contributions stemming from free propagation (represented by G_0). We will also need a generalization of this concept to the scattering of two particles, which reads as follows

$$\begin{aligned} S_{fi}^{(2)} =& G(p_{i_1})^{-1}G(p_{i_2})^{-1}G^{(2)}(\{p_i\},\{p_f\})G(p_{f_1})^{-1}G(p_{f_2})^{-1}|_{os} \\ &\times \delta\left(\sum_i \epsilon(p_i) - \sum_f \epsilon(p_f)\right) \times \delta(\sum_i p_i - \sum_f p_f) \end{aligned} \tag{2.59}$$

Note that we have introduced an object $G^{(2)}$, two particle Green's function defined as $G^{(2)}(\{p_i\},\{p_f\}) = \langle GS|\psi_{f_1}\psi_{f_2}\psi_{i_1}\psi_{i_2}|GS\rangle$ which describes the propagation of two instead of one particles. $(\{p_i\},\{p_f\})$ denotes the set of incoming and outgoing momenta. The procedure how to obtain scattering matrix elements out of Green's functions is called Lehmann-Symanzik-Zimmermann reduction (LSZ) [53, 48]. Note that we eliminated all the effects arising purely from one particle by amputating the full two-point correlation functions instead of just the bare one furthermore we made the on-shell condition explicit. Formulating this a little bit different

$$S_{fi}^{(2)} = 1 + i\mathcal{T}_{if} \tag{2.60}$$

where the object $\mathcal{T}_{if}$ is called the T-matrix which contains all the information about the actual two particle scattering process and the factor 1 describes free propagation (no interaction). Furthermore it is important to note that like in the one particle case all disconnected two particle contributions have been eliminated similar to the process which was leading us to 2.48. In the ϕ^4-theory up to second order perturbation theory a pictorial representation of the T-Matrix is given in FIG. 2.8

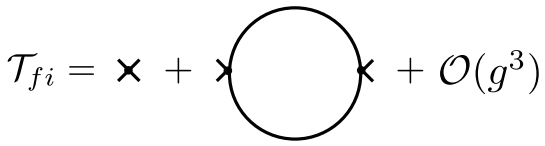

Figure 2.8: *The the T-Matrix in second order perturbation theory. The small lines indicate the amputated outer legs. All momenta/energy labels are suppressed*

Note that the first term is just the bare vertex (times some conservation rules). For this reason the two particle T-matrix is interpreted as a renormalized interaction vertex and diagrams containing such an object a said to include vertex corrections.

3 DIAGRAMMTIC APPROACH TO WQED WITH APPLICATIONS TO THE ONE TLS PROBLEM

We discuss how to construct a diagrammatic approach to tackle WQED problems with an inherent nonlinearity. We discuss in detail its application to a system consisting of a 1-D waveguide coupled to a single TLS. We reproduce results obtained before by other methods and gain new physical insights through the easy interpretability of the Feynman diagrams

3.1 Introduction

In this chapter we want to discuss the Hamiltonian 1.33, introduced in chapter one, which describes the interaction of 1-D optical waveguide with a TLS. We follow mainly the lines of our work published in [54], we may also note that a very similar approach was developed independently shortly thereafter [101]. It turns out that from a theoretical angle this system exhibits certain similarities with nano-electronic transport problems. This makes it possible to apply successfully methods originally developed in electron transport theory to the analysis of nano-scale quantum optical (NQO) systems. These include on the one hand a Bethe-Ansatz approach [72], the Lehmann-Symanzik-Zimmermann reduction technique [73] and the Input-Output formalism [74] where the multi-particle scattering matrix was succesfully derived and on the other hand a Green's function approach that exploits the chirality of effective low-energy field theories which can be derived from the basic Hamiltonian 1.33 [75]. These approaches have also been extended to the case of many photons [76, 77] and more complicated quantum impurities [78]. There are also numerical approaches [79, 80, 82] which may also be used to overcome the restricitions of the RWA [84].
We develop a flexible and intuitive quantum-field-theoretical framework for the analysis of our model Hamiltonian which can be easily extended to more complicated systems. For example the effects of a second scatterer are discussed in the next chapter. Also the implementation of a disordered waveguide was already successfully demonstrated [83]. Our framework is based on a

path-integral formulation from which we can derive the Feynman diagrams of the theory. This enables us to construct an efficient Green's function technique. With these tools at hand we can rederive the main results of the above-mentioned approaches and extend them to arbitrary dispersion relations, notably for the case of two photons. This generalization is an important step, because this enables us to describe a whole new class of physical states, the so called atom photon bound states (APS). They where already numerically found [79], but where not describable by the analytical techniques available so far. Furthermore our approach allows us to classify quite intuitively different non-linear effects like photon bunching and interaction induced radiation trapping by their corresponding Feynman diagrams.

For our approach it turns out to be convenient to replace the Pauli spin operators in (1.33) by auxiliary fermions [81]. We do this for two reasons: First off all it saves us from the heavy machinery to describe a generic spin 1/2 correctly via a path integral. Second it makes the resulting diagrammatics much more transparent and familiar. The transformation rules read as follows

$$\hat{\sigma}_z = \hat{e}^\dagger \hat{e} - \hat{g}^\dagger \hat{g} \tag{3.1}$$

$$\hat{\sigma}_- = \hat{g}^\dagger \hat{e}, \tag{3.2}$$

which requires that the constraint

$$\hat{e}^\dagger \hat{e} + \hat{g}^\dagger \hat{g} = 1, \tag{3.3}$$

has to be fulfilled. Here, $\hat{e}^\dagger$ and $\hat{g}^\dagger$ are, respectively, the creation operators of the excited and ground state of the TLS. Hence, the Hamiltonian which we use for the remainder of this work is [1]

$$\begin{aligned}\hat{H} = &\sum_k \epsilon(k) \hat{a}_k^\dagger \hat{a}_k + \frac{\Omega}{2}\left(\hat{e}^\dagger \hat{e} - \hat{g}^\dagger \hat{g}\right) \\ &+ \frac{U}{\sqrt{L}} \sum_k \left(\hat{a}_k^\dagger \hat{g}^\dagger \hat{e} + \text{h.c.}\right).\end{aligned} \tag{3.4}$$

Furhtermore we note that a generic state of the system can be decomposed into a direct product of TLS and waveguide states

$$|q\rangle = |\text{ph}_q\rangle \otimes |\text{TLS}_q\rangle. \tag{3.5}$$

Having reformulated the Hamiltonian successfully we can go on to perform actual calculations. They are organized as follows. We describe the path-integral formulation in Sec. 3.2. This formulation can be translated into Feynman diagrams, which is discussed in Sec. 3.3. Their properties in the single- and two-excitation sectors are derived in Secs. 3.4 and 3.5, respectively.

[1] Note that we switched for the moment to discrete momenta, this is mainly for the purpose to make the path integral calculations performed later well defined. This switching between discrete and continuous momenta is performed a few times in this thesis whenever it turn s out to be convenient

3.2 Path integral approach

As discussed in 2.5 the Green's function describe the propagation of a particle from one time point to another. From an heuristic point of view (the exponential in (3.6) is the time-evolution operator, which has exactly this property) it is easy to deduce that the formulation there is equivalent to the matrix element of an initial and a final state at different times

$$G(t_f - t_i) = -i\langle f|e^{-\int_{t_i}^{t_f}\hat{H}(t)dt}|i\rangle, \tag{3.6}$$

where $\hat{H}$ is a the Hamiltonian is defined in (3.4). In addition, $|i\rangle$ and $|f\rangle$ represent, respectively, the initial and the final state.
For a path-integral representation, we utilize the resolution of unity via coherent states

$$\mathbb{1} = \frac{1}{(2\pi i)^c}\int\prod_{\alpha}\mathrm{d}\psi_\alpha\mathrm{d}\psi_\alpha^* e^{-\sum_\alpha\psi_\alpha^*\psi_\alpha}|\psi_\alpha\rangle\langle\psi_\alpha|, \tag{3.7}$$

where $c = 1$ for complex fields, $c = 0$ for Grassmann fields, and α labels the set of associated one-particle states ($|\psi_\alpha\rangle\langle\psi_\alpha|$ being the corresponding projection operator). Following the standard procedure for constructing path integrals [91], we insert the resolution of unity twice into Eq. (3.6).This yields

$$G(t_f-t_i) = -i\int\prod_{m,n}\mathrm{d}\psi_{i,m}\mathrm{d}\psi_{i,m}^*\mathrm{d}\psi_{f,n}\mathrm{d}\psi_{f,n}^* e^{-\sum_m\psi_{i,m}^*\psi_{i,m}-\sum_n\psi_{f,n}^*\psi_{f,n}}\langle f|\psi_f\rangle\langle\psi_i|i\rangle\,\mathcal{G}(f,i;t_f-t_i). \tag{3.8}$$

Here $\mathcal{G}(f,i,t_f-t_i)$ is given by

$$\mathcal{G}(f,i;t_f-t_i) = \langle\psi_f|e^{-\int_{t_i}^{t_f}\hat{H}(t)dt}|\psi_i\rangle, \tag{3.9}$$

so that the labels i and f represent the initial and final fields, ψ_i and ψ_f, respectively. In the above equations, the indicies m and n run over all possible one particle states supported by $\hat{H}$.

To be more concrete, we need three types of fields to describe the Hamiltonian correctly: Complex fields ϕ_k for the bosonic modes in the waveguide and two Grassmann fields η and γ which represent the fermionic operators $\hat{e}$ and $\hat{g}$ associated with the TLS. Eq. (3.8) reads now as follows

$$G(t_f-t_i) = -i\int\prod_{k,k'}\mathrm{d}\phi_{i,k}\mathrm{d}\phi_{i,k}^*\mathrm{d}\phi_{f,k'}\mathrm{d}\phi_{f,k'}^* e^{-\sum_k\phi_{i,k}^*\phi_{i,k}-\sum_k\phi_{f,k}^*\phi_{f,k}}\langle\mathrm{ph}_f|\phi_f\rangle\langle\phi_i|\mathrm{ph}_i\rangle\mathcal{G}(f,i;t_f-t_i), \tag{3.10}$$

where we have redefined $\mathcal{G}(f,i,t_f-t_i)$ as follows

$$\begin{aligned}\mathcal{G}(f,i;t_f-t_i) = \int\mathrm{d}\gamma_i\mathrm{d}\gamma_i^*\mathrm{d}\gamma_f\mathrm{d}\gamma_f^*\mathrm{d}\eta_i\mathrm{d}\eta_i^*\mathrm{d}\eta_f\mathrm{d}\eta_f^* e^{-\gamma_i^*\gamma_i-\gamma_f^*\gamma_f-\eta_i^*\eta_i-\eta_f^*\eta_f}\\ \times\langle\mathrm{TLS}_f|\gamma_f\eta_f\rangle\langle\gamma_i\eta_i|\mathrm{TLS}_i\rangle\langle\phi_f\gamma_f\eta_f|e^{-\int_{t_i}^{t_f}\hat{H}(t)dt}|\phi_i\gamma_i\eta_i\rangle.\end{aligned} \tag{3.11}$$

For the calculation of $\mathcal{G}(f,i,t_f-t_i)$ we mainly follow the lines of Ref. [93], so that we will restrict ourselves to the relevant intermediate steps. Upon inserting the resolution of unity N times in Eq. (3.11), we arrive at

$$\begin{aligned}\mathcal{G}(f,i;t_f-t_i) = &\int \mathrm{d}\gamma_i \mathrm{d}\gamma_i^* \mathrm{d}\gamma_f \mathrm{d}\gamma_f^* \mathrm{d}\eta_i \mathrm{d}\eta_i^* \mathrm{d}\eta_f \mathrm{d}\eta_f^* e^{-\gamma_i^*\gamma_i-\gamma_f^*\gamma_f-\eta_i^*\eta_i-\eta_f^*\eta_f} \langle \mathrm{TLS}_f|\gamma_f\eta_f\rangle\langle\gamma_i\eta_i|\mathrm{TLS}_i\rangle \\ &\times \lim_{N\to\infty} \int \prod_{m=1}^{N} \prod_{n=1}^{N-1} \prod_k \frac{\mathrm{d}\phi_{n,k}\mathrm{d}\phi_{n,k}^*\mathrm{d}\eta_n\mathrm{d}\eta_n^*\mathrm{d}\gamma_n\mathrm{d}\gamma_n^*}{2\pi i} \\ &\times e^{-\sum_{n,k}(\phi_{n,k}\phi_{n,k}^*+\gamma_n\gamma_n^*+\eta_n\eta_n^*)} e^{-i\lambda H(\phi_m,\phi_{m-1}^*,\gamma_m,\gamma_{m-1}^*,\eta_m,\eta_{m-1}^*)}, \end{aligned} \tag{3.12}$$

where $\lambda = \frac{t_f-t_i}{N}$ and

$$\begin{aligned}H(\phi_n,&\phi_{n-1}^*,\gamma_n,\gamma_{n-1}^*,\eta_n,\eta_{n-1}^*) = \\ &\sum_k \epsilon(k)\phi_{n,k}\phi_{n-1,k}^* + \frac{\Omega}{2}(\eta_n\eta_{n-1}^* - \gamma_n\gamma_{n-1}^*) + \frac{U}{\sqrt{N}}\sum_k \left(\phi_{n,k}^*\gamma_n^*\eta_{n-1} + \eta_n^*\gamma_{n-1}\phi_{n-1,k}\right). \end{aligned} \tag{3.13}$$

The labels $n=0$ and $n=N$ correspond, respectively, to the initial and final fields. It is now straightforward to integrate out the fermionic degrees of freedom due to the Gaussian structure of the corresponding path integral

$$\begin{aligned}\mathcal{G}(f,i;t_f-t_i) = &\int \mathrm{d}\gamma_i \mathrm{d}\gamma_i^* \mathrm{d}\gamma_f \mathrm{d}\gamma_f^* \mathrm{d}\eta_i \mathrm{d}\eta_i^* \mathrm{d}\eta_f \mathrm{d}\eta_f^* e^{-\gamma_i^*\gamma_i-\gamma_f^*\gamma_f-\eta_i^*\eta_i-\eta_f^*\eta_f} \langle \mathrm{TLS}_f|\gamma_f\eta_f\rangle\langle\gamma_i\eta_i|\mathrm{TLS}_i\rangle \\ &\times \lim_{N\to\infty} \int \prod_{n=1}^{N-1} \prod_k \frac{\mathrm{d}\phi_{n,k}\mathrm{d}\phi_{n,k}^*}{2\pi i} e^{-\sum_{n,k}\phi_{n,k}\phi_{n,k}^*(1-i\lambda\epsilon(k))} e^{\vec{q}_N^{\,\dagger} R(\phi,\phi^*)\vec{q}_0}. \end{aligned} \tag{3.14}$$

Here, we have introduced the following abbreviations

$$\begin{aligned} q_i = (\eta_i,\gamma_i), \qquad R(\phi,\phi^*) = \mathcal{R}(\phi_N,\phi_{N-1}^*)\cdot\ldots\cdot\mathcal{R}(\phi_1,\phi_0^*), \\ \mathcal{R}(\phi_i,\phi_{i-1}^*) = \begin{pmatrix} 1-i\lambda\Omega/2 & 0 \\ 0 & 1+i\lambda\Omega/2 \end{pmatrix} - i\lambda\frac{U}{\sqrt{L}}\sum_k \begin{pmatrix} 0 & \phi_{i-1,k} \\ \phi_{i,k}^* & 0 \end{pmatrix}. \end{aligned} \tag{3.15}$$

The TLS can either be in the excited or in the ground state. Thus, we can identify the TLS state by a two component vector

$$|\mathrm{TLS}\rangle = \begin{pmatrix} |e\rangle \\ |g\rangle \end{pmatrix}, \tag{3.16}$$

which induces a 2×2 matrix structure to $\mathcal{G}(f,i;t_f-t_i)$

$$\mathcal{G}(f,i;t_f-t_i) = \begin{pmatrix} \mathcal{G}_\mathrm{e}(f,i;t_f-t_i) & \mathcal{G}_\mathrm{ab}(f,i;t_f-t_i) \\ \mathcal{G}_\mathrm{em}(f,i;t_f-t_i) & \mathcal{G}_\mathrm{w}(f,i;t_f-t_i) \end{pmatrix}. \tag{3.17}$$

We denote the case when the TLS is excited in the initial as well as in the final state by the diagonal element $\mathcal{G}_{\mathrm{e}}$. Consequently, $\mathcal{G}_{\mathrm{e}}$ covers the dynamics of the quantum impurity, i.e. the TLS that interacts with photons from the waveguide so that we call it the TLS-Green's function. Similarly, we denote the case when the TLS is in the ground state for both the initial and the final state by the diagonal element $\mathcal{G}_{\mathrm{w}}$. Clearly, this quantity describes the dynamics of the photons in the waveguide in the presence of the TLS and we, therefore, call it the waveguide Green's function. The off-diagonal element $\mathcal{G}_{\mathrm{ab}}$ features that the TLS is initially in the ground state, but ends up being in the excited state. This means that the TLS has absorbed a photon, hence we call $\mathcal{G}_{\mathrm{ab}}$ the absorption Green's function. Clearly, $\mathcal{G}_{\mathrm{em}}$ covers the complementary process where an initially excited TLS emits a photon and therefore we call this matrix element the emission Green's function.

We now utilize the fermionic resolution of unity and the identities [93] $\langle e|\eta\gamma\rangle = \eta$, $\langle g|\eta\gamma\rangle = \gamma$, and $\eta\gamma^* = e^{-\eta\gamma^*} - 1$ to perform the last integration over the initial and final fermionic fields. We will restrict ourselves to the TLS-Green's function, the other Green's functions can be determined in exactly the same way. After some algebra we obtain

$$\mathcal{G}_{\mathrm{e}}(f,i,t_f-t_i) = \lim_{N\to\infty}\int\prod_{n=1}^{N-1}\prod_k \frac{\mathrm{d}\phi_{k,n}\mathrm{d}\phi^*_{k,n}}{2\pi i} e^{-\sum_{n,k}\phi_{n,k}\phi^*_{n,k}(1-i\lambda\epsilon(k))} R(\phi,\phi^*). \tag{3.18}$$

In the next step, we want to integrate out the bosonic fields. Therefore, we use the matrix $R(\phi,\phi^*)$ (see Eq. (3.15)) and expand it up to $\mathcal{O}(\lambda)$ (This is sufficent, because the timestep might be chosen as small as necessary). Taking the limit $N\to\infty$ at the end, we find

$$\begin{aligned}
\mathcal{G}_{\mathrm{e}}(f,i;t_f-t_i) = &\sum_{r=0}^{\infty}\left(\frac{iU}{\sqrt{L}}\right)^r \int_0^{t_i-t_f}\mathrm{d}t_{2r}\int_0^{t_{2r}}\mathrm{d}t_{2r-1}....\int_0^{t_2}\mathrm{d}t_1\prod_k\prod_{m=1}^{2r}\frac{\mathrm{d}\phi_{m,k}\mathrm{d}\phi^*_{m,k}}{2\pi i}\\
&\times\mathcal{G}^0_{\mathrm{e}}(\phi^*_N,\phi_{2r},t_f-t_i-t_{2r})\,e^{-\sum_k\phi^*_{2r,k}\phi_{2r,k}}\sum_k\phi_{2r,k}\\
&\times\mathcal{G}^0_{\mathrm{w}}(\phi^*_{2r},\phi_{2r-1},t_{2r}-t_{2r-1})\,e^{-\sum_k\phi^*_{2r-1,k}\phi_{2r-1,k}}\sum_k\phi^*_{2r-1,k}\\
&\times\mathcal{G}^0_{\mathrm{e}}(\phi^*_{2r-1},\phi_{2r-2},t_{2r-1}-t_{2r-2})\,e^{-\sum_k\phi^*_{2r-2,k}\phi_{2r-2,k}}\sum_k\phi_{2r-2,k}\\
&.....\\
&\times\mathcal{G}^0_{\mathrm{e}}(\phi^*_1,\phi_0,t_1).
\end{aligned}\tag{3.19}$$

Here, we have introduced the free propagators of the excited TLS

$$\mathcal{G}^0_{\mathrm{e}}(\phi^*_i,\phi_j,t) = e^{-i\frac{\Omega}{2}t}\,e^{\sum_k\phi^*_{i,k}e^{-i\epsilon(k)t}\phi_{j,k}} \tag{3.20}$$

and the waveguide

$$\mathcal{G}^0_{\mathrm{w}}(\phi^*_i,\phi_j,t) = e^{+i\frac{\Omega}{2}t}\,e^{\sum_k\phi^*_{i,k}e^{-i\epsilon(k)t}\phi_{j,k}}. \tag{3.21}$$

Further, we would like to note that at this point the correspondence to a Dyson series, known from usual quantum mechanical pertubation theory, becomes clear. We have vertices with

strength $\frac{U}{\sqrt{L}}$ at which a photon is annihilated or created and the free propagation of photons or excitations between two successive scattering events.
In order to calculate the full Green's function, we have to evaluate Eq. (3.10). For an n-photon state, the projection on the coherent states is given by

$$\langle k_1 k_2 \dots k_n | \phi \rangle = \phi_{k_1} \phi_{k_2} \dots \phi_{k_n}. \tag{3.22}$$

Inserting these bosonic fields and integrating out the bosonic variables yields the full Green's functions. As our basic (and equivalent) Hamiltonians, Eqs. (1.33) and (3.4), conserve the total number of excitations, we can evaluate the TLS-Green's function separately in any $N-$excitation subspace and we do this explicitly in the one-excitation and the two-excitation sector. Therefore, a generic Green's function is of the form ${}_N G^{\alpha}_{\beta}$, where N indicates the excitation number, β denotes the initial and final state of the TLS according to Eq. (3.17) and α describes the level of interaction taken into account, i.e. $\alpha = 0$ for a free Green's function and a blank space for the full Green's function.

3.2.1 Single excitation sector

For a single excitation, we start the evaluation of the TLS-Green's function ${}_1 G_{\mathrm{e}}(t_f - t_i)$ by noting that we have an initial and final state where the TLS is excited and there are no photons in the waveguide. The TLS-Green's function then reads

$${}_1 G_{\mathrm{e}}(t_f - t_i) = -i \int \prod_{k,k'} \mathrm{d}\phi_{f,k} \mathrm{d}\phi^*_{f,k} \mathrm{d}\phi_{i,k'} \mathrm{d}\phi^*_{i,k'} e^{-\sum_k \phi_{f,k}\phi^*_{f,k} - \sum_k \phi_{i,k}\phi^*_{i,k}} \mathcal{G}_{\mathrm{e}}(f, i, t_f - t_i). \tag{3.23}$$

The two Gaussian functional integrals over ϕ_f, ϕ_i are easily carried out and we obtain

$$\begin{aligned} {}_1 G_{\mathrm{e}}(t_f - t_i) = &- i \sum_{j=0}^{\infty} \left(\frac{iU}{\sqrt{L}} \right)^{2j} \int_0^{t_i - t_f} \mathrm{d}t_{2j} \int_0^{t_{2j}} \mathrm{d}t_{2j-1} .... \int_0^{t_2} \mathrm{d}t_1 \\ &\times {}_1 G^0_{\mathrm{e}}(t_f - t_i - t_{2j}) \left[\sum_k {}_1 G^0_{\mathrm{w}}(k, t_{2j} - t_{2j-1}) \right] {}_1 G^0_{\mathrm{e}}(t_{2j-1} - t_{2j-2}) \dots {}_1 G^0_{\mathrm{e}}(t_1 - t_0) \\ = &\sum_j {}_1 G^{(j)}_{\mathrm{e}}(t_f - t_i) \end{aligned} \tag{3.24}$$

We note that every term of the sum has the form of a Dyson series and represents a convolution ${}_1 G^{(j)}_{\mathrm{e}} \sim \underbrace{{}_1 G^0_{\mathrm{e}} * {}_1 G^0_{\mathrm{w}} * {}_1 G^0_{\mathrm{e}} .... * {}_1 G^0_{\mathrm{e}}}_{2j+1 \text{ factors}}$ with

$${}_1 G^0_{\mathrm{e}}(t) = e^{-i\frac{\Omega}{2}t}, \qquad {}_1 G^0_{\mathrm{w}}(k, t) = e^{i\frac{\Omega}{2}t} e^{-i\epsilon(k)t}. \tag{3.25}$$

The convolution theorem states that a convolution in time domain equals a simple multiplication in frequency domain. This means that, after Fouriertransfrom (FT), we can recast the above

equation in purely algebraic form

$$ {}_1G_{\mathrm{e}}(\omega) = \sum_{j=0}^{\infty} \frac{1}{\omega - \Omega/2 + i\delta} \left(\frac{1}{\omega - \Omega/2 + i\delta} \sum_k \frac{U^2/L}{\omega + (\Omega/2 - \epsilon(k)) + i\delta} \right)^j . \tag{3.26} $$

Here, we have introduced the factors $+i\delta$ because we are working with retarded Green's functions exclusively [2] and the limit $\delta \to 0_+$ is implicit. Please note also the structural similarity to the Dyson series derived for the ϕ^4 model 2.49 in section 2.5. The above equation can be solved by simply adding the geometric series, and we arrive at the main equation of this section, the TLS-Green's function ${}_1G_{\mathrm{e}}(\omega)$ in the single-excitation sector

$$ {}_1G_{\mathrm{e}}(\omega) = \frac{1}{\omega - \Omega/2 + i\delta - {}_1\Sigma(\omega)}, \tag{3.27} $$

where the one-excitation self-energy ${}_1\Sigma(\omega)$ is given by

$$ {}_1\Sigma(\omega) = \frac{U^2}{L} \sum_k \frac{1}{\omega + \Omega/2 - \epsilon(k) + i\delta}. \tag{3.28} $$

The waveguide-Green's function in the single excitation sector can be calculated in a similar manner as the above TLS-Green's function. The main difference lies in the fact that the initial and final states feature a free photon. As a result, one has to add free photon fields in Eq. (3.23), which yields

$$ {}_1G_{\mathrm{w}}(k_i, k_f; t_f - t_i) = -i \int \prod_{k,k'} \mathrm{d}\phi_{f,k} \mathrm{d}\phi^*_{f,k} \mathrm{d}\phi_{i,k'} \mathrm{d}\phi^*_{i,k'} \phi^*_{i,k_i} \phi_{f,k_f} e^{-\sum_k \phi_{f,k}\phi^*_{f,k} - \sum_k \phi_{i,k}\phi^*_{i,k}} \mathcal{G}_{\mathrm{w}}(f, i; t_f - t_i). \tag{3.29} $$

Performing the integrations and again transiting to momentum space results in

$$ {}_1G_{\mathrm{w}}(k_i, k_f; \omega) = {}_1G^0_{\mathrm{w}}(k_i; \omega)\delta_{k_i,k_f} + \frac{U^2}{L} {}_1G^0_{\mathrm{w}}(k_i; \omega)\, {}_1G_{\mathrm{e}}(\omega)\, {}_1G^0_{\mathrm{w}}(k_f; \omega), \tag{3.30} $$

where

$$ {}_1G^0_{\mathrm{w}}(k; \omega) = \frac{1}{\omega + \Omega/2 - \epsilon(k) + i\delta}. \tag{3.31} $$

The expression (3.30) for the waveguide-Green's function ${}_1G_{\mathrm{w}}(k_i, k_f; \omega)$ consists of two terms, which can be identified with free propagation of the photon and scattering off the (renormalized) TLS, respectively. The corresponding absorption and emission Green's functions are derived in Appendix A, together with their diagrammatic representation.

[2] recall that this are the only type of Green's function in our system due to the lack of hole-like excitations which would require the existence of a Fermi surface

3.2.2 Two excitation sector

The calculations for the two excitation sub sector follow the same lines as before, but we will see that the resulting equations become much more complex in the sense that they are not of purely algebraic type, but consist of additional internal momentum integrations. Again, we start with determining the Green's function for an excited impurity in the initial and in the final state ${}_2G_\mathrm{e}$. We again start with the general expression given by Eq. (3.10). According to Eq. (3.22) and Pauli's exclusion principle which states that a TLS can only contain one excitation, the only particle we can add to the system in this situation compared to the one-excitation case is an additional photon which is represented by a bosonic state in the initial and final state

$$ {}_2G_\mathrm{e}(k_i,k_f;t_f{-}t_i) = -i\int\prod_{k,k'}\mathrm{d}\phi_{f,k}\mathrm{d}\phi^*_{f,k}\mathrm{d}\phi_{i,k'}\mathrm{d}\phi^*_{i,k'}\phi^*_{i,k_i}\phi_{f,k_f}\, e^{-\sum_k\phi_{f,k}\phi^*_{f,k}-\sum_k\phi_{i,k}\phi^*_{i,k}}\mathcal{G}_\mathrm{e}(f,i,t_f{-}t_i), \tag{3.32}$$

where $\mathcal{G}_\mathrm{e}(f,i,t_f-t_i)$ is given by (3.19). The Gaussian integrals can be performed as before. Additionaly we perform a Fourier transform and the Green's function is then given by

$$\begin{aligned} {}_2G_\mathrm{e}(k_f,k_i;\omega) = {}&{}_2G^\mathrm{r}_\mathrm{e}(k_i;\omega)\delta_{k_i,k_f} \\ &+\frac{U^2}{L}\,{}_2G^\mathrm{r}_\mathrm{e}(k_i;\omega)\,{}_2G^0_\mathrm{w}(k_f,k_i;\omega)\,{}_2G^\mathrm{r}_\mathrm{e}(k_f;\omega) \\ &+\frac{U^4}{L^2}\sum_k\,{}_2G^\mathrm{r}_\mathrm{e}(k_i;\omega)\,{}_2G^0_\mathrm{w}(k_i,k;\omega)\,{}_2G^\mathrm{r}_\mathrm{e}(k;\omega)\,{}_2G^0_\mathrm{w}(k,k_f;\omega)\,{}_2G^\mathrm{r}_\mathrm{e}(k_f;\omega) \\ &+\ldots, \end{aligned} \tag{3.33}$$

where

$$ {}_2G^0_\mathrm{w}(k,k';\omega) = \frac{1}{\omega+\Omega/2-\epsilon(k)-\epsilon(k')+i\delta} \tag{3.34}$$

and

$$ {}_2G^\mathrm{r}_\mathrm{e}(k;\omega) = \frac{1}{\omega-\Omega/2-\epsilon(k)+i\delta-{}_2\Sigma(k;\omega)}. \tag{3.35}$$

Here, the superscript r indicates that the TLS-Green's function is already renormalized by the self-energy

$$ {}_2\Sigma(k;\omega) = \frac{U^2}{L}\sum_{k'}{}_2G^0_\mathrm{w}(k,k';\omega). \tag{3.36}$$

Because we were not able to express ${}_2G_\mathrm{e}(k_f,k_i;\omega)$ in closed form (even if we replace the summations by integration) we can recast Eq. (3.33) in a T-Matrix representation which is well suited for numerical calculations.To be more concrete, the T-Matrix representation reads

$$ {}_2G_\mathrm{e}(k_f,k_i;\omega) = {}_2G^\mathrm{r}_\mathrm{e}(k_i;\omega)\delta_{k_i,k_f} + {}_2G^\mathrm{r}_\mathrm{e}(k_i;\omega)\,T(k_f,k_i;\omega)\,{}_2G^\mathrm{r}_\mathrm{e}(k_f;\omega) \tag{3.37}$$

where the T-Matrix is given by

$$ T(k_f,k_i;\omega) = \frac{U^2}{L}{}_2G^0_\mathrm{w}(k_f,k_i;\omega) + \frac{U^2}{L}\sum_k\,{}_2G^0_\mathrm{w}(k,k_i;\omega)\,{}_2G^\mathrm{r}_\mathrm{e}(k;\omega)\,T(k_f,k;\omega). \tag{3.38}$$

The above T-matrix representation of ${}_2G_\mathrm{e}(k_f, k_i; \omega)$, Eqs. (3.37) and (3.38), constitutes one of the main results of this PhD thesis. Eq. (3.37) describes the nontrivial behavior of an excited TLS in the presence of an additional photon. As announced previously, the result is more complicated than in the single-excitation case, where we were able to explicitly sum the corresponding Dyson series. In the present case of two excitations, however, we have found a self-consistent description of the Green's function, which can be solved numerically for arbitrary dispersion relations. In the special case of a linear dispersion relation, the TLS-Green's function can even be calculated analytically because the Dyson series truncates after just two terms (we consider this case in more details in section 3.5.2). The waveguide-Green's function, which describes the behavior of two photons in the presence of an TLS which is initially in its ground state is given by

$$\begin{aligned}{}_2G_\mathrm{w}(k_i, p_i, k_f, p_f; t_f - t_i) = -i \int \prod_{k,k'} \mathrm{d}\phi_{f,k} \mathrm{d}\phi^*_{f,k} \mathrm{d}\phi_{i,k'} \mathrm{d}\phi^*_{i,k'} \\ \times \phi^*_{i,k_i} \phi^*_{i,p_i} \phi_{f,k_f} \phi_{f,p_f} \, e^{-\sum_k \phi_{f,k}\phi^*_{f,k} - \sum_k \phi_{i,k}\phi^*_{i,k}} \mathcal{G}_\mathrm{w}(f, i, t_f - t_i).\end{aligned} \tag{3.39}$$

After performing the integrations, this finally reads

$$\begin{aligned}{}_2G_\mathrm{w}(\omega, k_f, p_f, k_i, p_i) =& {}_2G^0_\mathrm{w}(k_i, p_i; \omega) \left(\delta_{k_i,k_f} \delta_{p_i,p_f} + \delta_{k_i,p_f} \delta_{p_i,k_f} \right) \\ &+ \frac{U^2}{L} \, {}_2G^0_\mathrm{w}(\omega, k_i, p_i) \, {}_2G^\mathrm{sym}_\mathrm{e}(k_i, p_i, k_f, p_f; \omega) \, {}_2G^0_\mathrm{w}(\omega, k_f, p_f),\end{aligned} \tag{3.40}$$

where ${}_2G^\mathrm{sym}_\mathrm{e}$ is a symmetrized version (this symmetrization is necessary to include all the allowed permutations of initial and final momenta) of the full TLS-Green's function and is given by

$${}_2G^\mathrm{sym}_\mathrm{e}(k_i, p_i, k_f, p_f; \omega) = {}_2G_\mathrm{e}(k_f, k_i; \omega) + {}_2G_\mathrm{e}(k_f, p_i; \omega) + {}_2G_\mathrm{e}(p_f, k_i; \omega) + {}_2G_\mathrm{e}(p_f, p_i; \omega). \tag{3.41}$$

For the case of two excitations, the full waveguide-Green's function ${}_2G_\mathrm{w}(\omega, k_f, p_f, k_i, p_i)$ exhibits the same structure as in the single-excitation sector. It consists of a free propagation term and a second term that describes the scattering off a renormalized TLS. The corresponding absorption and emission Green's functions are discussed in Appendix A.

3.3 Feynman diagram representation

In this section, we illustrate the formulas obtained by the path integral approach by way of Feynman diagrams. Specifically, we will refrain from providing a rigorous derivation of the full diagrammatic technique but will instead represent the equations of the previous section by Feynman diagrams. This "visualization" provides a clear identification and interpretation of physical processes and, as already alluded to above, facilitates a very flexible and efficient framework for perturbative analyses.
In general, the Hamiltonian given by Eq. (3.4) features three distinct species of quantized excitations, i.e., bosons (photons) with a mode index k and two types of fermions, representing

the excited and the ground state of the TLS. In the following diagrammatic representation, these excitations will be depicted by a wavy, a dashed and a solid line, respectively. This mapping is also shown in Tab. 3.1 for clarification. Apart from these diagonal contributions, Eq. (3.4) also features a scattering vertex, which connects the individual lines and is also shown in Tab. 3.1.
As much of the physical insight to be gained originates from a comparison of the results for the case of a single excitations with the case of two excitations, we will proceed in a corresponding sequence of sub-sections.

3.3.1 Single excitation sector

In this section we want to find a diagrammatic representation of the TLS-Green's function ${}_1G_\mathrm{e}$ for the case of one excitation present in the system. From Eq. (3.24) it is immediately clear that we have essentially to deal with two different kind of processes. First we investigate

$$ {}_1G^0_\mathrm{e}(t'-t) = e^{-i\frac{\Omega}{2}(t'-t)} = \quad (3.42)$$

which describes the propagation of an excited TLS from time t to t'. The second contribution is given by (cf. Eq. (3.25))

$$ {}_1G^0_\mathrm{w}(k,t'-t) = e^{i\frac{\Omega}{2}(t'-t)}e^{-i\epsilon(k)(t'-t)} = \quad , \quad (3.43)$$

and describes the simultaneous transport of a TLS in the ground state together with a photon in the waveguide again from time t to t' (Note that a propagating ground state seems to be unphysical but it shows up naturally in the slave fermion description and makes good sense if it is always coupled to a real excitation, namely the photon in our case). Furthermore, we can assign to every pairing of a wavequide and groundstate Green's function in Eq. (3.24) a factor of $iU/\sqrt{L}$ which may therefore interpreted as an interaction vertex where one type of excitation is converted to an other one. Combining everything we can rewrite the TLS-Green's function

Photons	$\|e\rangle$	$\|g\rangle$	Vertex

Table 3.1: *Table of the representation of the individual species and the interaction vertex in terms of Feynman diagrams.*

diagrammatically as

$${}_1G_{\mathrm{e}}(t_f - t_i) = -i\Big\{$$

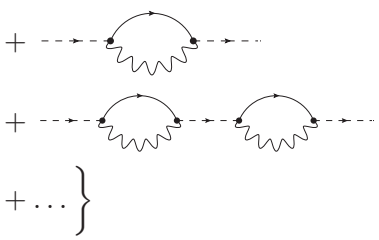

(3.44)

where each vertex provides an integration over internal times. Additionally, each photonic line sandwiched between two interaction vertices implies a summation over the corresponding momentum. At this point we are able to exploit one of the main advantages of the diagrammatic approach and provide an interpretation of the the individual terms in the perturbation series in terms of physical processes: The excited TLS goes to the ground state by emitting a photon. This photon is absorbed at a later time, setting the TLS to the excited state again. This process is repeated n times in the nth term of the perturbation series. Again the convolution integrals associated with the time-domain diagrams turn into simple products if we perform a FT, so that we may retain the free propagation and the bubble diagram as well as the entire perturbation series. Therefore, in the frequency domain no integration with regards to the scattering vertices are implied and per bubble only a weighting factor of $U/\sqrt{L}$ is added. Furthermore the global prefactor $-i$ can be omitted. However we have to perform a momentum summation to calculate explicitly the photon-ground state bubble which corresponds to an averaging over internal (not necessary on-shell) momenta. More explicitly, the free TLS-Green's function reads

$$= \frac{1}{\omega - \Omega/2 + i\delta} = {}_1G^0_{\mathrm{e}}(\omega). \tag{3.45}$$

Similarly, in the frequency domain, we evaluate the bubble diagram after cutting it free from the interaction vertices to

$$= \frac{1}{\omega + \Omega/2 - \epsilon(k) + i\delta}$$

$$= {}_1G^0_{\mathrm{w}}(k;\omega). \tag{3.46}$$

In the time-domain this Green's function describes the simultaneous propagation of a TLS in the ground state and a photon in the waveguide. Since both excitations are created and annihilated at the same times, the Fourier transform yields only one frequency argument and leads to the analytic form shown above. As usual, we can cast the perturbation series (3.44) into the well known form of a self-consistent Dyson equation

$${}_1G_{\mathrm{e}}(\omega) =$$

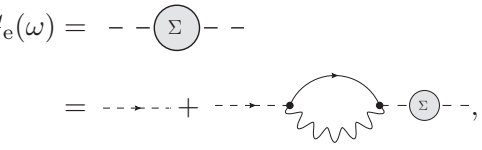

(3.47)

which can be solved directly and we obtain Eq. (3.27) with the (one-excitation) self-energy

$$ {}_1\Sigma(\omega) = \frac{U^2}{L} \sum_k {}_1G^0_{\mathrm{w}}(k;\omega) = $$ 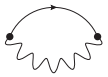 . (3.48)

By the same token, the full waveguide-Green's function is given by Eq. (3.30) and we can represent it in a diagrammatic form

$$ {}_1G_{\mathrm{w}}(k_f, k_i;\omega) = $$  . (3.49)

This expression comprises two terms. The first term on r.h.s. corresponds to the free propagation of a photon and the TLS in the ground state while the second term on the r.h.s. describes the scattering of the (renormalized) TLS. Upon reinserting Eq. (3.44) into Eq. (3.49), we obtain the perturbation series of the full waveguide-Green's function.

3.3.2 Two excitation sector

We now want to develop the diagrammatic description of Sec. 3.2.2 which describes the system with two excitations in it. From Eq. (3.33) we know that the perturbation series for the TLS-Green's function consists of two Green's functions, which we will depict diagrammatically as

$$ {}_2G^0_{\mathrm{w}}(k, k';t_f - t_i) = $$ 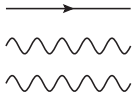 (3.50)

and

$$ {}_2G^{\mathrm{r}}_{\mathrm{e}}(k;t_f - t_i) = $$ 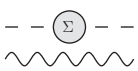 . (3.51)

Just as in the single-excitation case, these Green's functions describe the propagation of the excitations over a given time interval from t_i to t_f (this behavior can be immediately understood by the single frequency dependence in Eq. (3.34) and (3.35)). The Green's function ${}_2G^0_{\mathrm{w}}(k, k';t_f - t_i)$ describes the simultaneous propagation of two photons with momenta k and k', together with a ground state field of the TLS. Similarly, the Green's function ${}_2G^{\mathrm{r}}_{\mathrm{e}}(k;t_f - t_i)$ represents the propagation of an excited TLS and one additional photon. In addition, in Eq. (3.51) we have already accounted for single particle renormalizations of the excited TLS (as discussed in the single-excitation case) which is again depicted by the symbol Σ . With the help of these basic Green's function, we can now rewrite the TLS-Green's function in the

two-excitation case as given by Eq. (3.33) within as

$$
{}_2G_{\mathrm{e}}(k,k',t_f-t_i)
$$

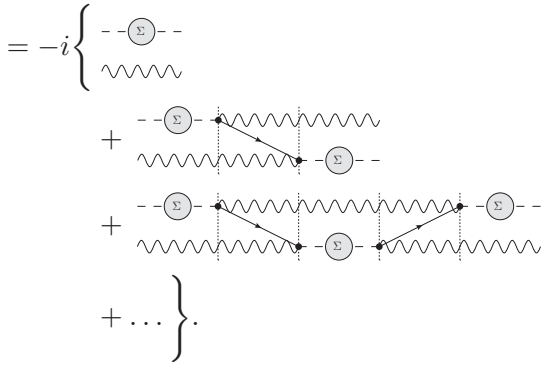

(3.52)

Here, the dotted lines serve as indicators that separate distinct Green's functions from each other and - in the time-domain formulation - imply an integration over the associated intermediate times. Furthermore, the momentum of the free photon is conserved (as long as it does not interact with a vertex), each interaction vertex provides as before a factor $iU/\sqrt{L}$ and photons sandwiched between two interaction vertices imply a summation over the corresponding momentum. We elaborate in some details how to derive this equal-time Green's functions in Appendix B. This diagrammatic formulation of the TLS-Green's function's perturbation series in the two-excitation case provides a clear physical interpretation. The first term of the perturbation series corresponds to the situation when the TLS is excited and the additional photon is and stays free throughout the entire propagation (the two excitations are independent so it is a simple combination of one particle processes). In the second term, the excited TLS emits a photon at some intermediate time, so for a given period of time two photons propagate freely in the waveguide (the photon ground state is also present). After a certain time the initially free photon is absorbed by the TLS, whereas the other photon continues to propagate freely. Clearly, this induces correlations between the photons. In the higher-order terms of the perturbation series this process is repeated many times, which effectively leads to photons that are emitted and reabsorbed, while the respective other photon is scattered by the TLS. Finally, we would like to note that all processes where the TLS directly reabsorbs the originally emitted photon without intermediate scattering are contained in the self-energy bubbles. In the case of a frequency-domain description, the intermediate convolutions integrals translate into multiplications and the common time-dependencies of the individual free-particle propagators that comprise the TLS-Green's function lead to a single frequency argument, just as in the case for the single-excitation case. The full waveguide-Green's function is given by Eq. (3.40) and can be obtained by adding free waveguide-Green's functions to the full TLS-Green's function ${}_2G_{\mathrm{e}}(k,k',\omega)$ in a symmetrized way consistent with Eq. (3.40)) and by augmenting the perturbation series by a further term that takes into account the free propagation as described by Eq. (3.50). A general and very important property of the system is that the TLS cannot interact with free photons if it is in the excited state (Again this is due to the Pauli exclusion principle for fermions). It is exactly this property which renders the system nonlinear, because loosely speaking the second photon knows if the first photon has been absorbed or not. For

a linear system (e.g., a one-dimensional waveguide with a site-coupled bosonic quantum dot instead of the TLS) with two excitations, we could just take the square of the single excitation propagator, which, in our model, would lead to double excitations of the bosonic quantum dot. As already noted, the two-excitation Green's functions which we use have only one time dependence, so that the particles (photons (bosons) and the two fermions corresponding to the TLS in the ground and excited state, respectively) are created and annihilated at the same times. This means that the second term on the r.h.s. of Eq. (3.52) can be interpreted as follows. A photon and an excited TLS are created at time t_i and propagate up to an intermediate time τ. At this time, the TLS emits an additional photon and goes to the ground state, until at time $\tilde{\tau} > \tau$ one photon is absorbed and the other one remains free. As all Green's functions in this series are retarded, at no point in time can double-excitation of the TLS take place. As a result, the few-photon nonlinearity emerges and induces complex correlations between the photons [95].

3.4 Properties of the Green's functions in the single-excitation sector

After having established the diagrammatic formulation of the theory in the single- and double-excitation case, we are now ready derive physical measurable quantities within this framework. Especially we calculate the spectral density of the TLS as well as the scattering matrix. This will also establish the connection of our framework to the other approaches discussed in Sec. 3.1. In Chap. 1, we have introduced the waveguide as a one-dimensional chain of length L with nearest-neighbor hopping, thus exhibiting a cosine-shaped dispersion relation $\epsilon(k) = -2t\cos(k)$. Although we employ the cosine-shaped dispersion relation in this section, we may also use other dispersion relations (see the discussion in Chap. 1). Specifically, we will also consider a linear dispersion relation with group velocity v, i.e., $\epsilon_\mu(k) = \mu v k$, which is, as already discussed, a good approximation for photons in the center of the cosine band. Furthermore, we go back to a continuum description replacing sums by integrals so the one-excitation self energy reads

$$\begin{aligned} {}_1\Sigma(\omega) =& U^2 \int \frac{\mathrm{d}k}{2\pi} \frac{1}{\omega + \Omega/2 - \epsilon(k) + i0} \\ =& U^2 \mathcal{P} \int \frac{\mathrm{d}k}{2\pi} \frac{1}{\omega + \Omega/2 - \epsilon(k)} \\ & - i\pi U^2 \int \frac{\mathrm{d}k}{2\pi} \sum_n \delta(k - k_n) \frac{1}{\partial\epsilon/\partial k}\bigg|_{k=k_n}, \end{aligned} \tag{3.53}$$

where $\mathcal{P}$ denotes the Cauchy principal value and the k_n are given by the roots of $\omega + \Omega/2 = \epsilon(k)$. If all these roots are real (this means that the energy is inside the photonic band), the principal value in Eq. (3.53) becomes zero. The second term can be identified as the density-of-states of the free waveguide $\nu(\omega)$ [3]. This gives

$${}_1\Sigma(\omega) = -i\pi U^2 \nu(\omega). \tag{3.54}$$

[3] This follows from the continuum definition of the density of states as a integral over allowed modes $\nu(\omega) = intdk\delta(\omega - \epsilon(k))$ followed by an application of the rule $\delta(f(x)) = \sum_l \frac{1}{f'(x_l)}\delta(x - x_l)$ where x_l denotes the zeros of $f(x)$

As a result, we find that the self-energy for the cosine dispersion as

$$ {}_1\Sigma_{\cos}(\omega,\Omega) = \frac{U^2}{\omega+\Omega/2+i\delta-2t}\sqrt{\frac{\omega+\Omega/2+i\delta-2t}{\omega+\Omega/2+i\delta+2t}}, \tag{3.55} $$

and for the linear dispersion as

$$ {}_1\Sigma_{\mathrm{lin}}(\omega) = -i\frac{U^2}{v}. \tag{3.56} $$

In the case of linear dispersion, the frequency-independent density-of-states leads to a frequency-independent self-energy. The self-energy of the cosine band exhibits a more complicated structure, it is purely imaginary when ω lies inside of the band and purely real when ω is outside the band. Note that the given representation of the self-energy is chosen in such a way that the square-root is evaluated at the correct side of the branch cut. Furthermore we might also add that an ω-independent self-energy is typical for a system which is Markovian. In the opposite case of an explicit ω-dependence the system is non-Markovian which means that it exhibits a memory [94].

With these two self-energies, we are able to compute the spectral density of the TLS (which can be interpreted as a measure for the distribution of states) in the single-excitation case as

$$ {}_1A(\omega) = -\frac{1}{\pi}\mathrm{Im}\left[{}_1G_{\mathrm{e}}(\omega)\right]. \tag{3.57} $$

In Fig. 3.1, we depict the spectral density for both dispersion relations. The spectral density for the linear dispersion relation is a simple Lorentzian with width U^2/v. In the case of the

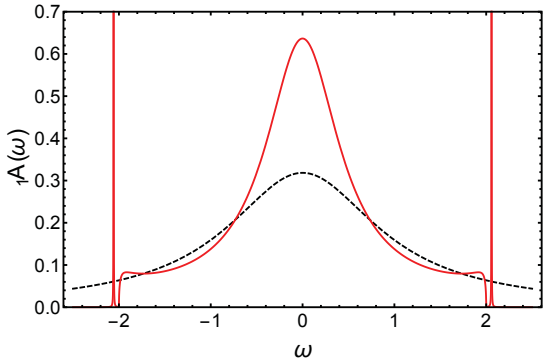

Figure 3.1: *Spectral density of the TLS with $\Omega = 0$, $U = 1$, $v = 1$ and $t = 1$ for the linear (black, dashed) and cosine (red) dispersion relation. ω is measured in units of v (t) for the linear (cosine) dispersion relation and the spectral density in units of v^{-1} (t^{-1}). The spectral density of the cosine band clearly displays the band edges and features spectrally ultra-sharp bound states in the band gaps on either side of the band (when plotting the spectral density for the cosine band, we have introduced an artificial broadening $\delta = 10^{-4}$ in order to enhance the visibility of the bound states). By contrast, the spectral density for the linear dispersion relation corresponds to a simple Lorentzian.*

cosine dispersion, we clearly observe the frequency span of the band. In addition, we observe two sharp spectral lines in the band gaps on either side of the band that correspond to two atom-photon bound states [73, 80, 114]. The finite width of the peaks corresponding to the APBs is due to a small but finite *delta* for a better visibility. Because this are eigenstates of the system in limit $\delta \to$ they should be imagined as infinitely sharp. As discussed in 2.5 the knowledge of the Green's functions enables us to compute the scattering matrix, where we have obtained the transition matrix (T-matrix) via the LSZ reduction formula

$$S_{k,p} = \delta_{k,p} + i2\pi\delta\left(\epsilon(k) - \epsilon(p)\right) T_{k,p}, \tag{3.58}$$

with

$$iT_{k,p} = -iG_0^{-1}(k)G(k,p)G_0^{-1}(p)\Big|_{os}. \tag{3.59}$$

In this expression, $G_0(k)$ and $G(k,p)$ denote, respectively, the free and the full, time-ordered Green's function. Further, the subscript *os* indicates again that the expression is taken on-shell, i.e., the scattering is elastic (or alternatively $\omega = \sum_i \epsilon(k_i) = \sum_f \epsilon(k_f)$, where the sums are over the initial and final momenta, respectively). This formulation resembles strongly results from electronic transport theory [96]. Using Eqs. (3.31) and (3.30) for the free and for the full Green's function, respectively, and omitting the free propagating part yields

$$iT_{k,p} = -i\frac{U^2}{2\pi}{}_1G_{\mathrm{e}}(\omega)\Big|_{os}. \tag{3.60}$$

We now rewrite the energy-conserving δ-function that implements elastic scattering in terms of δ-functions with momentum arguments and the density-of-states of the free waveguide

$$\delta\left(\epsilon(k) - \epsilon(p)\right) = \pi\nu\left(\delta_{k,p} + \delta_{k,-p}\right), \tag{3.61}$$

Upon combining Eqs. (3.58) and (3.60) with Eq. (3.61) yields

$$S_{k,p} = (1 + r_k)\delta_{k,p} + r_k\delta_{k,-p}, \tag{3.62}$$

where the reflection amplitude r_k is given by

$$r_k = \frac{-i\pi\nu U^2}{\epsilon(k) - \Omega/2 + i\pi\nu U^2}. \tag{3.63}$$

3.62 clearly describes the elastic scattering of a photon at the TLS which is reflected with probability $|r_k|^2$ and transmitted with probability $|t_k|^2 = |1 + r_k|^2$. In order to compare our results with the results from earlier works [72, 97, 73], we perform a shift of the energy $\omega \to \omega - \Omega/2$. Explicitly, for the linear dispersion relation we obtain

$$r_k^{\mathrm{lin}} = \frac{-iU^2/v}{vk - \Omega + iU^2/v}, \tag{3.64}$$

while we obtain for the cosine dispersion relation

$$r_k^{\cos} = \frac{-iU^2}{2t|\sin(k)|}\frac{1}{-2t\cos(k) - \Omega + iU^2/2t|\sin(k)|}. \tag{3.65}$$

These expressions are in agreement with the results obtained in earlier works by way of Bethe-Ansatz and LSZ-techniques which means that our approach appears to be a valid alternative at least in the one-excitation sector [72, 97, 73].

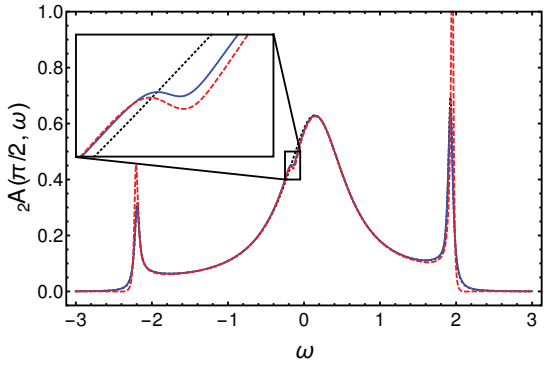

Figure 3.2: *Two-excitation spectral density ${}_2A(\pi/2,\omega)$ (obtained via the Green's function approach (solid blue) and DMRG (dashed red)) of the TLS with $\Omega = 0.3$ and $U = 1$ for a tight-binding waveguide with $L = 600$ discrete sites and cosine dispersion relation $\epsilon(k) = -2t\cos(k)$ $(t = 1)$, together with the corresponding single-excitation spectral density ${}_1A(\omega)$ (black dotted). ω is measured in units of t and the spectral density in units of t^{-1}. In ${}_2A(\pi/2,\omega)$, we clearly observe a Fano-resonance just below $\omega = 0$ (see text for details). This Fano-resonance is absent in the single-excitation spectral density of the TLS. When plotting the spectral densities, we have introduced an artificial broadening $\delta = 0.04$ in order to enhance the visibility of the Fano-resonance and to improve numerical convergence.*

3.5 Properties of the Green's functions in the two-excitation sector

We now proceed to analyze the Green's functions in the two-excitation case for the cosine and linear dispersion relations. It turns out that the existence of band edges and, related to that, the bound photon-atom states, have again a great influence on the structure of the perturbation series so we will discuss this feature of our model system in great detail.

3.5.1 Cosine dispersion relation - discrete waveguide

The full Green's function of the TLS is given by Eq. (3.33) in the form of a perturbation series. This perturbation series can be cast in the form of a T-Matrix equation, given by Eq. (3.37). For a discrete waveguide, we can solve this equations simply by (numerical) matrix inversion and we defer the discussion of the continuum limit of the cosine band to sections 3.5.2 (band center, approximately linear dispersion) and 3.5.3 (band edge, approximately quadratic dispersion). In analogy to the one-excitation case 3.4 we define the two-excitation spectral density of the TLS as

$$ {}_2A(k,\omega) = -\frac{1}{\pi}\mathrm{Im}\left[{}_2G_\mathrm{e}(k,k;\omega)\right]. \tag{3.66}$$

In Fig. 3.2, we depict the two-excitation spectral density of the TLS, ${}_2A(\pi/2,\omega)$, and compare with the corresponding single-excitations spectral density, ${}_1A(\omega)$ (see Fig. 3.2 for details of

the systems). While both spectral densities exhibit an overall similar behavior, we observe an additional small dip (highlighted by the inset) in the two-excitation spectral density which we attribute to a Fano resonance between the occupied (renormalized) TLS and the additional photon in the waveguide. A Fano resonance appears [98] when a broad continuum of states interacts with a single sharp mode. In our case, the renormalized TLS has a continuous frequency distribution whereas the additional photon can be thought of a delta like peak in frequency space. We would like to note that we have introduced an artificial broadening of $\delta = 0.04$ in order to enhance the visibility of the Fano resonance and to improve numerical convergence of the matrix inversion. As a result, the bound states are not as sharp as in Fig. 3.1 and the band edges are almost completely smeared out. We have confirmed the results of the matrix inversion displayed in Fig. 3.2 via computations of the spectral density by using an expansion in Chebyshev polynomials within the framework of the Density-Matrix-Renormalization-Group (DMRG) technique as described in [99] (This calculations where actually performed by P. Schmitteckert). In addition, we would like to stress that a similar Fano-resonance occurs in (analytically solvable) case of linear dispersion (see Sec. 3.5.2) so that we conclude that the occurrence of such a Fano-resonance between the occupied (renormalized) TLS and the additional photon in the waveguide is a generic feature of the few-photon nonlinearity in the n-photon-transport through a waveguide with embedded TLS for $n > 1$ and is furthermore no effect which is related to the existence of band edges in the dispersion relation. Although we have solved Eq. (3.37) for a cosine dispersion relation only, we would like to stress that our formalism is certainly not limited to this case (see the discussion in chapter 1). In fact, the T-matrix equation (3.37) is applicable to every possible dispersion relation that can be realized in a one-dimensional waveguide.

3.5.2 Linear dispersion relation

We now turn to our attention to the case of an (infinitely extended) linear dispersion relation $\epsilon_\mu(k) = \mu v k$ and thus ignore the effects of band edges, notably bound photon-atom states and slow light regimes. Just as in the single-excitation case, we transit to the continuum limit. Then, the self-energy of the renormalized TLS-Green's functions is

$$ {}_2\Sigma_{\mathrm{lin}}(k;\omega) = -i\frac{U^2}{v}, \tag{3.67} $$

which is the same expression as in the single-excitation sector. We rewrite the perturbation series as

$$ {}_2G_{\mathrm{e}}(k_f, k_i;\omega) = \sum_i {}_2G_{\mathrm{e}}^{(i)}(k_f, k_i;\omega). \tag{3.68} $$

Since the first two terms contain no internal integration there are no further work required

so we can concentrate on the third term which is given by

$$\begin{aligned}
&{}_2G_{\mathrm{e}}^{(3)}(k_f,k_i;\omega)\\
&\quad=\frac{U^4}{2\pi}\int\frac{\mathrm{d}k}{2\pi}\,{}_2G_{\mathrm{e}}^{\mathrm{r}}(k_i;\omega){}_2G_{\mathrm{w}}^{0}(k_i,k;\omega)\\
&\qquad\qquad\times{}_2G_{\mathrm{e}}^{\mathrm{r}}(k;\omega)\,{}_2G_{\mathrm{w}}^{0}(k,k_f;\omega)\\
&\qquad\qquad\times{}_2G_{\mathrm{e}}^{\mathrm{r}}(k_f;\omega),
\end{aligned}\tag{3.69}$$

Here the integral only extends over the three internal Green's functions. As all these Green's functions have single poles that are shifted into the upper half plane because we are only dealing with retarded quantities. We can now can now choose a contour of integration closed in the lower half plane (convergence is assured because the integrand goes as k^{-3} for big enough k) which gives us as according to Cauchy's theorem that the integral and hence the entire third term in the perturbation series vanishes. Because terms of order higher will have essentially have the same structure, containing the same type of integrals, this means also that, in the case of a linear dispersion, the full TLS-Green's function is completely determined by the first two terms

$$\begin{aligned}
&{}_2G_{\mathrm{e}}(k_f,k_i;\omega)\\
&=\,{}_2G_{\mathrm{e}}^{\mathrm{r}}(k_i;\omega)\,\delta_{k_i,k_f}\\
&\quad+\frac{U^2}{2\pi}\,{}_2G_{\mathrm{e}}^{\mathrm{r}}(k_i;\omega)\,{}_2G_{\mathrm{w}}^{0}(k_f,k_i;\omega)\,{}_2G_{\mathrm{e}}^{\mathrm{r}}(k_f;\omega).
\end{aligned}\tag{3.70}$$

We are now in a position to provide a physical explanation for this termination of the perturbation series for linear dispersion relations after the first two terms by inspecting the first vanishing Feynman diagram (i.e., the third diagram on the r.h.s. of Eq. (3.52)) in the time domain

$${}_2G_{\mathrm{e}}^{(3)}(k_f,k_i;\omega)=$$ 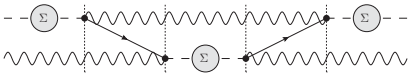

(3.71)

The particle of interest is the (intermediary) upper photon, which is emitted and reabsorbed by the TLS. During the time that the upper photon "lives", the initial photon propagates and eventually gets absorbed. After a while, the photon is re-emitted and propagates further for a certain time. The entire process occupies a certain time $\tau > 0$. During this time, the upper (intermediate) photon moves a certain distance due to the fixed group velocity $v > 0$ of the linear dispersion and the absence of back-scattering mechanisms. This means that the photon has moved away from the TLS and actually cannot be reabsorbed, hence the diagram vanishes. We would like to note that this is a special property of the linear dispersion relation and does not hold for general dispersions relations, notably not near band edges and/or waveguide cut-off frequencies, i.e., in the vicinity of slow-light regimes where the photon may stay in the vicinity of the TLS and may get reabsorbed.

We have calculated the two-excitation spectral density according to Eq. (3.66) and depict the results together with the single-excitation spectral density in Fig. 3.3. Similar to the numerical calculations for the cosine dispersion relation we, again, find again a Fano resonance located this time at $\omega_F = 2vk - \Omega/2$, which is much more pronounced than in the cosine-shaped dispersion

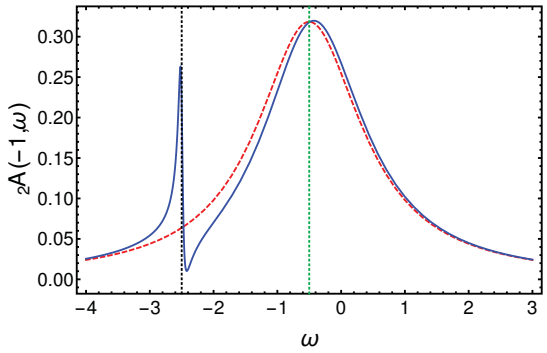

Figure 3.3: *Two-excitation spectral density* ${}_2A(-1,\omega)$ *(solid blue) of the TLS with* $\Omega = 1$ *and* $U = 1$ *for a waveguide with linear dispersion relation* $\epsilon(k) = \mu v k$ *and* $v = 1$ *considered in the continuum limit, together with the corresponding single-excitation spectral density* ${}_1A(\omega)$ *(red dashed).* ω *is measured in units of* v *and the spectral density in units of* v^{-1}*. We have shifted the single-excitation spectral density* ${}_1A(\omega)$ *by* $\omega \to \omega - vk$*, so that the maxima of both plots overlap. The green dotted line is at* $vk + \Omega/2$ *and indicates the maximum of* ${}_1A(\omega)$*. In* ${}_2A(-1,\omega)$*, we clearly observe a Fano-resonance at* $\omega = 2vk - \Omega/2$ *(black-dotted line) which is more pronounced than for the case of tight-binding waveguide in Fig. 3.2. As in the case of the tight-binding waveguide, this Fano-resonance is absent in the single-excitation spectral density of the TLS. When plotting the spectral densities, we have introduced the same artificial broadening* $\delta = 0.04$ *as in the case of the tight-binding waveguide in order to enhance the visibility of the Fano-resonance and make the graph comparable to that in Fig. 3.2.*

case. Comparing both dispersion relations, the Fano resonance appears in two different ways: In the linear case it emerges from the second term in the perturbation series ${}_2G_{\mathrm{e}}^{(2)}(k_f, k_i; \omega)$ which consists of an internal free waveguide Green's function ${}_2G_{\mathrm{w}}^{0}(k_i, k_f; \omega)$ of the form $(\omega - \omega_F + i\delta)^{-1}$. The Fano resonance is therefore the consequence of a first order pole, regularized by a finite imaginary factor $i\delta$. This means it should be considered as infinitely sharp for $\delta \to 0$.This means that the spectral density can assume negative values which looks suspicious on first sight. However, one has to take into account that we are not considering the spectral density of the full system, but only the TLS subsystem. Therefore, a negative spectral density is acceptable and can be interpreted as sort of a gain mechanism where energy is taken from the photonic "bath" realized by the waveguide. This sort of behavior indicates effects such as photon bunching [100, 72, 95]. Moreover, we would like to point out that the Fano resonance is less pronounced in Fig. 3.2, although all energies (transition energy of the TLS, photon energy) are in the linear regime of the cosine band. We attribute this regularization to higher-order diagrams which are not present in the linear dispersion relation. In fact, the deeper reason behind the termination of the perturbation series for the linear dispersion is the separation of the photons on the Hamiltonian level into two kinds of photons (left- and right-moving ones). This changes the symmetry of the original Hamiltonian, i.e., the chirality is introduced as a new

good quantum number, and eventually leads to the special analytic structure of the Green's functions and, as a consequence, to the termination of the perturbation series [4]. Finally, we can now construct the two-excitation S-matrix by generalizing the LSZ formalism presented in Sec. 3.4. Explicitly, the two-excitation S-Matrix is given as

$$\begin{aligned} S_{k_i p_i, k_f p_f} =& \left(\delta_{k_i,k_f}\delta_{p_i,p_f} + \delta_{p_i,k_f}\delta_{k_i,p_f}\right) \\ &+ i2\pi\delta(E)\, T_{k_i p_i, k_f p_f}, \end{aligned} \tag{3.72}$$

where

$$\delta(E) = \delta(\epsilon(k_i) + \epsilon(p_i) - \epsilon(k_f) - \epsilon(p_f)) \tag{3.73}$$

ensures elastic scattering and the associated T-matrix is defined as

$$\begin{aligned} &iT_{k_i p_i, k_f p_f} \\ &\quad = -iG_0^{-1}(k_i, p_i)\, G(k_i, p_i; k_f, p_f)\, G_0^{-1}(k_f, p_f)\Big|_{os}. \end{aligned} \tag{3.74}$$

In this expression, $G_0(k,p)$ and $G(k,p;k',p')$ denote, respectively, the free and the full waveguide Green's function. With the help of Eq. (3.40), we explicitly find

$$iT_{k_i p_i, k_f p_f} = -i\frac{U^2}{2\pi}\, {}_2G_{\mathrm{e}}^{\mathrm{sym}}(k_i, p_i, k_f, p_f; \omega)\Big|_{os}, \tag{3.75}$$

where ${}_2G_{\mathrm{e}}^{\mathrm{sym}}(k_i, p_i, k_f, p_f; \omega)$ is defined by Eq. (3.41). In order to compare these results with results of earlier works, we again perform a frequency shift $\omega \to \omega - \Omega/2$. We now state the results for the S-Matrix. Because the corresponding calculations are quite lengthy we shift them to Appendix C and only state the results here

- $k_i^R p_i^R \to k_f^R p_f^R$

$$\begin{aligned} S^{RR,RR}_{k_i p_i, k_f p_f} =& t_{k_i} t_{p_i} \left(\delta_{k_i,k_f}\delta_{p_i,p_f} + \delta_{k_i,p_f}\delta_{p_i,k_f}\right) \\ &+ S^{2,\mathrm{P.V.}}_{k_i p_i, k_f p_f}, \end{aligned} \tag{3.76}$$

- $k_i^R p_i^R \to k_f^R p_f^L$

$$\begin{aligned} S^{RR,RL}_{k_i p_i, k_f p_f} =& t_{k_i} r_{p_i} \delta_{k_i,k_f}\delta_{p_i,-p_f} + r_{k_i} t_{p_i} \delta_{k_i,-p_f}\delta_{p_i,k_f} \\ &+ S^{2,\mathrm{P.V.}}_{k_i p_i, k_f p_f}, \end{aligned} \tag{3.77}$$

- $k_i^R p_i^R \to k_f^L p_f^L$

$$\begin{aligned} S^{RR,LL}_{k_i p_i, k_f p_f} =& r_{k_i} r_{p_i} \left(\delta_{k_i,-k_f}\delta_{p_i,-p_f} + \delta_{k_i,-p_f}\delta_{p_i,-k_f}\right) \\ &+ S^{2,\mathrm{P.V.}}_{k_i p_i, k_f p_f}. \end{aligned} \tag{3.78}$$

[4] This also explains why the Bethe Ansatz is successful in this case: The additional conserved integrals of motion related to the additional symmetry make the system fully integrable

In these expressions, the superscript of the momenta indicates the chirality, r_k is the single-excitation reflection amplitude (c.f. Eq. (3.64)), $t_k = 1 + r_k$ is the single-excitation transmission amplitude and $S^{2,\mathrm{P.V.}}_{k_i p_i, k_f p_f}$ is given by

$$\begin{aligned} S^{2,\mathrm{P.V.}}_{k_i p_i, k_f p_f} =& \frac{iU^4}{\pi v} \delta_{k_i + p_i, k_f + p_f} \\ & \times \frac{\left(k_i + p_i - 2\Omega + iU^2/v\right)}{(vp_i - \Omega + iU^2/v)(vk_i - \Omega + iU^2/v)} \\ & \times \frac{1}{(vp_f - \Omega + iU^2/v)(vk_f - \Omega + iU^2/v)}. \end{aligned} \tag{3.79}$$

Again our formulas are in accordance with the results obtained by other techniques in earlier works, which proves the validity of our approach also in the two excitation sector [100, 72, 73]. Furthermore we can also give a quite clear explanation of the term $S^{2,\mathrm{P.V.}}_{k_i p_i, k_f p_f}$. In the first place, this term appears by replacing the free waveguide-Green's function in ${}_2G^{(2)}_{\mathrm{e}}$ by the Dirac identity

$$\frac{1}{\omega - vk - vp + i0} = \mathcal{P}\frac{1}{\omega - vk - vp} - i\pi\delta\left(\omega - vk - vp\right). \tag{3.80}$$

The two terms in the Dirac identity can be interpreted as follows. The imaginary part that is proportional to a δ-function corresponds to long-time, real processes, because the δ-function sets the particles on-shell which can be interpreted as composition of single particle scattering processes. The real part that contains the principal value, however, does not place a constraint on the momenta. The momenta can be chosen freely and are only restricted by energy conservation. Therefore, this term corresponds to short times, which are on the scale of the Heisenberg uncertainty principle, i.e., they correspond to *virtual processes* and are also hallmarks of the photon-photon interaction because they are responsible for photon (anti-) bunching.

3.5.3 Band edge effects

Finally, we address the case of band edges by following the same line of reasoning as in section 3.5.2. Because we are only interested in band edge effects, we can perform a Taylor expansion in the dispersion relation around $k = \pm Pi$ which yields a quadratic dispersion relations $\epsilon(k) = tk^2$ with $t > 0$. In this case, the self-energy is given by

$${}_2\Sigma_{\mathrm{qu}}(k;\omega) = -i\frac{\pi U^2}{\sqrt{t(\omega - tk^2 + i0)}}, \tag{3.81}$$

where we scaled out the factor $\Omega/2$. The first two terms of the perturbation series given by Eq. (3.68) can again be computed straightforwardly, but the third term (and all higher-order terms) exhibit different characteristics. First of all, the quadratic dispersion relation induces poles on both sides of the complex half-plane, which means that the integral over internal momenta is not vanishing, hence ${}_2G^{(3)}_{\mathrm{e}}(k_f, k_i; \omega)$ is finite. This was expected, since the quadratic dispersion relation exhibits a state where the group velocity $v_g = 0$, which means that an emitted photon can be reabsorbed by the TLS after a certain amount of time (c.f.

discussion in section 3.5.2). Secondly, the self-energy ${}_2\Sigma_{\mathrm{qu}}(k;\omega)$ leads to two branch cuts, one in each half space of the complex plane. These branch cuts represent major obstacles in the integration over the internal momenta and we have been unable to find a closed form-solution for ${}_2G_{\mathrm{e}}^{(3)}(k_f,k_i;\omega)$. From a more physical point of view, however, we expect that the higher-order processes encapsulate the effect of interaction-induced radiation trapping (IIRT) [80, 114], because this phenomenon is absent in the linear case and therefore have to be a feature of the additional diagrams present here. It describes the excitation of the atom-photon bound state by a two-photon pulse as the result of a nonlinear process (or in this case equivalently the photon-photon interaction induced by Pauli's principle). This expectation can be motivated by the diagrammatic form of ${}_2G_{\mathrm{e}}^{(3)}(k_f,k_i;\omega)$,

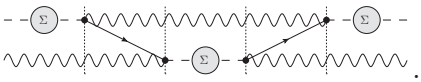

In the top line the TLS emits a photon, which is reabsorbed at a later time. This is exactly the behavior one would expect from the atom-photon bound state, since the radiation cannot leave the the surrounding of TLS yielding a new kind eigenstate of the system which is of composite light-matter nature. The prototypical process of IIRT includes two initial photons, which are transformed into an atom-photon bound state and a photon with a different momentum. Energetically, this process is described by

$$\omega = \epsilon(k_i) + \epsilon(p_i) = \omega_{\mathrm{BS}} + \epsilon(k_f), \tag{3.82}$$

where k_i and p_i are the momenta of the initial photons, k_f is the momentum of the final photon, ω is the total energy and ω_{BS} is the energy of the bound atom-photon state, which can be found by solving the equation

$$\omega_{\mathrm{BS}} - \Omega + i\frac{U^2\pi}{\sqrt{t\omega_{\mathrm{BS}}}} = 0. \tag{3.83}$$

In fact, setting ${}_2G_{\mathrm{e}}^{(3)}(k_f,k_i;\omega)$ on-shell (thus making it proportional to a scattering matrix element) and computing the integration over the internal momenta numerically yields a sharp peak at precisely the momenta k_f which fulfill $\omega = \omega_{\mathrm{BS}} + \epsilon(k_f)$ (cf. Fig. 3.4). This indicates that ${}_2G_{\mathrm{e}}^{(3)}(k_f,k_i;\omega)$ (together with the higher-order processes) describes indeed the physics behind the IIRT. Moreover, treating the sharp peak as a pole (which is motivated by the fact that the width of the resonance scales with the small imaginary part $i\delta$) enables us to compute the residue of the resonance via

$$\mathrm{Res}\left[{}_2G_{\mathrm{e}}^{(3)},k_0\right] = \frac{1}{2\pi i}\oint_C \mathrm{d}z\, {}_2G_{\mathrm{e}}^{(3)}(z,k_i;\omega)\Big|_{os}, \tag{3.84}$$

where k_0 is the solution of Eq. (3.82), the subscript *os* indicates that the expression is taken on-shell and the contour C is a circle centered at k_0 with radius λ such that no other energy eigenvalue in the complex plane is enclosed. We have plotted the residue in Fig. 3.5, together with the conditions that the two initial photons are on resonance with the TLS individually ($\Omega = \epsilon(k_i)$) and collectively ($\Omega = \omega = 2\epsilon(k_i)$). We can see here that the strength of the pole

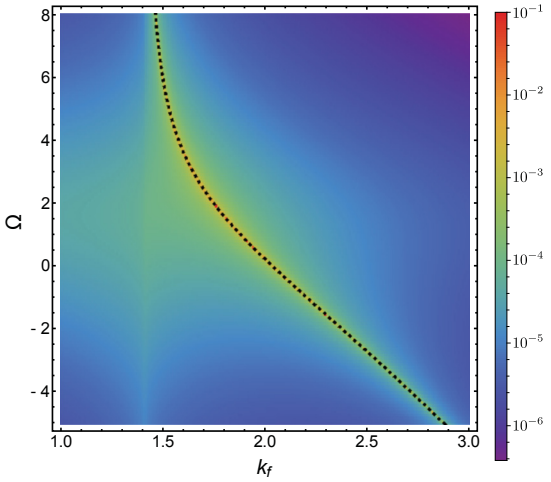

Figure 3.4: *Logarithmic plot of* $\left|{}_2G_{\mathrm{e}}^{(3)}(k_f, k_i; \omega)\right|$ *(in units of* t^{-1}*) with* $k_i = p_i = 1$, $t = 1$, $U = 1$, $\omega = \epsilon(k_1) + \epsilon(k_2)$ *and* Ω *is measured in units of* t*. We have added a small imaginary part* $\delta = 10^{-3}$ *to* ω *for an artificial broadening of the resonance. The black dotted line represents the solution of* $\omega = \omega_{\mathrm{BS}} + \epsilon(k_f)$*. The resonance approaches* $k_f \to \sqrt{2}$ *for large values of* Ω*, since the bound state energy* $\omega_{BS} \to 0$ *in this case.*

is sensitive to the TLS being on resonance with the collective photonic excitation, rather than with the individual ones. This is another indicator that IIRT emerges as the result of the nonlinear behavior of the TLS in the presence of two or more photons. Furthermore, this result shows that an analytic solution for ${}_2G_{\mathrm{e}}^{(3)}(k_f, k_i; \omega)$ is still highly desirable as this would provide further insights into the physics of IIRT.

Finally, we would like to conclude this section by recalling the physical interpretation of each term in the perturbation series of ${}_2G_{\mathrm{e}}(k_f, k_i; \omega)$: The first term describes the single-photon scattering and does not induce correlations between the two photons. The second term gives rise to photon bunching and is always finite, independent of the dispersion relation. The third term and all higher-order terms are nontrivial, since they include integrations over internal momenta. In the case of a linear dispersion relation their contribution vanishes. Conversely, these higher-order terms become particularly relevant for frequencies near band edges and/or waveguide cut-offs and lead to the effect of IIRT.

3.6 Conclusion

In this section we showed how to set up a Feynman diagram approach to WQED, using a path integral approach. After deriving the Feynman rules, we set up the necessary equations to determine the full Green's function in the one- as well as in the two excitation sector. It permits for novel physical interpretation of the atom-photon bound states as well as for the related phenomenon of IIRT. We also found a Fano resonance in the two excitation sector

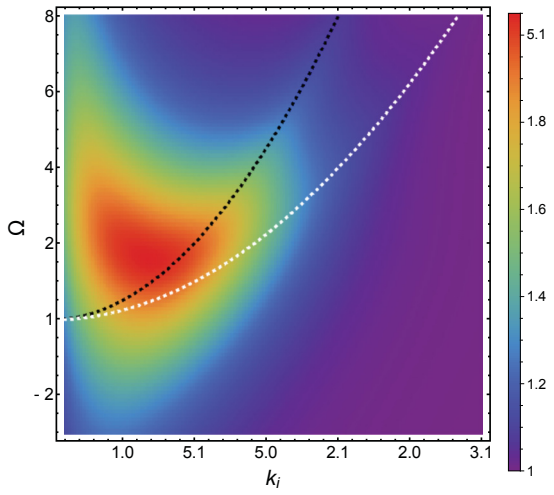

Figure 3.5: *Plot of* $\left|Res\left[{}_2G_e^{(3)}, k_0\right]\right|$ *(in units of* t^{-1}*) for two identical initial photons* $\omega = 2\epsilon(k_i)$*,* $U = 1$*,* $t = 1$*,* $\delta = 10^{-4}$*,* $\lambda = 10^{-6}$ *and* Ω *is measured in units of* t*. The black and white lines represent the parabolas* $\Omega = 2\epsilon(k_i)$ *and* $\Omega = \epsilon(k_i)$*, respectively.*

that was unknown previously and which serves as a signature of the few-photon nonlinearity inherent in our systems. We solved the system exactly for a linear dispersion and showed that only a restricted class of diagram is necessary to describe the system completely in this case whereas in the cosine case the number of relevant diagrams is of infinite order.

4 THE TWO SCATTERER PROBLEM AND FLUCTUATING FORCES

We discuss the exact solution of two two-level-systems coupled to a 1-D waveguide, using a Feynman diagram approach. Furthermore we give a complete analysis of the energy spectrum of the problem. We also make a connection to fluctuation forces, especially we discuss the occurrence of Förster Resonance Energy Transfer (FRET) in this system.

4.1 Introduction

In this section we are interested in what happens if we couple an additional two-level-system (TLS) to our waveguide. The reason is twofold, on the one hand it is a very natural generalization of the system with just one TLS and we expect that the techniques developed so far are well suited to apply also to this slightly more difficult problem. On the other hand we also expect to find interesting new physics on our way. The reason is that the two TLS should start to interact. Specifically it will turn out that we have new kinds of communication channels mediated by the different kind of eigenmodes of the system, which are quite different from usual photon scattering. For example, due to the level repulsion present between the different APS one can expect to find novel possibilities to manipulate the system. We also try to gain some understanding of the fluctuation forces which are present in the system due to the photonic waveguide. This forces turn out to be of the Förster type. We classify the effects of curvature and band edges on this force, which turn out to be dramatic. As a last point we investigate the dynamics that are induced by a totally different kind of eigenmodes which we call cavity modes or bound states in continuum. They result from the possibility of radiation trapping between the two TLS. Some related work was already done in the context of this model (and slight generalizations of it) but most of that was concerned with the properties of the system for a linear dispersion only. Some topics which where investigated there were photon-photon correlation [102] and qubit entanglement (a topic we will also discuss to some extent in 4.6.5) [103]. [106] also is investigating our model system with an emphasis on fluctuation forces but

only in first order perturbation theory, whereas we will solve the system exactly. Their results are included as certain limits in our calculation.

4.2 The model

We consider the following system which consists of a one dimensional waveguide with dispersion relation $\epsilon(k)$ and the two TLS, which again can represent a whole bunch of physical realizations (QD, superconducting qubits etc.). The level splittings are denoted by Ω_1 and Ω_2 the corresponding strengths are given by U_1 and U_2.

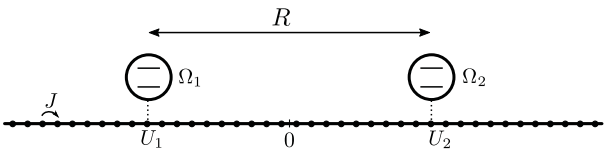

Figure 4.1: *The System*

The Hamiltonian of the system is given by

$$H = \sum_k \epsilon(k) a_k^\dagger a_k + \sum_{j=1}^{2} \frac{\Omega^{\{j\}}}{2} \sigma_z^{\{j\}} + \sum_{k,j=1}^{2} \left[U_j e^{i s_j k R/2} a_k^\dagger \sigma_-^{\{j\}} + h.c \right] \tag{4.1}$$

where the subscript $j \in \{1, 2\}$ discerns the two TLS and $s_j = (-1)^j$ takes care of the proper sign of the $R-$dependent phase factors. The above Hamiltonian can be straightforwardly obtained by a FT of the corresponding x-space counterpart which can be written down intuitively (Note that R is measured in units of the lattice constant a, which we set to 1 for convenience).

For the following diagrammatic approach to the problem it is again convenient to change to a slave fermion description as we did before. We obtain

$$H = \sum_k \epsilon(k) a_k^\dagger a_k + \sum_{j=1}^{2} \frac{\Omega^{\{j\}}}{2} \left[f^{\dagger\{j\}} f^{\{j\}} - g^{\dagger\{j\}} g^{\{j\}} \right] \tag{4.2}$$

$$+ \sum_{k,j=1}^{2} \left[U_j e^{i s_j k R/2} a_k^\dagger f^{\{j\}} g^{\dagger\{j\}} + h.c \right] \tag{4.3}$$

We consider again two kind of dispersion relations, linear $\epsilon(k) = vk$ and cosine shaped $\epsilon(k) = 2J\cos(k)$ which will yield qualitatively different results.

4.3 Diagramatic solution

In the diagrammatics of this chapter we suppress the ground state propagators which we used extensively in the last chapter. The reason for this is that we only perform calculation in the single excitation sector and so don't have to take care of a proper treatment of the Pauli exclusion principle.

4.3.1 Preliminaries & Notations

First of all we want to introduce some changes in notation, beginning with some basic Green's functions which describe the two isolated TLS and the waveguide (this one is exactly the same as in the one scatterer case). Note that we drop the excitation number index in front of the Green's functions because we are concerned with the the single-excitation sector only.

$$G_j^0(\omega) = \frac{1}{\omega - \Omega_j + i\delta} \tag{4.4}$$

$$G_w^0(\omega, k) = \frac{1}{\omega - \epsilon(k) + i\delta} \tag{4.5}$$

Furthermore we need the same one-scatterer self-energy as in the last chapter

$$\Sigma(\omega) = \frac{1}{2\pi} \int \frac{1}{\omega - \epsilon(k) + i\delta} \mathrm{d}k \tag{4.6}$$

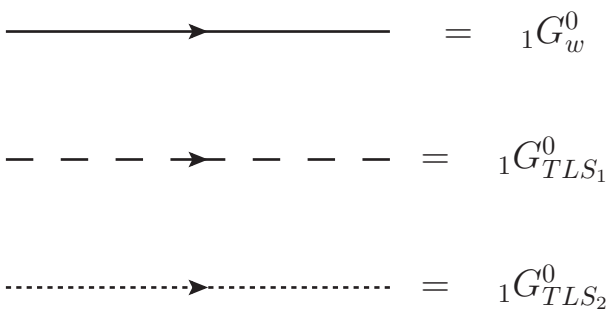

Figure 4.2: *Free Green's functions*

For the dispersion relations of interest, they are given by (see section 3.3.1)

$$\Sigma_j = \begin{cases} -i\pi \frac{1}{v} & \text{if } \epsilon(k) = \mu v k \\ -\frac{1}{J} \frac{1}{\sqrt{(\omega/J)^2 - 4}} & \text{if } \epsilon(k) = 2J\cos(k) \end{cases} \tag{4.7}$$

the full Green's functions consisting of scattering on only one impurity are then given by following self consistent equations (see section 3.4)

$$G_j = G_j^0 + U_j^2 G_j^0 \Sigma G_1$$
$$G_{w,j} = G_w^0 + U_j^2 G_w^0 \Sigma G_w \tag{4.8}$$

Note that these expressions are exactly the same then in the last chapter, except that we

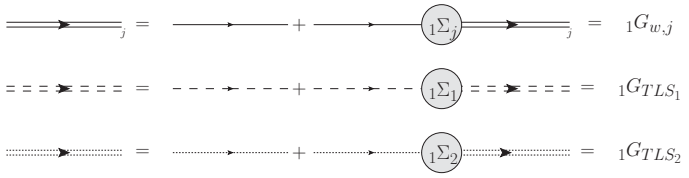

Figure 4.3: *Free Greensfunctions*

added an additional index j that labels the different TLS. We can therefore interpret them as the Green's functions of the system in the absence of any interaction between two scatterers or equivalently as the Green's functions when the two TLS have an infinite distance: $R = \infty$.

4.3.2 The full Green's function

With this ingredients we can go on to construct the full Green's functions of the problem. We start by letting the the excitation travel one time from the first to the second TLS. This process is mediated by a virtual photon. Afterwards the excitation is reemitted and comes back to the first scatterer. We use calligraphic letters to denote the full Green's functions. Furthermore the subscripts 11/22 denote full two scatterer Green's functions which describes the propagation that starts and ends at the same scatterer ($1 \to 1$ or $2 \to 2$) whereas subscripts 12/21 describe propagation between different TLS ($1 \to 2$ or $2 \to 1$).

$$\begin{aligned}
&\mathcal{G}_{11} = \\
&G_1 + \\
&|U_1 U_2|^2 G_1 \left[\int_{-y}^{y} G_w^0 e^{-ikR} \mathrm{d}k\right] G_2 \left[\int_{-y}^{y} G_w^0 e^{ikR} \mathrm{d}k\right] G_1 \\
&+ ....
\end{aligned} \tag{4.9}$$

were ... consists of all terms with additional self energy insertions and y corresponds to the edge of the Brillouin Zone (π for the cosine dispersion and ∞ for the linear dispersion).
Note that we already included the fully one scatterer renormalized Green's functions 4.8 instead of the bare G_j^0, which makes sense because we know already how to tackle this part of the problem from the last section. There are also no problems stemming from double counting as

one can see by expanding the whole expression up to $\mathcal{O}(U^6)$. Taking ω in units of J and setting $J = 1$ for the cosine dispersion, the integrals can be calculated analytically and are given by

$$\Gamma(R) = \int_{-y}^{y} G_w^0(k) e^{(-1)^j ikR} \mathrm{d}k = \left\{ \begin{array}{ll} \frac{i}{v} e^{i(\omega/v)R} \Theta((-1)^j \mu) & \text{if } \epsilon(k) = \mu v k \\ \frac{1}{2^R} \frac{(\omega - \mathrm{sign}(\omega)\sqrt{\omega^2-4})^R}{\sqrt{\omega^2-4}} & \text{if } \epsilon(k) = 2J\cos(k) \end{array} \right\} \tag{4.10}$$

It is clear, that in the case of the cosine band one has to be careful how to choose the correct branch of the square root which is implicitly done in the above equations. Note that we can interpret $\Gamma(R)$ heuristically as the distance-dependent and momentum averaged probability that a photon travels from the first to the second TLS. It is again very useful to employ a Feynman diagram representation to visualize the perturbation series

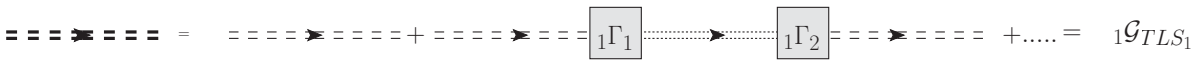

Figure 4.4: *Pertubation Series for $\mathcal{G}_{11}$, fat lines are full Green's functions*

The first describes the part of the TLS Green's function which is not affected by the second scatterer.The second summarizes all contributions where the excitation travels exactly once to the second TLS interacts an arbitrary numbers of times and comes back to the first scatterer. The terms hidden in the "..." describe the same kind of physics with the difference that the journey of the excitation contains $2, 3...n$ visits to the second TLS.
Keeping this in mind, it is easy to deduce the following self consistent equation

$$\mathcal{G}_{11} = G_1 + |U_1 U_2|^2 \Gamma(R) G_1 \Gamma(R) G_2 \mathcal{G}_{11} \tag{4.11}$$

This means that the effect of the second TLS onto the Green's function of the first TLS is mediated by photons that propagate from TLS one to TLS two, are reflected at the second TLS and come back to the first TLS. During this process they accumulate a $R-$dependent (complex valued) phase, whose absolute value is the same on the forward and backward way due to time reversal symmetry, yielding a factor $\Gamma^2(R)$.
The corresponding diagrammatic representation looks as follows

We also want to mention that everything we have done so far could also be obtained from scratch by using a similar path integral approach then in chapter 3. Especially the above Green's function could directly be read of from the effective action obtained by first integrating over all

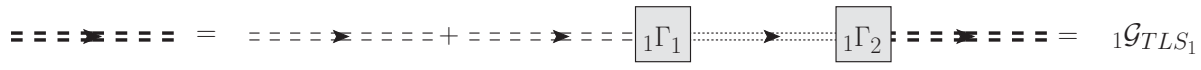

Figure 4.5: *Self consistent diagrammatic representation of $\mathcal{G}_{11}$,fat lines are full Green's functions*

bosonic degrees of freedom (which is equivalent as taking an average over the photon "bath"). It can be shown that this effective action contains an additional part $\sim U^2\Gamma(R)(\sigma_1^-\sigma_2^+ + h.c.)$ which shows that the induced interaction is of the flip-flop type (which is exactly the kind of interaction we observe in the diagrams, one TLS goes to the ground state whereas the other gets excited and vice-versa) well known from nuclear magnetic resonance (NMR) physics [105]. Going back to our actual problem, we can furthermore observe two important limits.

$$\lim_{R\to\infty}\Gamma(R) = 0 \tag{4.12}$$

$$\lim_{R\to 0}\Gamma(R) = \Sigma(\omega) \tag{4.13}$$

The first case corresponds to the limiting cases of a single two level system (in the limit as R goes to infinity, the influence of the second TLS vanishes and we have two independent scatterers).
The second limit leads, in the one excitation subspace, to a three level system with V-level structure [113] because the second TLS degenerates (for $R \to 0$) simply in an additional energy level which can be occupied if an excitation decays into the photonic waveguide and gets reabsorbed by the second energy level.

It is now straightforward to construct all other Green's functions by adding appropriate additional external legs

$$\mathcal{G}_{22} = G_2 + |U_2|^2\Gamma[R]^2 G_2\mathcal{G}_{11}G_2 \tag{4.14}$$

and the photon Green's function is given by

$$\begin{aligned}\mathcal{G}_w =& G_w + |U_1|^2 G_w\mathcal{G}_{11}G_w + \\ & \{TLS_1 \leftrightarrow TLS_2,\ U_1 \leftrightarrow U_2\}\end{aligned} \tag{4.15}$$

Also processes corresponding to emission (this quite similar to the case of one TLS, see A) of a photon can be described in the following way:

$$\mathcal{G}_{e,j} = U_j^* e^{-is(j)kR}\mathcal{G}_{jj}G_w \tag{4.16}$$

Due to time reversal symmetry, the complementary process of the absorption of a photon is given by

$\mathcal{G}_{a,j}(\omega) = \mathcal{G}^*_{e,j}(-\omega)$
The last type of correlation functions we encounter are the ones which describe propagation between different TLS ($i \neq j$)

$$\mathcal{G}_{ij} = \Gamma[R] U_i U_j^* \mathcal{G}_{ii} G_j \tag{4.17}$$

We may again note that, by time reversal symmetry the connection $\mathcal{G}_{21}(\omega) = \mathcal{G}^*_{12}(-\omega)$ holds We now can summarize all the results of this section with the help of a matrix valued Green's function:

$$\hat{\mathcal{G}} = \begin{pmatrix} \mathcal{G}_{11} & \mathcal{G}_{12} & \mathcal{G}_{e1} \\ \mathcal{G}_{21} & \mathcal{G}_{22} & \mathcal{G}_{e2} \\ \mathcal{G}_{a_1} & \mathcal{G}_{a_2} & \mathcal{G}_w \end{pmatrix} \tag{4.18}$$

or in a written out form

$$\begin{aligned} \hat{\mathcal{G}} =& \frac{1}{1 - |U_1 U_2|^2 \Gamma[R]^2 G_1 G_2} \times \\ & \begin{pmatrix} G_1 & U_1^* U_2 \Gamma[R] G_1 G_2 & U_1^* e^{ikR} G_1 G_w^i \\ U_1 U_2^* \Gamma(R) G_1 G_2 & G_2 & U_2^* e^{-ikR} G_2 G_w^i \\ U_1 e^{-ikR} G_1 G_w^f & U_2 e^{ikR} G_2 G_w^f & |U_1|^2 G_w^i G_1 G_w^f \end{pmatrix} \end{aligned} \tag{4.19}$$

At this point we can make a very general and important observation, namely that all the dependence of the energy eigenvalues on the distance R is stored in the common prefactor.This follows from the general fact that energy eigenvalues are given by the poles of the Green's function and also because $\Gamma(R)$ contains no poles whose values depend on the distance. The modes which are contained inside the matrix correspond to energy eigenvalues that are related to the single TLS problem. Furthermore we observe that the prefactor is independent of k, which means that the energies of the scattering states are not influenced by the presence of the second scatterer. Putting this into more mathematical language, we may say that

$$\hat{\mathcal{G}} = \frac{1}{Q(\omega, R)} \hat{M}(\omega, k, R) \tag{4.20}$$

where $M(\omega, k, R)$ is a matrix which is analytic in the variable R and $\frac{1}{Q(\omega,R)}$ is meromorphic in ω with simple poles for any finite R. It is important to notice that in the limit of $R \to \infty$ the system becomes two independent TLS whose eigenvalues might be degenerate so the poles are not simple anymore in this case.

4.4 Analysis of eigenvalues

4.4.1 Cosine dispersion relation

As we have seen in the previous paragraph, the eigenvalues which are new compared with the case of two decoupled TLS are corresponding to the zeros of the denominator of the prefactor

in equation (4.19).In what follows we concentrate on the case of identical atoms $U_1 = U_2 = U$, $\Omega_1 = \Omega_2 = \Omega$ (we shortly discuss the case of different atoms at the end of this section). The equation which determines the eigenvalues looks as follows:

$$Q(\omega, R) = f_+(\omega, R) f_-(\omega, R) = (\omega - \Omega - U^2\Sigma(\omega))^2 - U^4\Gamma^2(R, \omega) = 0 \tag{4.21}$$

Here $f_\pm(\omega, R) = (\omega - \Omega - U^2[\Sigma(\omega) \pm \Gamma(\omega, R)])$. Using the expressions for $\Sigma(\omega)$ and $\Gamma(\omega, R)$ (4.7,4.10), we find in the case of a cosine dispersion (we assume the correct analytical continuation of the square root implicitly) for $\omega > 0$ [1]

$$\left(\omega - \Omega - U^2 \frac{1}{\sqrt{\omega^2 - 4}}\right)^2 - U^4 \frac{(\omega - \sqrt{\omega^2 - 4})^{2R}}{\omega^2 - 4} = 0 \tag{4.22}$$

We now have to distinguish between two cases, $\omega > 2$ which means the we are dealing with energies above the band gap and $2 > \omega \geq 0$ where the energy is inside the band of the waveguide.

Outside the band

In the case of $\omega > 2$, me make the substitution $\operatorname{arccosh}(\omega/2) = \Theta$ with $\Theta > 0$ (We concentrate on this case, the corresponding solutions below the band can be obtained by a similar analysis replacing $\Theta \to \Theta + i\pi$). This makes the analysis of the eigenvalue equation much more transparent from an analytical point of view because we can eliminate explicitly any (redundant) multivaluedness induced by the square roots. Also the corresponding numerical analysis in Mathematica gets much faster. It is furthermore important to remember that for this choice of energy we only obtain the solutions corresponding to atom-photon bound states (APB) because they are the only eigenstates of our system living outside of the band.
We obtain

$$f_\pm(\Theta, R) = 2\sinh(\Theta)(2\cosh(\Theta) - \Omega) - U^2(1 \pm e^{-R\Theta}) = 0 \tag{4.23}$$

To get started, we sketch the result of typical evalution of the above equation in FIG. 4.6

We see that apparently some of the eigenvalues exists only for some $R > R_{cr_\pm}$ where the subscript $cr_\pm$ stands for critical above $(+)$ or below $(-)$ the band . If the distance gets smaller then this value the corresponding state resides inside the continuum of scattering states.
To be more precise, it can be shown that the equation $f_-(\Theta, R) = 0$ only gives a real solution if

$$R > R_{c,+} = \frac{2(2 - \Omega)}{U^2} \tag{4.24}$$

To visualize the following considerations, we plotted a sketch of (4.23) in FIG. 4.7

The statement (4.24) can be proven using the following observations:

1.) $U^2(1 - e^{-R\Theta})$ is positive, monotonically increasing function bounded by U^2.

[1] We concentrate on $\omega > 0$ because it turns out that the case $\omega < 0$ can simply be obtained by a change of $\omega \to -\omega$ in all equations that follow from here on.

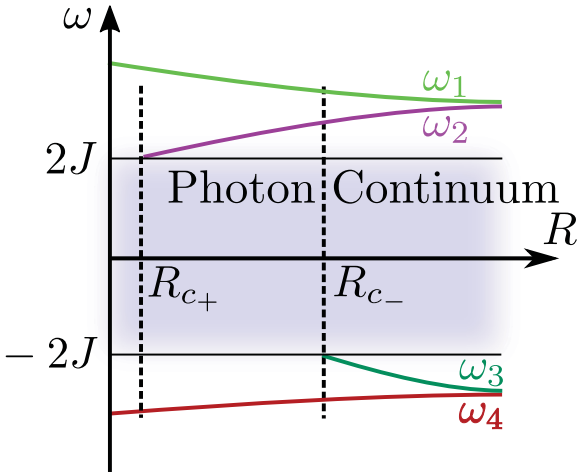

Figure 4.6: *A sketch of the typical behaviour of the solutions of 4.23*

2.) $2\sinh(\Theta)(2\cosh(\Theta) - \Omega)$ goes to positive infinity as $\Theta \to \infty$
3.) $\Theta = 0$ is a trivial solution

From these points, we may conclude that $f_-(\Theta, R) = 0$ only has a solution, if the absolute value of the derivative of the R-independent part of (4.23) is smaller then the one of the R-dependent part at $\Theta = 0$.
This is because otherwise the the two functions can never cross. The possibility that the R-independent part starts to grow fast and then fall down to a minimum value which is smaller

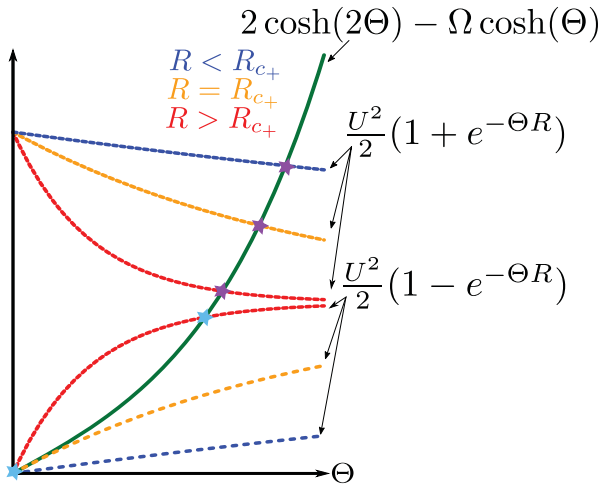

Figure 4.7: *A sketch of the R-dependent and the R− independent parts of* $f_\pm$
The curves corresponding to f_- only cross if $R > R_{cr\_}$

then the right-hand side is excluded by the fact that it is equivalent to a symmetric polynomial of order 4 (substitute $x = e^{\Theta}$ in (4.23) to see this) which can at least have one extreme value for $x > 0$ which forbids the described behavior necessary for an additional crossing.
All what is left is to calculate the derivative of (4.23) at $\Theta = 0$:

$$\partial_\Theta f_-(\Theta, R)|_{\Theta=0} \Leftrightarrow 4 - 2\Omega = RU^2 \tag{4.25}$$

and the stated result follows . A similar inequality might be obtained for the case that $\omega < 0$ yielding $R_{c,-} = 2(2 + \Omega)/U^2$.
It furthermore follows, that depending on $\Omega > 2$ or $\Omega < 2$ we have a different number of atom-photon bound states (We consider $\Omega > 0$ here only, because we can get the other case by just letting $\Omega \to -\Omega$). We can summarize the different cases in Table 4.1

-	$\Omega < 2$	$2 < \Omega$
$R < R_{c-}$	2	3
$R_{c-} < R < R_{c+}$	3	3
$R_{c+} < R$	4	4

Table 4.1: *The number of bound states given the distance of the two TLS and their energy*

The numbers in the table are the number of bound states which exists for different values of Ω. Note this number is independent of the coupling U, which is quite interesting. The first entry on the right is due to the fact that $R \geq 0$ by definition and $R_{c-} < 0$ in this case which is a contradiction. The physical interpretation of this table is clear. For large R we have all the possible atom photon bound states, but as soon as they start to get closer they start to repel each other (this phenomenon is called level repulsion and is well known from many physical systems, for an introduction, see [107])
In a next step we have analyzed the asymptotic behavior of the $R-$dependence of the eigenvalues. We did this in four cases

1.) For $R\Theta_\infty \gg 1$ which means that we discuss the influence of a finite distance on the initially degenerate two TLS. Here Θ_∞ denotes the eigenvalue at $R = \infty$

2.) Then we discuss $R\Theta_{0,\pm} \ll 1$ which means that we start out of the degenerate $V-$system and see what the effects of a finite distance are ($\Theta_{0,\pm}$ denote the two eigenvalues at $R = 0$).

3.) In a third step, we analyze the behavior of the eigenvalues near $R_{c\pm}$ where $\Theta \approx 0$.

4.) Last but not least we discuss the Markovian limit $U \to 0$, where the coupling of both TLS to the waveguide is assumed to be small .

For the sake of a clear presentation, we postpone the derivations concerning the first three cases to Appendix E and merely state the results here. The derivation of case four will be carried out here, because it is particularly easy, independent from the other cases and furthermore reproduces nicely a result given previously.[106]

Because the coupling is assumed to be small we might expect that the shift of the resonance energy due to the self energy contributions is small. It is therefore legitimate to perform a Taylor expansion in $\omega - \Omega$ because we can assume that the energy will be not too far away from the non-interacting value $\omega = \Omega$. $Q(\omega, R) = 0$ then takes the following form:

$$(\omega - \Omega - U^2\Sigma(\Omega)^2 - U^4\Gamma(R, \Omega) \tag{4.26}$$

Setting this to zero we get the following Poles (again concentrating on the equations above the band):

$$\omega_\pm(R) = \Omega + \frac{U^2}{\sqrt{\Omega^2 - 4}} \left[1 \pm \left(\frac{\Omega - \sqrt{\Omega^2 - 4}}{2} \right)^R \right] \tag{4.27}$$

Subtracting $\omega(\infty)$ we get

$$\omega(R)_{reg} = \pm \frac{U^2}{\sqrt{\Omega^2 - 4}} \left(\frac{\Omega - \sqrt{\Omega^2 - 4}}{2} \right)^R \tag{4.28}$$

which corresponds to (19) in [106]. The subscript "reg" means regularized. Please note that this limit is equivalent to a Wigner-Weisskopf approximation [104], which is essentially a lowest order expansion in U and is very common in quantum optics. In the case $\Omega < 2$ the above yields in general no real solution which gives us a strong hint that we miss a good amount of interesting physics if we compare this with the rather rich behavior we expect from Tab. 4.1.
We now state the asymptotic results for the $R-$ dependence of Θ. We give not the full asymptotics we derived because everything would become quite lengthy. Instead, we only state the leading order results, the full expansions can be found in Appendix E together with their derivations. Furthermore all the formulas below only hold for energies above the band. The corresponding values below the band can be obtained by a simultaneous transformation $R \to -R$, $\Omega \to -\Omega$ together with a replacement of $\Theta_{0/\infty,\pm}$, which are the numerical values at $R = 0$ and $R = \infty$, by the their appropriate values below the band.

Here and later on, f denotes the R-independent part of $f_\pm$ defined in (4.23), and primes denote derivatives with respect to Θ. We get (E.4) for $R\Theta_{0,\pm} \ll 1$

$$\omega_\pm = 2\cosh(\Theta_{0,\pm}) \mp \frac{\sinh(\Theta_{0,\pm})U^2 R}{f'(\Theta_{0,\pm})} \tag{4.29}$$

which means that we have a linear dependence on R near the origin. The approximation gets worse for very big U, but because this is beyond the RWA the results would be questionable even if this wouldn't be the case.
Next we calculated perturbative results for $\Theta(R - R_{c+}) \ll 1$. The way this asymptotics are obtained is a bit more tricky, because there are cancellations taking place in the eigenvalue equations which forces us to keep track of terms $\mathcal{O}(\Theta(R-R_c))^3$ and furthermore the asymptotic behavior changes drastically in the limit $\Omega \to 2$ where observe a crossover between $\Theta \sim (R-R_c)$

if $R_c \sim \mathcal{O}(1)$and $\Theta \sim (\sqrt{R - R_c})$ if $R_c \to 0$.
The exact leading order behavior is given by

$$\omega = 2 + \frac{4\Delta R}{R_c^2} \text{ if } R_c \sim \mathcal{O}(1), \tag{4.30}$$

where $\Delta R = R - R_c$ and

$$\omega = 2 + \frac{U\sqrt{3\Delta R}}{\sqrt{8 - \Omega}} \text{ if } R_c \to 0. \tag{4.31}$$

We see that the jump in the derivative $\partial_R \omega(R)$ at ΔR is also different in both cases. For a discussion of possible issues for $\Omega > 8$ please consult Appendix E.

Last but not least we obtained an asymptotic expansion for the case $e^{R\Theta_\infty} \gg 1$ reading (E.12)

$$\omega_\pm = 2\cosh(\Theta_\infty) \pm U^2 \frac{\sinh(\Theta_\infty)}{f'_\pm(\Theta_\infty)} e^{-R\Theta_\infty} \tag{4.32}$$

Observe how the $\pm$ signs is taking care of the level repulsion: Initially at $R = \infty$ we have two degenerate solutions which start to split up in opposite directions as the distance becomes finite.
The behavior of the eigenvalues in (Fig.4.8) and below (Fig.4.9) the band is shown in the picture below. Note that in this particular case $\Omega = 2.5$ and $U = 1$ so we have $R_{c-} = 9$

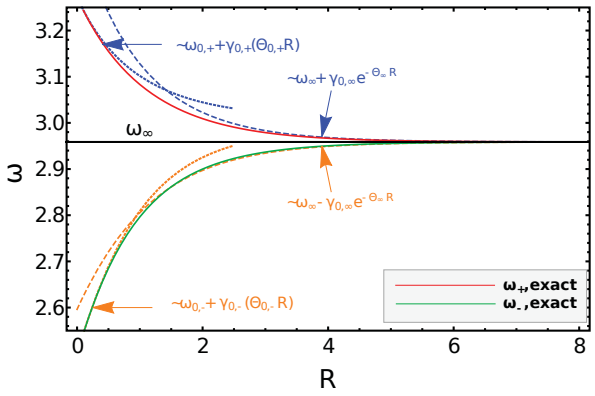

Figure 4.8: *The energy values above the band. Level repulsion is clearly visible for $R \approx 4$. Note that both curves stay finite for $R = 0$, which is not visible*

The R-independent coefficients can be read out from the formulas (4.29,4.30,4.32). If the symbol $\sim$ shows in a plot it means "to lowest order". In every other context it means "asymptotically equal to".

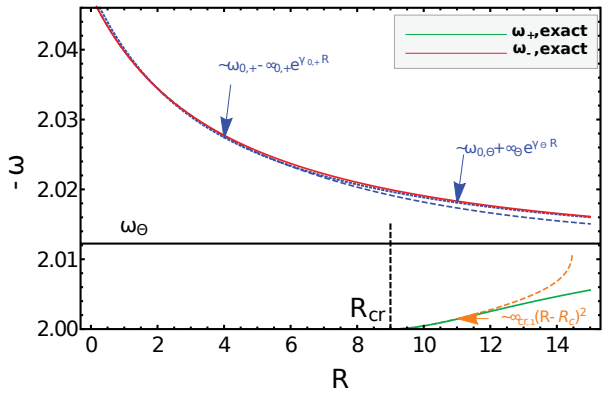

Figure 4.9: *The energy values below the band. At $R = R_c$, we can observe how one of the eigenvalues slips out the band.*

The plots nicely confirm the expectations from the calculations we did so far:
The level repulsion between the two initially degenerate eigenvalues is clearly visible. Furthermore, we observe the disappearance of one of the bound states into the photon continuum. Also our asymptotics seems to work quite well for a wide range of R values. A point we want to stress here is that the behavior at R_c is not analytic. As soon as the band edge is hit, this state becomes a scattering state with constant energy which is distributed over the whole waveguide. The consequence of this is that we obtain a jump in the derivative of the energy eigenvalue, which should be visible also in at least some (experimentally) measurable quantities which can be derived from them, namely the fluctuation forces. We will come back to this point in more detail in the next chapter.
One should also mention again that all these nice features wouldn't be visible if we would have just assumed a linear dispersion, because it has none of the bound states we discussed here. What features survive in the case of linear dispersion will be part of the next section.

Inside the band

For $2 > \omega > 0$ we can use a very similar substitution in the general eigenvalue equation 4.21, namely $\omega = 2\cos(\theta)$. This results in

$$-i2\sin(\theta)(2\cos(\theta) - \Omega) = U^2(1 \pm e^{-iR\theta}) \tag{4.33}$$

Surely these equations aren't solvable exactly by analytic means but one particular interesting set of solutions can be obtained straightforwardly by nullifying both terms inside of the brackets separately. We obtain

$$\Sigma_j = \begin{cases} 2\cos(\frac{2N\pi}{R}) & \text{if } f_+ = 0 \\ 2\cos(\frac{(2N+1)\pi}{R}) & \text{if } f_- = 0 \end{cases} \tag{4.34}$$

where N is an integer number. We can now conclude that for every fixed pair of R and Ω there is just one state fulfilling these conditions. This follows from the fact that the above is

equivalent to a quantisation condition

$$\Omega = 2\cos(\frac{\pi N}{2R}) \tag{4.35}$$

It corresponds to one of the eigenmodes of the cavity build from the two TLS (This point will be discussed in more details later). It is furthermore straightforward to prove that these are the only real and finite solutions to (4.33). This follows from the fact that the LHS of (4.33) is, apart from the above solution, always imaginary if the bracket is nonzero whereas the RHS always has finite real part if the bracket is nonzero which leads to a contradiction if we assume that $\theta \in \mathbb{R}$.
The states of the system corresponding to the energies we found above are quite uncommon. First of all despite the fact that they are located energetically inside the photon continuum, they are no scattering states as they have no momentum dependence. For this reason they belong to a class of states called bound state in continuum (BIC) which, despite not occurring very often in literature, have a long history going back to Wigner and von Neumann [108] and where thoroughly studied by Stillinger [109] for separable Schrödinger equations. In the last years, they where also found to play a role in the context of qubits coupled to an electronic waveguide (which is on a theoretical level similar to our systems, at least in the single excitation sector) [110].
Their occurrence is rather non surprising if one remembers that a single atom can act as a perfect mirror if a photon is on resonance with it [114]. Coupling two atoms and putting them one resonance with the photon therefore results in a perfect cavity, trapping one specific mode. It is furthermore [113] interesting to note, that in the case of $R = 0$ the BIC energy turns into the well known energy for the dark state (DS) of the $V-$system which is called this way because it cannot be probed by the photons in the waveguide
Another fascinating fact about BICs at least in our system (for arbitrary dispersion relations as we will see later) is that their occurrence is totally independent of the size of the coupling constant U, as long it is bigger then 0. They are, therefore, a pure interference effect, mediated by the two atoms.
The different kind of eigenstates in the system are sketched in the picture below

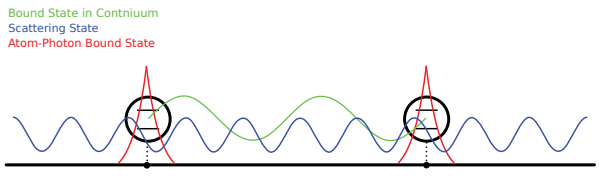

Figure 4.10: *Sketch of different classes of Eigenstates*

We may also note that there exist some kind of connection between APBs and BICs due to resonance located at $\Omega = \omega$. As noted above the BIC becomes a Dark State for R=0. This is indeed true as long as $\omega = \Omega < 2$. If this condition is not fulfilled, the energy of a BIC

would be larger then the band edge of the wavequide which contradicts its nature of a state living inside the continua of scattering states. Instead, the DS turns into an additional APS if $\omega = \Omega > 2$ and R becomes finite.

4.4.2 Linear dispersion relation

To obtain a better understanding of the BICs, we now investigate the case of a linear dispersion. Clearly any sign of the APBs is gone in this case, because the band edges are pushed to infinity. From (4.10) and (4.19) we get the following equation which determines the eigenvalues

$$(\omega - \Omega - i\frac{U^2}{v}) = \pm i\frac{U^2}{v}e^{2iR\omega/v} \tag{4.36}$$

Following the same line of reasoning as in the last subsection, it is easy to see that the BICs appear again but with slightly different energies.

$$\omega = \Omega \wedge \omega = \frac{v\pi N}{R} \tag{4.37}$$

where N is again an integer number. Note that this is exactly the resonance condition for a particle in an infinite square well potential, which gives our interpretation of the BIC as something trapped into a perfect cavity even more credit.
In contrast to the cosine case, it is also possible to give an "explicit" solution to this equation.

$$\omega_{n\pm} = \Omega - iU^2 - i\frac{W_n\left(\pm RU^2 e^{iR(\Omega+iU^2)}\right)}{R} \tag{4.38}$$

Here $W_n(z)$ denotes the n-th branch of the Lambert W-function which is implicitly defined as $z = W(z)e^{W(z)}$. Note that the only eigenmodes arising from this equation are the BICs from above, because all other solutions have finite imaginary part and are therefore decaying (this solutions describe a leaky instead of a perfect cavity). It is worth to mention that this kind of modes is closely related to the well known quasi-normal modes which are commonly used in the description of leaky cavities in the context of classical optics [111]. Using the well known expansions [112] $W_0(z) \approx z$ for $z \to 0$ and $W_n(z) \approx \log(z)$ for $z \to \infty$ we recover easily the limiting cases of a 3-level system and of two decoupled 2-level systems (which also follows directly from (4.36) if we keep in mind that exponential is always implicitly damped (by a factor of $e^{-\delta R}$) for $R \to \infty$: $\omega(\infty) = \Omega - iU^2/v, \omega(0,\pm) = i\Omega - iU^2/v \pm iU^2/v$)
Because in the case of a linear dispersion there are no APBs (see the discussion in 3.4), these are according to (4.20) the only $R-$dependent eigenvalues of the system.
We sketch the different modes below, which shows the differences to FIG. 4.10 quite nicely.

4.4.3 General existence condition for bound states in the continuum

It follows from equation 4.21 that the condition to have a BIC is

$$\pm\,\Sigma(\omega) = \Gamma[R,\omega] \wedge \omega = \Omega \tag{4.39}$$

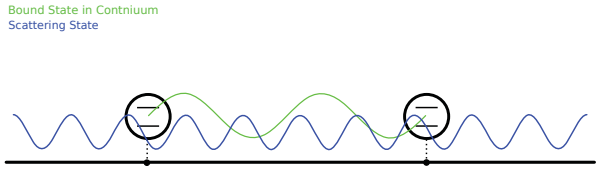

Figure 4.11: *Sketch of different classes of eigenstates for the linear dispersion*

Here $\wedge$ denotes a logical and.
Furthermore we might observe that both BIC conditions, (4.34) and (4.37) are of the form

$$\omega = \epsilon\left(\frac{\pi N}{R}\right) \wedge \omega = \Omega \tag{4.40}$$

This also makes sense heuristically: For a mode to be trapped in a infinite potential well, it has to fulfill such a condition. We now want to prove that (4.39) and (4.40) are indeed equivalent statements for generic dispersion relations. Therefore, we might look at the definition of $\Gamma(R,\omega)$ in (4.10) and perform a change of variables $\epsilon(k) = z$ to obtain:

$$\Gamma(R) = \sum_j \int_{\epsilon(k_{min})}^{\epsilon(k_{max})} \partial_z \epsilon_j^{-1}(z) \frac{e^{iR\epsilon_j^{-1}(z)}}{\omega - z + i\delta} dz \tag{4.41}$$

Here the $\sum_j$ runs over all different branches of $\epsilon^{-1}(z)$. Using Dirac's identity $\frac{1}{x+i\delta} = P\frac{1}{x} + \imath\pi\delta(x)$ we get

$$\Gamma(R) = i\pi \sum_j \partial_z \epsilon_j^{-1}(z)\Big|_{z=\omega} e^{iR\epsilon_j^{-1}(\omega)} + \Re[....]_j \tag{4.42}$$

In section 3.4 we showed that the real part $\sum_j \Re[...]_j$ vanishes for great the class of dispersion relations (The ones with an inversion symmetry $k \to -k$). Therefore if this is the case, and furthermore the condition $\epsilon_j^{-1}(\omega)R = \pi N$ is fulfilled, we obtain

$$\Gamma(R) = \pm i\pi \sum_j \partial_z \epsilon_j^{-1}(z)\Big|_{z=\omega} = \pm\Sigma(\omega) \tag{4.43}$$

This is in agreement with the general condition we imposed in (4.39), and therefore we have proven that the resonance condition which has to be fulfilled for a BIC to occur is indeed

$$\Omega = \epsilon(\pi N/R) \tag{4.44}$$

for every dispersion with the symmetry $k \to -k$. As a side remark, we might note (4.39) is trivially fulfilled for $R = 0$ which means that for every dispersion relation there is a darkstate (DS) at this point.

4.5 Dynamics of the TLS for the linear spectrum

In this section we want to discuss briefly how the BICs affect the dynamics of the two TLS. We therefor calculate $|\mathcal{G}_{12}(t)|^2$ which gives us the probability that the system in which at $t = 0$ the first TLS is excited has the second TLS excited at time t. We, therefore, have to take the inverse Fourier transform of the $(1, 2)$ entry of (4.19):

$$\mathcal{G}_{TLS_{12}}(t) = \tag{4.45}$$
$$U^2 \int_{-\infty}^{\infty} \frac{\mathrm{d}\omega}{2\pi} \frac{e^{-i\omega t} e^{i(\omega/v)R}}{(\omega - \Omega - iU^2(1 + e^{i(\omega/v)R})(\omega - \Omega - iU^2(1 - e^{i(\omega/v)R})}$$

The evaluation of this integral can be done by the help of the residue theorem. Depending on the sign of the quantity $t - R/v$ we close the contour in the appropriate half plane and pick up all the residues. Inspecting the above formula we see that imaginary part of the denominator is always negative which means that all poles lie in in the region with $\Im(\omega) \leq 0$. This means that if we have to close our contour in the upper half plane (if $t < R/v$) the integral is just zero. This can be also understood from an more intuitive direction by remembering that R/v is the time a photon needs to travel from one TLS to another (the retardation time). If t is smaller than this time the two atoms can't influence each other and we expect that the Green's function is zero. We obtain

$$\mathcal{G}_{TLS12}(t) =$$
$$iU^2 \Theta(t - R/v) \sum_{n=0}^{\infty} \mathrm{Res}(\mathcal{G}_{TLS12}(\omega) e^{i\omega t}, \omega = \omega_n) \tag{4.46}$$

From here on we want to focus on the limit of $R/v \ll t$ where the effects of the BICs are most dramatic.The reason is that they are the only contribution to the above sum which are not decaying exponentially in time because the corresponding poles have zero imaginary part (as they should because they are eigenstates of the system). Therefore, we restrict our attention to the poles containing the BIC ($n = 0$) and the one with smallest imaginary part because everything else will be exponentially suppressed for times that are long enough (The reason for this is that $W_0(-x) = W_{-1}^*(-x)$ for $x \in \mathbb{R}$, so the corresponding eigenvalues in (4.38) are equally important if the argument of the Lambert function becomes purely negative). We obtain

$$\mathcal{G}_{TLS12}(t) =$$
$$iU^2 \Theta(t - R/v) \sum_{n=0, l=\pm}^{-1} \mathrm{Res}(\mathcal{G}_{TLS12}(\omega) e^{i\omega t} \omega = \omega_{l,n}). \tag{4.47}$$

Calculating the residues explicitly we get

$$\mathcal{G}_{TLS12}(t) = iU^2 \sum_{l=\pm} \Theta(t - R/v) \left(\alpha_{l,0} e^{i\Omega_{0,l} t - \gamma_{0,l} t} + \alpha_{l,1} e^{i\Omega_{1,l} t - \gamma_{1,l}} \right), \tag{4.48}$$

where $\alpha_{0,1}$ are t independent constants,

$$\Omega_{\pm,0,1} = \Omega + \Re[W_{0,-1}(\pm(R/v)U^2 e^{(R/v)(U^2+i\Omega)}]/R, \tag{4.49}$$

is the renormalized oscillation frequency and

$$\gamma_{\pm,0,1} = U^2/v + \Im[W_{0,-1}(\pm(R/v)U^2 e^{(R/v)(U^2+i\Omega)}]/R, \tag{4.50}$$

describes the modified inverse decay time of the TLS.
Note, that in the special case of a BIC, $\Im(\Omega_{\pm,0}) = 0$ if N is even/odd and we have a finite contribution even in the stationary limit $t \to \infty$. From a mathematical point of view, this follows from the fact the zeroth branch of the Lambert-W function is the only one which is real for real positive arguments [112].
We now want to resolve the influence of the BIC a bit further. We use that by definition $W_0(ze^z) = z$ for $z \in \mathbb{R}_+$ and $e^{i\pi N} = (-1)^n$. Therefore

$$W_0(\pm e^{(R/v)U^2 + i\pi N} RU^2) = (R/v)U^2 \text{ if } \left\{ \begin{matrix} N \text{ even } (+) \\ N \text{ odd } (-) \end{matrix} \right\} \tag{4.51}$$

where $(\pm)$ refers to the sign of the argument of the Lambert-W function. Together with (4.38) we see that depending on N one of the exponents in (4.48) gets nullified so this contribution will not decay in time. The last piece we need are the corresponding prefactors. After a little algebra we obtain

$$\alpha_{\pm,0} = \frac{i}{2} \frac{1}{1 + W(0, \pm RU^2 e^{-(R/v)U^2})} \tag{4.52}$$

Using again (4.51) and assuming again that (4.37) is fulfilled we obtain

$$\alpha_{\pm,0} = \frac{i}{2} \frac{1}{1 + (R/v)U^2} \text{ if } \left\{ \begin{matrix} N \text{ even } (+) \\ N \text{ odd } (-) \end{matrix} \right\} \tag{4.53}$$

and therefore $(\Theta(x)^2 = \Theta(x))$

$$|\mathcal{G}_{TLS12}(t)|^2 = \frac{\Theta(t - R/v)}{4} \frac{1}{(1 + (R/v)U^2)^2} \tag{4.54}$$

if the BIC condition is fulfilled. Note that this result is not only true for large times but for every time t because none of the other branches of W can give us another non-decaying contribution. Plots of the modulus of (4.46) and (4.54) are shown below in Fig. 4.12

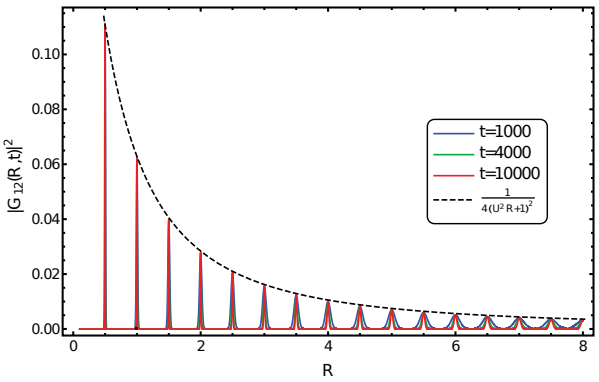

Figure 4.12: *Square Modolus of* $G_{12}(t)$ *for* $R = 0$

We observe a dramatic effect if the BIC is present in the system: In the long time limit, the probability goes as $\sim \frac{1}{U^4 R^2}$ at the position of the BIC and decays (it is literally not visible in the plot) exponentially in time far away from it. Furthermore at finite times we see that these peaks still have finite width, which come from solutions of (4.36) with very small imaginary part that are located in direct neighborhood of the BIC. A quite similar mechanism occurs in connection with the investigation of single three level systems [113] and the corresponding modes were coined Almost Dark States (ADS). Because our system in the one excitation subspace turns out to be exactly a V-system in the limit of $R \to 0$ we suspect that the slowly decaying modes we observed will share some similarities with them.
To summarize: if we are close to the BIC conditions the second TLS will have a finite excitation even for long times. Otherwise all occupation will disappear exponentially fast into the waveguide. This might open the path for a more efficient storage of information in TLS even in linear (Markovian) waveguides.

The special case $R = 0$

As a side note, we consider the case $R = 0$ where we effectively solve a V-System. In this case the bound state is the dark state and resides at $\omega = \Omega$. (4.45) becomes fairly easy to calculate and we obtain

$$G_{12}(t) = \frac{e^{i\Omega t}}{2}\left(1 + e^{-tU^2/v}\right) \tag{4.55}$$

This result is remarkable because it implies that the amount of excitation transferred from one degenerate energy level to another is given in the long-time limit by the universal constant

$$\lim_{t\to\infty} |G_{12}(t)|^2 = \frac{1}{4} \tag{4.56}$$

independent of any system parameter. Please note also that this non-decaying part is purely a result of the Dark state. This in agreement with (4.54) for the special case of $R = 0$.

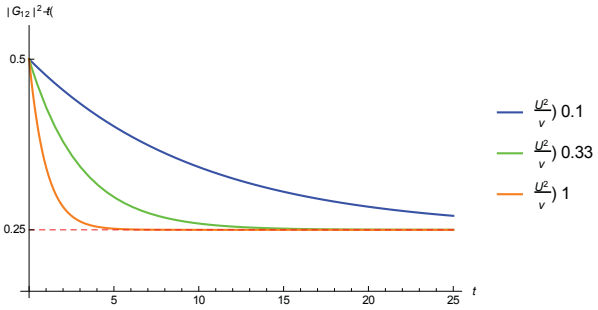

Figure 4.13: *Square Modolus of* $G_{12}(t)$ *for* $R = 0$

4.6 Förster Energy Transfer

4.6.1 Introduction

In this chapter we want to calculate fluctuation forces (or their corresponding potentials). We expect them to be present in our system for the reason that if we focus our attention onto the TLS we see that they are coupled via a photonic environment, namely the waveguide which mediates an effective interaction between them. This situation is very similar to the case of the well known Casimir-Polder interaction, originally derived 1948 for an atom in front of a metallic plate [115] where the interaction is induced by vacuum fluctuations of the EM field. This concept was generalized in 1959 to more or less generic, arbitrary formed solids separated by a liquid as described in the seminal paper by Dzyaloshinskii, Lifshitz and Pitaevskii [116]. Since then many new important discoveries had been made in this field (see [117] for an overview) most notably it opens the door to whole new branch of mechanics, the so called nanomechanics where objects with a size of a few hundred nanometers are manipulated [119].
In our work we focus on a special case of fluctuating force, the so called Förster energy [2] transfer (FRET) which was predicted in 1948 [120] and describes the radiationless transfer of energy between quantum objects due to dipolar forces. The reason for this is that as we discussed in the last chapter, the energy of the scattering modes are independent of R so they will not give rise to any (non-constant) fluctuating energy between the two atoms so we can only expect radiationless energy transfer. Remembering that a TLS is an approximation too, for example, an atomic dipole it makes also well sense to expect the interaction to be of dipolar type. We might want to add that the force we are talking about here is mediated by the near field part of the EM field which is for our system related directly to the APBs (their photonic part is exponentially located around the atoms). Its existence is therefore closely tied to the presence of a band edge in the dispersion relation which is crucial for the existence of APBs. In its original work Förster showed, that the lifetime of two molecules or atoms at distance R in 3D free space is modulated due to dipolar interactions by $(R/R_0)^6$ where R_0 sets the

[2] One might ask how we can be sure that we are really dealing with a Förster like energy transfer which is not always easily distinguishable from another type of energy transfer, the so called Dexter transfer. The reason is, that our interaction is mediated by virtual photons (as it is clear from the diagramatics) which is typical for Förster like processes, whereas in Dexter like processes the interaction is mediated directly by overlapping wavefunctions of the polaritonic states

scale where the lifetime becomes that of an isolated atom and is typically on the size of 10nm [120]. This is intuitively clear if one keeps in mind that by Fermi's golden rule the lifetime is proportional to the inverse of the square of the dipole interaction which scales as R^{-3} . FRET found numerous applications in biochemistry like the measurement of distances between molecules [121, 122] or signal transport in biological systems [123]. Also some of the microscopic techniques which circumvent the Abbe limit are relying on this effect [124, 125]. Furthermore the biochemical processes that are responsible for photosynthesis in plants are essentially based on FRET [128].It turned out that this not only of importance for pure science but also crucial for the design of efficient organic solar cells [129]. We want to discuss this phenomena in the context of WQED where it is not commonly applied so far. We are doing this for two reasons: On the one hand, our simple model system gives us the opportunity to discuss FRET in a very clean environment whereas in the context of the above applications the underlying physical models are much more involved (lots of different and big molecules, different decay channels and complicated electromagnetic environment, so one can hope to earn some better understanding of this phenomena at least in one dimension. On the other hand one can hope that FRET will also yield some new interesting effects and opportunities in WQED like additional communication channels between quantum dots or the design of trapping potentials.
We start with a general discussion of how to define FRET in our system and we will see that it is quite important to know the occupation numbers of the energy eigenstates if we prepare our system in a generic quantum state, so we will discuss their calculation in the following section. Then we discuss the occupation numbers as well as the Förster energy on two particular examples: First the case where only one of the atoms is initially excited. Secondly the case where the system is prepared in a way that the two atoms are initially in a symmetric superposition (or in other words a triplet configuration)

4.6.2 The definition of the Förster Energy

In most applications of Casimir physics (an exception would be the thermal Casimir effect [117]), the involved constituents are in the quantum mechanical ground state. In contrast to that, our system is always in an excited state because and we have excitations in it (at least one) which, according to the superposition principle of quantum mechanics can be divided arbitrarily between the different parts of our model system (as long as normalization is granted) which means that we expect that the potential $\phi(R)$ which describes the fluctuating potential between the two atoms, is tuneable by preparing our system in one of its infinitely many initial states .
Furthermore we might remember (or have a look at 4.19) that our system for general R only supports at most four different energy eigenmodes that are distance dependent. So as a first important result we may conclude that they are the only states that can contribute to $\phi(R)$. This also implies that in the system with unbounded dispersion relation there will be no fluctuating forces because there are no APBs, as already mentioned in the introduction. We can also reformulate this conclusion as follows:
The only fluctuating forces in the system (for generic R) are due to the near field part of the dipolar interaction because the far field part mediated by the scattering states will not support any distance dependent contributions. Because it also turns out that the BICs are suppressed

if the APB are strongly occupied and topsy-turvy [118] we exclude them form our discussion here but notice that the corresonding force would anyway only exist for a very restricted set of parameters (4.39) and be of ultra shortrange type $\sim \delta'(R - R_c)$. The above discussion brings us to the following definition of the Förster energy[3]

$$\phi_\Psi(R) = \sum_{i=1}^{n_b} [\alpha_{\Psi,i}(R) E_i(R) - \alpha_{\Psi,i}(\infty)\omega_i(\infty)] \tag{4.57}$$

where $|\Psi\rangle$ is a generic quantum state $\alpha_{\Psi,i} = |\langle\omega_i|\Psi\rangle|^2$ is the occupation of a specific APB given an generic $|\Psi\rangle$ and n_b is the number of APB (whose energies are denoted by ω_i). We subtract the (finite) value at infinity so that the Förster energy becomes zero there, which makes sense because the atoms shouldn't influence each other there. This definition resembles very much the original definition of the Casimir energy [115] with the important difference that every energy got weighted by the corresponding occupation number of its eigenstate (for a usual,linear Casimir setup the system is in its ground state and the occupation of any mode is just $\frac{1}{2}$).

4.6.3 Calculating overlap integrals via Green's functions

In this subsection we want to discuss how we can extract occupation numbers out of our Greens functions formalism. This is important because we have seen that they are, together with the eigenenergies which where analyzed in detail previously, one of the two main ingredients showing up in the definition of the potential energy between the two atoms (4.57)
We recall that a general quantum state can be expanded in its energy eigenbasis:

$$|\Psi\rangle = \sum_i \langle\omega_i|\Psi\rangle|\omega_i\rangle \tag{4.58}$$

Furthermore we might define an associated Green's operator (denoted by a $\mathbf{G}$) to every Green's function. To see why this makes sense we consider the Green's function G_w as an example. It is given in Heisenberg representation by $G_{11} = \langle 0|a_k a_k^\dagger|0\rangle$ and we can identity $\mathbf{G}_w = a_k a_k^\dagger$ as the corresponding operator. For our purpose it is very convenient to express this operator in a Lehmann representation (this corresponds to the energy eigenbasis) [130]

$$\mathbf{G}(\omega) = \sum_i \frac{|\omega_i\rangle\langle\omega_i|}{\omega - \omega_i} \tag{4.59}$$

In a next step, let us squeeze this operator with an arbitrary quantum state decomposed in it's energy eigenbasis (4.58). Keeping in mind that $\langle\omega_j|\omega_i\rangle = \delta_{ij}$ we get:

[3] A more formal motivation can be given by looking at the expectation value of the Hamiltonian regarding some generic state $|\Psi\rangle$ expanded in an energy eigenbasis. This gives the energy of a quantum system: $E_\Psi = \langle\Psi|H|\Psi\rangle = \sum_{i,j} c_i^* c_j \langle\omega|H|\omega_j\rangle = \sum_i |c_i|^2 \omega_i$ where $|c_i|^2$ is the occupation corresponding to the i-th energy eigenstate

$$\langle\Psi|\mathbf{G}(\omega)|\Psi\rangle = \sum_i \frac{|\langle\omega_i|\Psi\rangle|^2}{\omega-\omega_i} \tag{4.60}$$

Because the poles of the above functions are simple, we may conclude immediately [4]

$$\alpha_{\Psi,i} = |\langle\omega_i|\Psi\rangle|^2 = \mathrm{Res}(\langle\Psi|\mathbf{G}(\omega)|\Psi\rangle, \omega=\omega_i) \tag{4.61}$$

4.6.4 First case-study: One atom excited

In this subsection we discuss in detail the occupation numbers $\alpha_{\Psi,i}$ and the corresponding Förster energies when we prepare the system in the state $|1\rangle = |0,\uparrow,\downarrow\rangle$, which means that the first atom is excited whereas the second has zero occupation (because we are dealing with identical atoms, this is equivalent to the case where the second atom is excited) and no excitation is initially in the wavequide (this is formalized by 0 in the bra-ket). As we have seen in the last section we have to calculate

$$\alpha_{|1\rangle,i} = \mathrm{Res}(\langle 1|\mathbf{G}(\omega)|1\rangle, \omega=\omega_i) = \tag{4.62}$$

$$\mathrm{Res}(\mathcal{G}_{11}(\omega), \omega=\omega_i) \tag{4.63}$$

where we have used (4.19). We did this in two ways. On the one hand, we calculated the residues directly by numerical methods. On the other hand we performed a perturbative analysis around the same values of R as we did for the energy eigenvalues $R = 0, R_c, \infty$. We will now discuss this second approach in some detail.
We used the fact that we are dealing with simple poles which means that the residue can be calculated (using (4.20,4.21) and performing the same substitutions then we did for the calculation of the energy eigenvalues) by decomposing G_{11} into an analytic and an meromorphic part[5].

$$\mathrm{Res}(\mathcal{G}_{11}(\Theta), \Theta=\Theta_\pm) = \underbrace{\frac{M_{11}(\Theta_\pm)}{f_\mp(\Theta_\pm)}}_{analytic} \underbrace{\frac{1}{f'_\pm(\Theta_\pm)}}_{meromorphic} \tag{4.64}$$

We concentrate ourselves on the occupations corresponding to energy eigenvalues above the photonic band ($\omega > 2$), the values corresponding to energies below the band can be obtained by the same methods using again the substitutions $\Omega \to -\Omega, R \to -R$ and replacing $\Theta_{0/\infty,\pm}$ by the appropriate values below the band. Furthermore we assumed that $\Omega > 2$ so we only have, according to Tab. 4.1, one bound state which can disappear into the scattering state

[4] This step can be made more rigorous by integrating around a closed contour which contains exactly one eigenvalue

[5] We used the general rule for the residue of an meromorphic function: Let $f(z) = h(z)/g(z)$ where $h(z), g(z)$ both analytic and $g(z_0) = 0$.Then $\mathrm{Res}(f(z), z=z_0) = h(z_0)/g'(z_0)$

continuum.
We now give the different asymptotic expansions to first non vanishing order in R, for the sake of readability we again shift their derivations into Appendix E (together with higher order corrections). Please note that we omit the subscript on $|1\rangle$ for the rest of this section.
In the case of $\Theta_{0,\pm}R \ll 1$ we get (E.41),(the subscript $\pm$ discriminates between the occupations corresponding to the two different solutions of (4.21) with energies above the band)

$$\alpha_\pm = \alpha_{0,\pm} - \chi_{0,\pm}U^2\Theta_{0,\pm}R \tag{4.65}$$

with $\alpha_{0,\pm} = 4\frac{\sinh^2(\Theta_{0,\pm})}{f'_(\Theta_{0,\pm})}$ and $\chi_\pm = 2\frac{\sinh(2\Theta_{0,\pm})}{f'^2_(\Theta_{0,\pm})}$. In the case of $R \approx R_c, x \approx 0$ we get (E.42)

$$\alpha_- = \chi_{R_c,1}\Delta R \;\text{ if } R_c \sim \mathcal{O}(1) \tag{4.66}$$

with $\chi_{R_c,1} = \frac{8}{R_c^2}$. For small R_c the lowest order term is given by (E.43)

$$\alpha_- = \chi_{R_c,2}\sqrt{\Delta R} \;\text{ if } R_c \to 0 \tag{4.67}$$

with $\chi_{R_c,2} = \sqrt{\frac{3}{8-\Omega}}$
Whereas the last two cases are obtainable through a straightforward expansion of the explicit version of (4.64), the third case $R\Theta_\infty \gg 1$ is quite delicate due the occurrence of degenerate eigenvalues at $R = \infty$ which makes the original simple pole a pole of order two. For an in depth discussion of this point, see E.2.1

$$\alpha_\pm(R) = \alpha_\infty\left(1 \mp \frac{RU^2e^{-\Theta_\infty R}}{f'(\Theta_\infty)}\right) \tag{4.68}$$

where $\alpha_\infty = \frac{2\sinh^2(\Theta_\infty)}{f'(\Theta_\infty)}$ is the occupation at $R = \infty$ which is the same for both boundstate energies due to degeneracy. Please note that in contrast to the expansion for the energy eigenvalue equation (4.32) this are not monotonically decreasing/increasing functions and allow for a minimum or maximum at $R \approx 1/\Theta_\infty$ (this is not a good approximation but it gets highly improved by including higher order contributions). We summarize these calculations in the pictures below (Fig. 4.14 and Fig. 4.15). Again we choose $U = 1, \Omega = 2.5$

We might observe that the expected minimum in the occupation number is indeed visible also in the numerical calculations.The bound state corresponding to this occupation can be identified with an energy eigenvalue that is given by the solution to $f_+(\Theta, R) = 0$. It can approximately be calculated by use of the asymptotic expansion around $R = \infty$ using equations [E.37,E.38,E.40]. We obtain

$$R_{min} = \frac{1}{\Theta_\infty} - \frac{f''_\infty(\Theta_\infty)}{f'_\infty(\Theta_\infty)} + 2\coth(\Theta_\infty) \tag{4.69}$$

This gives for the above set of parameters $R_{min} \approx 0.44$ which fits sufficiently well with the numerical value read of from Fig. 4.14. A qualitative explanation for the occurrence of this minimum is as follows:
As R becomes finite, there is room for additional scattering states between the two TLS which

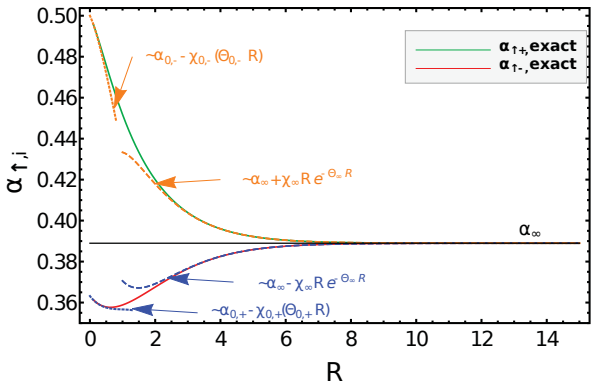

Figure 4.14: *The occupations above the band. We observe a minimum at $R \approx 0.7$ in the state corresponding to ω_+. Note that by comparing the colors of the lines with Fig. 4.8 we can identify the occupations numbers and the corresponding eigenenergy. Furthermore the DS at $R = 0$ which occupation 0.5 is clearly visible*

have to be occupied so the amount of occupation of the APB which is related to the atoms has to decrease (this is supported by the fact that the asymptotics for $R \approx 0$ predicts that the occupation behaves as $U^2 R$ which means that the coupling to the waveguide gets stronger for small but increasing distances), which means in turn that its photonic part gets more pronounced. On the other hand, after a certain value of R the occupation has to grow again because the degenerate value at infinity has to be reached (due to vanishing level repulsion which we expect to take over from the energy eigenvalues because we expand the occupations in the same small parameter $e^{-R\Theta_\infty}$), these two competing effects will eventually balance out to support the minimum value shown in the plot.
Even more interesting the second occupation number doesn't support an extreme value (regardless of the fact that the asymptotic expansion (4.68) predict this in both cases). [6].
Again, as explained above, new photonic states between the TLS occur for finite R and the state has to lose weight. But contrary to the case above this process is not opposed but supported by the vanishing level repulsion (they both have the same direction) so the relaxation to the value at infinity is monotonic and no extreme value appears.
It is quite interesting to see how different both occupation numbers behave, something one would not anticipate from the regular behavior of the corresponding eigenvalues shown in Fig. 4.8. We can perform the same calculations for the energy eigenvalues lying below the photonic band, which results in Fig.4.15.

Having a close look at Fig. 4.15 we might observe that the positions of the two curves are switched for large and small distances, which means that there should be a crossing somewhere

[6]Note that the corresponding eigenstate at $R = 0$ is a dark state. This means that at this point the occupation has to be always higher then the one corresponding to Θ_+ because otherwise the system would be completely non-radiative (no spectral weight in the scattering state because the overall occupation is one due to the RWA).Furthermore we can also explain why both curves don't cross. The reason for that is that $|\Theta_- - \Omega| < |\Theta_+ - \Omega|$ which means that the overlap with the atom is always bigger for the curve corresponding to Θ_-

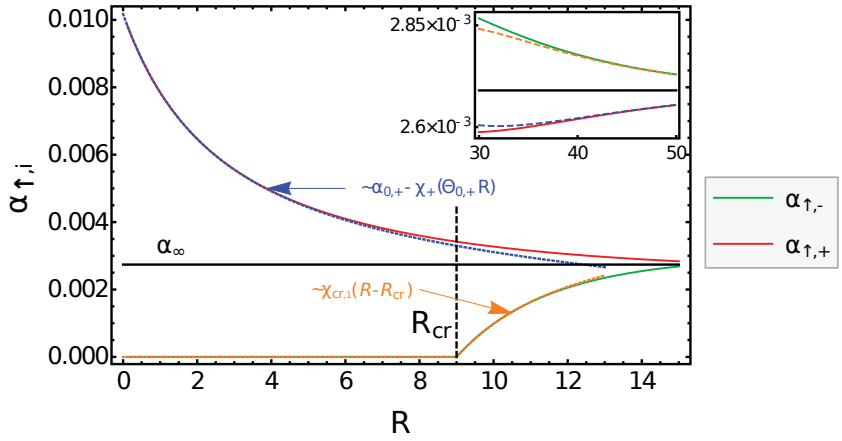

Figure 4.15: *The occupations below the band. At $R = R_c$ we can observe that one of the states starts to become populated. The two curves cross at point not visible neither in the plot nor in the inset*

in between. To make this behavior more clear let's have a look at another plot with a different range of R but otherwise same parameters (Fig. 4.16).

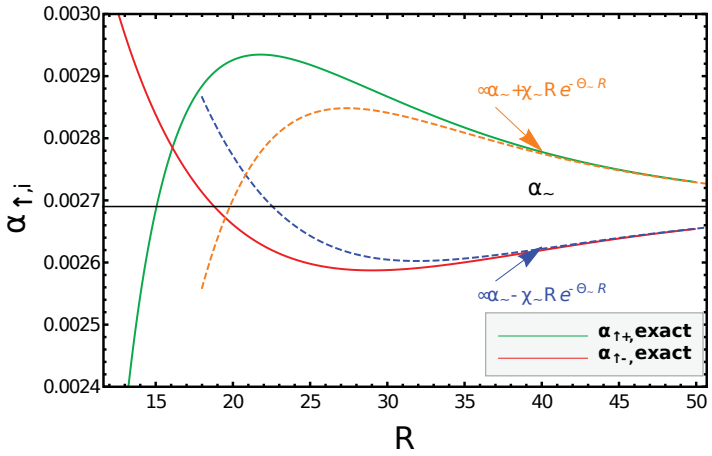

Figure 4.16: *The occupations below the band for larger distances*

We see that the two curves indeed cross. The occurrence of the extreme values as well as the crossing can be explained in a very similar fashion to the case above the band. For finite R the occupation again has to get smaller due to the additional photonic states which can be occupied. The difference is that one of the states is initially a scattering state and occurs first at $R = R_c$ where he starts to gain occupation. Furthermore because it is energetically closer to Ω it will eventually gain a bigger overlap with the atom than the other state which explains the crossing. In the end, due do vanishing level repulsion both values have to reach the same value for $R \to \infty$ so the need to have a maximum or minimum for some R.

From the asymptotic expansions (4.68,4.65) we also see that the occupation numbers are connected to the eigenvalues $\Theta_{0,\pm}, \Theta_\infty$ which are much smaller below than above the band. This induces the smaller occupation numbers below the band as well their much slower convergence to the limiting value at $R = \infty$, which can both be observed in the plots (Fig. 4.16,Fig.4.15 and Fig.4.14). Furthermore setting the derivative w.r.t R of the asymptotic expansion of the occupations for $R \to \infty$ to zero shows that the minimum and maximums values are given approximately by

$$R_{min/max} = \frac{1}{\Theta_\infty} \pm \frac{f''_\infty(\Theta_\infty)}{f'_\infty(\Theta_\infty)} + 2\coth(\Theta_\infty) \tag{4.70}$$

Using the parameters from used in the plot, this yields $R_{min} \approx 27.6$ and $R_{min} \approx 27.1$ which again is no too far away from the numerical values read off from FIG. 4.16.

Förster Potential

In the last part of the subsection we want to discuss the Förster potential. After calculating its two ingredients, the eigenenergies as well as the occupation numbers it is easy to calculated according to (4.57). Again numerical as well as analytical calculations were performed. The resulting plot is shown in Fig. 4.17 (The parameters are again $U = 1$ and $\Omega = 2.5$).

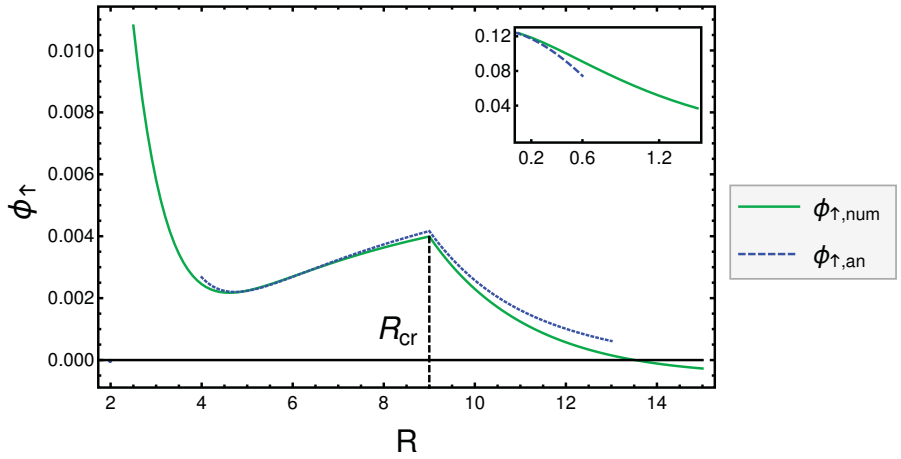

Figure 4.17: *The Förster energy for the case where the first atom is excited. At $R = R_c$ there is a cusp due to the disappearance of one of the polaritonic eigenstates. The potential has a minimum value at $R \approx 4.5$*

The minimum at $R \approx 4.5$ can be explained by the observation that the contributions above the band are initially much bigger then the contributions from below the band but they also disappear much faster for $\omega > 0$ (this follows directly from taking the product of (4.68) and (4.32) for both cases). At some point the value of the contributions from above the band is

therefore smaller than the part from below the band which results in the formation of a minimum. Following the R axis to the right end, we observe that the potential crosses zero. This is due to the fact that the contribution from the bound state which is initially a scattering state finally overtakes the occupation of the bound state which exists already at $R = 0$.This results in another, very shallow, minimum. This follows from the observation that the the potential has to reach 0 for very big distances due to the degeneration of the bound state energies.
The cusp at $R = R_c$ is clearly due to the sudden appearances of an additional non-radiative eigenstate of the system. The force at this point, which is the derivative $\partial_R \phi(R)|_{R=R_c}$, is proportional to the constants $\chi_{cr_{1/2}}$ that are defined in (4.66) and (4.67).
We may also observe that the asymptotic expansions didn't match as good as for the single constituents of the Förster potential. This is mainly due the fact that to obtain the approximation around $R = R_c$ we mixed the the expansions around R_0 for the first eigenvalue below the band together, the expansions around $R = \infty$ for the two eigenvalues above the band which induces some error because that are not perfectly valid at $R = R_c$.
Another point we want to discuss is the non-existence of an extreme value corresponding to the one we observed in the occupation numbers (FIG. 4.14).The reason for this is that the leading order contributions responsible for that vanish up to summation. This can to some extent be explained in (4.19) due to the different signs in the asymptotic expansion around $R = \infty$ (4.68).

The structure of the Förster potential is much richer then one would expect from free space calculations where the potential is monotonous and of the typical dipole-dipole form $\sim R^{-3}$
This shows again the crucial rule played by the electromagnetic environment characterized by the bounded waveguide dispersion. The novel features discussed above may lead to interesting applications First of all, we imagine that the non-analytic behavior in the derivative of $\psi(R)$ might be used to detect an atom photon bound state explicitly in experiment (which is still an open problem) because we expect that it can be translated into a very clear signal in an appropriate measurement.
Secondly one may think about trapping atoms because they should tend to assemble themselves in the potential minimums if they are allowed to move freely. Furthermore one could expect an even richer behavior of the potential landscape if one uses more then two atoms because more atom photon bound states are available ($2N$ for N two level systems).This might be interesting in the context of quantum simulation.
As a third point we may mention that the Förster energy seems to play a role on a scale of at least 10 lattice constants. Typical CROWs have a lattice constant of a few hundred nanometers which means that the radiationless processes should be something relevant at distances of at least 1μm which is bigger by a factor of 10^2 compared to typical applications in biochemistry.This shows that FRET might be an important mechanism on length-scales that are bigger then the ones one would typically expect.

4.6.5 Second case-study: Entangled states

Going a step further, we want to study what happens if we prepare our system in symmetric or anti-symmetric states and compare the results to what we got in the last subsection. This is

particularly interesting because we now have, in contrast to the case where only one atom was excited, entangled states. Especially we want to discuss the interplay between the symmetries of the APB and the symmetries of the initial state. To get started, the symmetric and the anti-symmetric state are given as follows.

$$|\pm\rangle = \frac{1}{\sqrt{2}}(|0,\downarrow,\uparrow\rangle \pm |0,\uparrow,\downarrow\rangle) \tag{4.71}$$

To obtain the corresponding occupation numbers which are necessary to calculate (4.57) we again project the states onto the Green's operator, yielding (we supress the scattering state vacuum $|0,..\rangle$ from here on)

$$\begin{aligned}\alpha_{|\pm\rangle,i} =& \text{Res}(\langle\pm|\mathbf{G}|\pm\rangle, (\omega=\omega_i)) = \\ & \frac{1}{2}\text{Res}(\langle\downarrow,\uparrow|\mathbf{G}|\downarrow,\uparrow\rangle + \langle\uparrow,\downarrow|\mathbf{G}|\uparrow,\downarrow\rangle \pm \qquad (4.72)\\ & \langle\uparrow,\downarrow|\mathbf{G}|\downarrow,\uparrow\rangle \pm \langle\downarrow,\uparrow|\mathbf{G}|\uparrow,\downarrow\rangle, \omega=\omega_i) \qquad (4.73)\end{aligned}$$

but because we are dealing with identical atoms $\langle\downarrow,\uparrow|\mathbf{G}|\downarrow\uparrow\rangle = \langle\uparrow,\downarrow|\mathbf{G}|\uparrow,\downarrow\rangle$ and $\langle\downarrow,\uparrow|\mathbf{G}|\uparrow,\downarrow\rangle = \langle\uparrow,\downarrow|\mathbf{G}|\downarrow,\uparrow\rangle$ and therefore using (4.18)

$$\alpha_{|\pm\rangle,i} = \text{Res}(\mathcal{G}_{11} \pm_s \mathcal{G}_{12}, (\omega=\omega_i)) \tag{4.74}$$

To make the further considerations a bit more transparent we marked the sign which refers to the state of our system by an subscript s.
Because we already know $\mathcal{G}_{11}$ from (4.64) what remains is to calculate $\mathcal{G}_{12}$. According to (4.19) we have that (outside the band, Θ is the same quantity then in previous calculations)

$$\mathcal{G}_{12} = U^2 G_{22}\mathcal{G}_{11} \times \left\{\begin{matrix} e^{-\Theta R} \text{ if } \omega_i > 2 \\ e^{-(\Theta+i\pi)R} \text{ if } \omega_i < 2 \end{matrix}\right\} \tag{4.75}$$

but inspecting (4.8) and (4.22) we also obtain that if Θ is an eigenvalue of our system then $G_{22}^{-1} = G_{11}^{-1} = \pm U^2 e^{-\Theta R}$ which means that

$$\mathcal{G}_{12} = \pm_e \mathcal{G}_{11} \left\{\begin{matrix} 1 \text{ if } \omega_i > 2 \\ e^{i\pi R} \text{ if } \omega_i < 2 \end{matrix}\right\} \tag{4.76}$$

where $\pm_e$ refers to one of the solutions of the eigenvalue equation (4.22) and we labeled the sign by an subscript e. We are now ready to calculate the occupations in terms of $\mathcal{G}_1 1$

$$\alpha_{|\pm\rangle,i} = \text{Res}\left(\mathcal{G}_{11}(\pm_s)(\pm_e)\mathcal{G}_{11}\left\{\begin{matrix} 1 \text{ if } \omega_i > 2 \\ e^{\imath\pi R} \text{ if } \omega_i < 2 \end{matrix}\right\}, \omega=\omega_i\right) \tag{4.77}$$

We see that for this kind of initial states we get very different results depending on if we are dealing with eigenstates which are above or below the band.

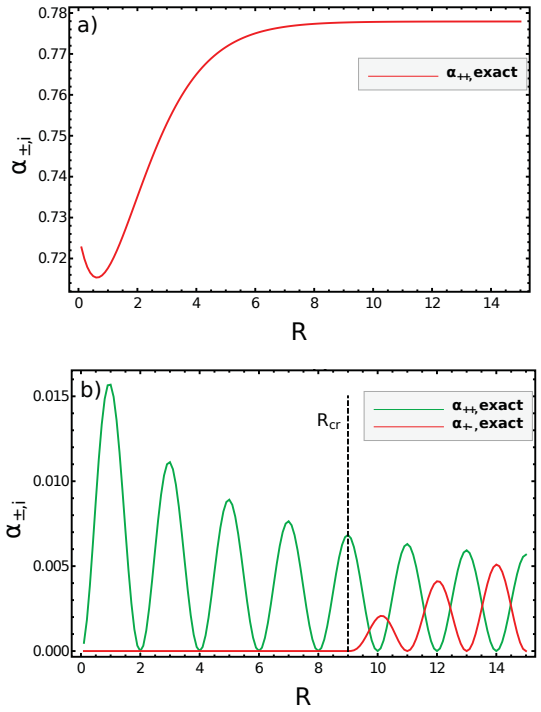

Figure 4.18: *The occupations above and above the band.*
a) Above the band only the state $|+\rangle$ couples.
b) Below the band the coupling of the two energy eigenstates oscillates in units of $R = 1$

For the first case we see that only the terms with $(\pm_s)(\pm_e) = +$ give a finite contribution which is twice as big as for the case where just one atom is excited (4.62).

$$\alpha_{|\pm\rangle,i} = 2\mathrm{Res}(\mathcal{G}_{11}, \omega = \omega_i) \text{ if } \omega_i > 2 \wedge (\pm_s)(\pm_e) = + \tag{4.78}$$

this can be explained by remembering that our initial states have a distinct parity $(\pm_s)$, so they are maximally coupled to bound states with the same parity and orthogonal to th APB with opposite parity, yielding the prefactors of 2 and 0. The distinct parity of the states $|\omega_i\rangle$ can be explained that for finite distances the wave functions of the two bound states above the band will hybridize either in an symmetric or an antisymmetric fashion (resulting in $\pm_e$). The situation is very similar to a quantum mechanical particle in a potential consisting of two delta peaks with distance R where exactly the same mechanism is working [131]. Surprisingly, the situation below the band is very different, we obtain

$$\alpha_{|\pm\rangle,i} = [1(\pm_s)(\pm_e)\cos(\pi R)]\mathrm{Res}(\mathcal{G}_{11}, \omega = \omega_i) \text{ if } \omega_i < 2 \tag{4.79}$$

We see that instead of having just a prefactor of two of zero the occupation oscillates be-

tween these two values on the length of a lattice spacing[7] (remember that a is set to one). The reason for this very different behavior can be explained by the fact that the atom photon bound state is a state which contains of atomic as well as photonic degrees of freedom. From the last chapter we know that the APB can be imagined as photons which steadily hop into the atom, get reemmited and hop back into the atom again. This can only happen if the photons have a velocity which is zero $\partial_k \epsilon(k) = 0$, because otherwise they just would disappear from the atom. Looking at the Brillouin zone (FIG. 1.1) we see that there are only three points which fulfill this condition 0 and $\pm\pi$. The former case corresponds to the bound states above the band and the second case to APB below the band, which explains the occurrence of the oscillations in (4.79) because the constituting photons have an momentum of $\pm\pi$ (for $k = 0$ the oscillations in (4.78) vanish).
This behavior is quite interesting, first because it makes the photonic part of the APB much clearer visible than in all other calculations we have done so far. Secondly these oscillations can't be explained by referring to the simple quantum mechanical model we used to explain the behavior above the band.
To back up the above considerations we performed some numerical calculations for $|+\rangle$, where we again set $U = 1, \Omega = 2.5$ (Fig. 4.18).The results are shown in Fig. 4.18. For asymptotic calculations one could simply recycle the results of the last section but because this doesn't yield any deeper insight we spare them here. We indeed observe the expected oscillations below the band as well as only one state is occupied above the band (as has exactly a value which is twice as much, see (4.15)). Furthermore we see that contrary to Fig. 4.15 there is now sign of a sharp cusp in the surrounding of $R_{c-} = 9$, the reason for that is that the cosine term in (4.79) is quite small in this region, suppressing the effects of the non-analytic behavior.

The Förster potential

Last but not least we want to see how the Förster potential behaves for the initial state $|+\rangle$ (the parameters are the same as before).

The Förster potential shows a different behavior then in Fig. 4.17. First of all we have a minimum at $R \approx 1.5$ which is much deeper by a factor of 50 then compared to the case where only one atom is excited. Furthermore there is again no sign of the cusp, for the same reason then it was absent for the occupation numbers. Also the oscillations we expect from our former analysis are present initially but are fading out for $R > R_{c+}$. This proves our claim that the potential between the two atoms is highly sensible on the initial state we choose to prepare the system.

[7] This is the first time we see features which explicitly take place on the length scale of the lattice constant. Because we are dealing with a cosine dispersion relation, the underlying lattice has finite spacing. In an experiment we would be only able to observe effects with spatial extent $\delta x \sim a$, so we interpret anything which is smaller then this length as an interpolation between physical realizable quantities

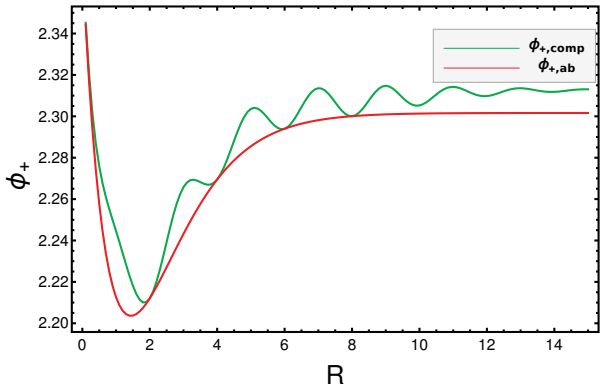

Figure 4.19: *The Förster potential $\phi_{+,comp}$ for the symmetric state. It is dominated by the contribution above the band $\phi_{+,ab}$, modulated by oscillations which start to fade out for $R > R_c$*

4.7 Conclusion

In this chapter we analyzed the properties of a 1-D waveguide coupled to two TLS. For that we generalized the Green's function approach developed in 3, which enabled us to give an exact solution in the one-excitation subspace. We analyzed the different eigenmodes of the system. The first result of this analysis was the insight that the scattering state energy is independent of the distance R between the scatterers. This essentially induces that every fluctuating force present in system (as along as the RWA is valid) is necessarily of short range type and can be interpreted as Förster resonance energy transfer, which is mediated by the second type of eigenstates of the system, the atom photon bound state which live outside the waveguide continuum (which only exists for bounded dispersion relations). We showed that the number of APBs depends on the distance between the atoms, resulting in a critical distance $R_{c\pm} = 2(2 \pm \Omega)/U^2$ and the value of the resonance energy of the TLS. We also found out that there is a third type of eigenstates which may be present,the BICs that are located inside the waveguide continuum. We then derived a general existence condition for them. We then moved on and discussed the effect of the BICs on the time dynamics of the system. Our main finding was that they induce a finite occupation of the TLS even in the limit $t \to \infty$. In the last part of the chapter we calculated the Förster energy for two types of initial states, first for the case where only one atom is initially excited and second when the system is initially in the symmetric entangled state. It turned out that the shape of the potential landscape heavily depends on the chosen initial state qualitatively as well as quantitatively. We furthermore found out that this potentials may have singular points related to R_c, which is in sharp contrast to expectations one could have had from free space calculations which again showed the crucial influence of band edges in the waveguide dispersion relation. Last but not least we analyzed the occupation numbers of the APBs which are, despite of there occurrence in the defining equation for the Förster energy, interesting features which make them an interesting subject in their own right.

5 CONCLUSION & OUTLOOK

Now that we have reached the end of this PhD thesis we want to take the opportunity to summarize our results and furthermore have a look in the future and collecting some ideas what else could be done on the basis of the calculations we did so far.

5.1 Conclusion

When the project of this thesis started, the idea was to collect some of the things the author had learned during his diploma thesis in condensed matter field theory and apply them in waveguide quantum electrodynamics (WQED) where, back then, their use was not as established than in other branches of theoretical physics. A bunch of unsuccessful attempts told us that despite the fact that there are many similarities shared by the two fields there are nevertheless also many differences which require a big amount of care and good ideas to make them treatable by the tools we had in mind. The result of this learning process was a Feynman diagram approach, matched to the special features of WQED.

In the first chapter we discussed the quantization of the electromagnetic field and light matter interaction in general. Afterwards we proceeded with a short overview of the experimental status of WQED and discussed how it can be modeled theoretically.

In the second chapter we gave an introduction to QFT. We started by a presentation of the different time pictures of quantum mechanics and discussed the important theorems of Wick and Gell-Mann Low. Afterwards, we introduced the concept of Green's functions and used it to perform some perturbative analyses on the basis of a specific example, the ϕ^4 -model. We laid a special emphasis on the usefulness of Feynman diagram for the simplification of calculations as well as for clear physical interpretations of the corresponding physical processes. Last but not least, we discussed important physical concepts like self energies and $S-$ matrices in the context of the formalism of QFT.

The newly developed Feynman diagram approach mentioned above was the topic of chapter three. After setting up all the necessary diagrams and formally justify their occurrence by a path integral calculation, we started to reproduce some already known results about $S-$Matrices, density of states and other physical quantities. It turned out that our approach is far more transparent and compact then alternative calculations done by other groups. This is mainly due to the easy interpretability of the underlying Feynman diagrams, which allowed us

to classify different nonlinear effects (photon bunching, interaction induced radiation trapping) by corresponding diagrams. We furthermore discussed in great depth that it is important to keep track of the non linear parts of the dispersion relation (contrary to condensed matter physics where linearization is almost always possible due to the existence of a Fermi surface) because they are entirely responsible for a whole class of important physical effects, most prominently the occurrence of atom-photon bound states (APB). In this context we were also able to show that the fundamental difference between a linear and a non-linear dispersion in the two particle subspace manifests itself directly on the level of the corresponding Dyson series. Whereas in the linear case it truncates after a finite number of terms, in the nonlinear case we have an infinite number of contributions which are directly related to the occurrence of APBs. Due to this additional terms methods for a direct analytical solution failed, so we performed the calculations by the help of a self-consistent T-matrix equation. Last but not least, we discussed the occurrence of a Fano resonance which is due to the interference between the continuous spectrum in the waveguide and the discrete energy levels of the two level system (TLS).

In the fourth chapter, we generalized the model system of the previous section by adding an additional TLS. After setting up a diagrammatic approach in the single excitation sector, which is very similar to the one developed for the case of one scatterer, we performed an in depth analysis of the different eigenmodes of the system. We found that the system essentially contains three different kinds of eigenstates. First, the usual scattering states, whose energies interestingly do not show any R dependence. Second, the APBs, whose number crucially depends on the distance between the two scatteres because some of them can become scattering states if $R < 2(2 \pm \Omega)/U^2$. The third species of eigenstates we found are the so called bound states in continuum whose energy lies inside the photon continuum and they exist due to the trapping of light between the two atoms and only occur if the special resonance condition $\omega = \Omega = \epsilon(\frac{\pi N}{R})$ is fulfilled.
We then moved on and analyzed the fluctuating forces present in the system. We showed that they are of the Förster type and therefore mediated by virtual photons, related to the APS, because in our model system the far field contributions mediated by scattering states vanish. We furthermore discussed that a sensible definition of the corresponding fluctuating potentials heavily depend on the chosen initial state of the system. We analyzed two of them in depth, namely the state $|0,\uparrow,\downarrow\rangle$ where the first atom is excited initially and the symmetric entangled state $\frac{1}{\sqrt{2}}(|0,\downarrow,\uparrow\rangle + |0,\uparrow,\downarrow\rangle)$. The potential corresponding to the first state showed interesting non-analytic behavior near R_c which gives a clear signature of one of the APBs. Furthermore we observed the occurrence of two minimal values which is in sharp contrast to the monotonic behavior known from free space calculations. The potential related to the symmetric state had a totally different behavior: The non-analytic point was missing but the potential was instead oscillating on the length scale of the inverse lattice spacing. Additionally, the minimum of this potential was around 50 times deeper.
Because they are an important part of the Förster potential, we also discussed the occupation numbers of the different APS. We observed interesting non-monotonic behavior which could be explained by a complicated interplay between level repulsion, the distance of their energy to the atomic resonance Ω and the occurrence of additional scattering states for finite R.

In addition, we discussed the dramatic effects of the BICs onto the time dependence of a specific physical process, namely the transfer of excitation from one atom to another. We showed that if the BIC condition is not fulfilled the probability for this process is exponentially suppressed whereas in the opposite case it is given by a constant $\sim R^{-2}$.

5.2 Outlook

After establishing the Green's function formalism and proving its capability to describe novel and interesting physical processes, there are several possible promising paths to tread in the future.
On the one hand, there are loads of small extensions to the work we have already done. First of all, it would be interesting to investigate what happens for the two TLS problem if we go to the two excitation subspace. We have already set up the diagrammatics and it seems that there is, compared to the one scatterer case, only one additional class of physical processes, which describes the simultaneous emission and re-absorption of two photons. The corresponding basic diagram is shown in FIG.5.1

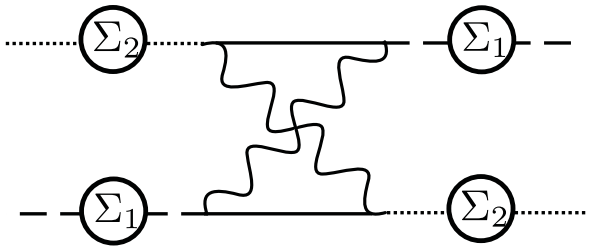

Figure 5.1: *The basic diagram in the two particle subspace for the two scatterer problem*

Despite of the fact that this looks like a fairly innocent complication of our previous results for the one scatterer case, our analysis in the one particle subspace has told us that many unexpected and in the first place counter-intuitive things are going on in this toymodel, so we wouldn't be surprised to see again a whole new world of physical effects after analyzing the corresponding mathematical expressions properly. For example, in contrast to our analysis for a single TLS, even in the case of a linear dispersion relation the perturbation series will not truncate after the first non-trivial term. The reason for this is simply that the second scatterer induces an additional lengthscale R into the system which breaks Markovanitiy. We are also quite confident, that some kind of BIC condition also exists in the two particle sector (essentially because again if the system fulfills the resonance condition the TLS act as prefect mirrors, allowing for the trapping of excitation between them), but it is far from clear what additional kind of effects we have to expect.

Another, very straightforward, extension would contain the inclusion of additional TLS. We expect in this case a maximum of $2N$ APBs (N is the numbers of scatterers) each with its own critical distance where it disappears into the waveguide continuum. This might allow the construction of very rich Föster potential landscapes with a more or less arbitrary number of minimums, maximums and points with non-analytic behavior. It would be also very interesting

to understand the crossover between a system with a low number of scatterers and its counterpart where every site is coupled to an TLS which is essentially the well known Bose-Hubbard model.

It is also tempting to connect existing work which was done by other PhD students in our group during the last years. Most interestingly would be the connection to the work which was done on the disordered single TLS system. For example we expect the APBs to survive moderately strong disorder, but become unstable if the disorder strength gets too strong (they will essentially be eaten up by the Lifshitz tails emerging in density of states of the disordered waveguide) therefore destroying essentially all signs of fluctuation forces beyond this point because the scattering states they transform into have again energies independent of the distance R.

On the other hand, one could also think about more ambitious projects which would require additional work on a more fundamental level then the topics we discussed above. During the whole thesis we take the rotating wave approximation as given which is fine if we are only dealing only with moderate coupling strengths, but experiments done in recent years show that this is not a valid assumption in every waveguide QED experiment. Therefore it would be quite interesting to generalize our approach beyond the RWA. The main challenge here are the additional difficulties induced by the violation of particle number conservation which gives rise to an infinite number of new diagram classes. This makes it necessary to truncate the Hilbert space and/or to isolate the diagrams which gives the most relevant additional contributions to the physical quantities of interest. We already set up an valid diagrammatic formalism for a linear dispersion relation (again for this particular case many of diagrams evaluate to zero which simplifies things a lot) so it can be expected that at least under this circumstances new results could be obtained in a relatively short amount of time.

Another important question which needs to be answered is what happens if we couple our model systems to a bath which models the coupling to the environment (on the numerical side there exists already some work in this direction [134]), like the substrate on which the waveguide is located. Especially if the spectrum of the APBs overlaps with that of the bath (which will always be the case if it is of ohmic type), we expect that they are no longer true eigenstates of the system but instead dissipate into the environment (accompanied by decoherence effects). On the one hand one would like to know under which circumstances this process is small enough so that the APBs can still used for the purpose of storing and manipulating information. On the other hand this instability of might be used to gain information about the physical properties of the bath which can presumably be used to design new types of pump-probe experiments. On the technical side there are different options to tackle this problem, but a possible route which is close to what we did so far would be to employ a path integral representation of the problem and integrate out the bath degrees of freedom. From the resulting effective Hamiltonian, one should be able to employ a diagrammatic representation of the problem which is more or less the same then the one we worked with so far.

On the whole, we showed that Feynman diagrams , an inevitable tool in many branches of physics, can also be a useful approach to light-matter interactions in the context of WQED which can lead to interesting new physical insights. We hope it may be of use to other researchers on the long journey to build an optical quantum computer or to explore exciting new

physics we would never even think about...

A ABSORPTION AND EMISSION GREEN'S FUNCTIONS

A.1 Single-excitation sector

In this appendix we give the derivations of the emission and absorption Green's function in the one-excitation sector The full TLS- and waveguide-Green's functions have been derived in Sec. 3.2.1. We have to to initialize the system with a photonic excitation which gets absorbed later on, so the general expression for the absorption-Green's function is given by

$$\begin{aligned} {}_1G_{\mathrm{ab}}(k_i;t_f-t_i) = &-i\int\prod_{k,k'}\mathrm{d}\phi_{f,k}\mathrm{d}\phi^*_{f,k}\mathrm{d}\phi_{i,k'}\mathrm{d}\phi^*_{i,k'} \\ &\times\phi^*_{i,k_i}e^{-\sum_k\phi_{f,k}\phi^*_{f,k}-\sum_k\phi_{i,k}\phi^*_{i,k}} \\ &\times\mathcal{G}_{\mathrm{ab}}(f,i,t_f-t_i), \end{aligned} \tag{A.1}$$

where $\mathcal{G}_{\mathrm{ab}}(f,i,t_f-t_i)$ is given by Eqs. (3.17) and (3.18). The Gaussian integrals over the photonic modes are performed as in Sec. 3.2 and yield

$${}_1G_{\mathrm{ab}}(k_i;\omega) = \frac{U}{\sqrt{L}}{}_1G^0_{\mathrm{w}}(k_i;\omega){}_1G_{\mathrm{e}}(\omega), \tag{A.2}$$

where, ${}_1G^0_{\mathrm{w}}(k_i;\omega)$ and ${}_1G_{\mathrm{e}}(\omega)$ are defined in Eqs. (3.31) and (3.27), respectively. The diagrammatic representation of this process is quite straightforward. A free photon is annihilated and excites the TLS which gets renormalized by additional emission and absorption processes which are summarized by Σ

$${}_1G_{\mathrm{ab}}(k_i;\omega) =$$ 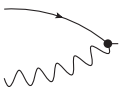 . (A.3)

The calculation of the emission-Green's function follows exactly the same lines with the only difference that the final state consists of a photon instead of an excited TLS

$$\begin{aligned} {}_1G_{\mathrm{em}}(k_f;t_f-t_i) = &-i\int\prod_{k,k'}\mathrm{d}\phi_{f,k}\mathrm{d}\phi^*_{f,k}\mathrm{d}\phi_{i,k'}\mathrm{d}\phi^*_{i,k'} \\ &\times\phi_{f,k_f}e^{-\sum_k\phi_{f,k}\phi^*_{f,k}-\sum_k\phi_{i,k}\phi^*_{i,k}} \\ &\times\mathcal{G}_{\mathrm{em}}(f,i,t_f-t_i). \end{aligned} \tag{A.4}$$

In turn, this yields

$$ {}_1G_{\mathrm{em}}(k_f;\omega) = \frac{U}{\sqrt{L}}\,{}_1G_{\mathrm{e}}(\omega)\,{}_1G^0_{\mathrm{w}}(k_f;\omega), \tag{A.5} $$

together with a straightforward diagrammatic representation. An excited TLS gets renormalized by various intermediate absorption and emission processes (summarized again by Σ) and finally emits a photon finding itself in the ground state

$$ {}_1G_{\mathrm{em}}(k_f;\omega) = $$ 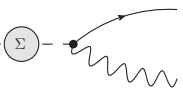 . (A.6)

A.2 Two-excitation sector

Just as in the single-excitation case, we can also derive absorption- and emission-Green's functions for the case of two excitations. However, we will omit the representation of the Green's functions by Feynman diagrams, since they become quiet complicated do to the necessity to include certain symmetrizations such as those in section 3.3.2 and are furthermore not needed during further calculations in the main text.

Explicitly, the absorption Green's function is given by (We initialize the system with two photons from which finally only one survives whereas the second gets absorbed by the TLS)

$$ \begin{aligned} &{}_2G_{\mathrm{ab}}(k_i,p_i,k_f;t_f-t_i) \\ &\quad = -i\int\prod_{k,k'}\mathrm{d}\phi_{f,k}\mathrm{d}\phi^*_{f,k}\mathrm{d}\phi_{i,k'}\mathrm{d}\phi^*_{i,k'} \\ &\qquad \times \phi^*_{i,k_i}\phi^*_{i,p_i}\phi_{f,k_f}e^{-\sum_k\phi_{f,k}\phi^*_{f,k}-\sum_k\phi_{i,k}\phi^*_{i,k}} \\ &\qquad \times \mathcal{G}_{\mathrm{ab}}(f,i,t_f-t_i), \end{aligned} \tag{A.7} $$

where $\mathcal{G}_{\mathrm{ab}}(f,i,t_f-t_i)$ is given by Eqs. (3.17) and (3.18).

Integrating out the bosonic fields results in

$$ \begin{aligned} &{}_2G_{\mathrm{ab}}(k_i,p_i,k_f;\omega) \\ &\quad = \frac{U}{\sqrt{L}}\,{}_2G^0_{\mathrm{w}}(k_i,p_i;\omega) \\ &\qquad \times \Big[{}_2G_{\mathrm{e}}(k_f,k_i;\omega)+{}_2G_{\mathrm{e}}(k_f,p_i;\omega)\Big]. \end{aligned} \tag{A.8} $$

Initializing the system with one photon and excited TLS which becomes unexcited in the final state we can give the general formula for the emission-Green's function

$$ \begin{aligned} &{}_2G_{\mathrm{em}}(k_i,k_f,p_f;t_f-t_i) \\ &\quad = -i\int\prod_{k,k'}\mathrm{d}\phi_{f,k}\mathrm{d}\phi^*_{f,k}\mathrm{d}\phi_{i,k'}\mathrm{d}\phi^*_{i,k'} \\ &\qquad \times \phi^*_{i,k_i}\phi_{f,k_f}\phi_{f,p_f}e^{-\sum_k\phi_{f,k}\phi^*_{f,k}-\sum_k\phi_{i,k}\phi^*_{i,k}} \\ &\qquad \times \mathcal{G}_{\mathrm{em}}(f,i,t_f-t_i). \end{aligned} \tag{A.9} $$

Performing again a standard functional integration over the bosonic modes yields

$$\begin{aligned} {}_2G_{\mathrm{em}}(k_i, k_f, p_f; \omega) \\ &= \frac{U}{\sqrt{L}} \left[{}_2G_{\mathrm{e}}(p_f, k_i; \omega) + {}_2G_{\mathrm{e}}(k_f, k_i; \omega) \right] \\ &\quad \times {}_2G^0_{\mathrm{w}}(k_f, p_f; \omega), \end{aligned} \tag{A.10}$$

B EQUAL TIME GREEN'S FUNCTIONS

Because their appearance is rather unfamiliar from standard diagrammatic approaches of condensed matter theory [133] we will discuss in this Appendix the appearance of equal-time Green's functions in the perturbation series derived for the the two-excitation sector. We will-not go into too many mathematical details but instead argue from an heuristic point of view discussing only the example diagram

$$g(t_f - t_i) = \quad , \tag{B.1}$$

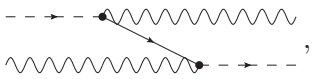

which is written down in the standard diagramtic representation. Translating it into mathematical formulas using standard Feynman rules we get

$$\begin{aligned} &g(k,k';t_f-t_i) \\ &\quad = i\frac{U^2}{L}\int \mathrm{d}t\mathrm{d}t' g_{\mathrm{e}}(t-t_i)g_{\mathrm{ph}}(k,t'-t_i)g_{\mathrm{g}}(t'-t) \\ &\qquad\qquad \times g_{\mathrm{ph}}(k',t_f-t)g_{\mathrm{e}}(t_f-t'), \end{aligned} \tag{B.2}$$

where the free Green's functions are given by

$$g_{\mathrm{e}}(t) = e^{-i\Omega t/2}, \quad g_{\mathrm{g}}(t) = e^{i\Omega t/2}, \quad g_{\mathrm{ph}}(k,t) = e^{-i\epsilon(k)t}, \tag{B.3}$$

the according Feynman diagrams are given in Tab. 3.1 and the time integrations stem from the interaction vertices (we essentialy don't know at which time exactly the interaction takes place). The crucial step now is to split every Green's function by the help of the simple identity $e^{-x}e^{x} = 1$, for example

$$\begin{aligned} g_{\mathrm{ph}}(k,t_f-t_i) &= e^{-i\epsilon(k)(t_f-t_i)} \\ &= e^{-i\epsilon(k)(t_f-t)}e^{-i\epsilon(k)(t-t_i)} \\ &= g_{\mathrm{ph}}(k,t_f-t)g_{\mathrm{ph}}(k,t-t_i). \end{aligned} \tag{B.4}$$

In this way Eq. (B.2) can be rewritten (splitting always two Green's functions at the arbitrary interaction times t, t') as

$$
\begin{aligned}
g(k,k';t_f-t_i) &= \\
&= i\frac{U^2}{L}\int \mathrm{d}t\mathrm{d}t' \left[g_\mathrm{e}(t-t_i)g_\mathrm{ph}(k,t-t_i)\right] \\
&\qquad \times \left[g_\mathrm{g}(t'-t)g_\mathrm{ph}(k,t'-t)g_\mathrm{ph}(k',t'-t)\right] \\
&\qquad \times \left[g_\mathrm{e}(t_f-t')g_\mathrm{ph}(k',t_f-t')\right], \qquad \text{(B.5)}
\end{aligned}
$$

so the whole formula can be expressed by equal-time Green's functions which are obviously defined by the content of the brackets. Diagrammatically, this expression can be depicted as

$g(t_f - t_i) =$ 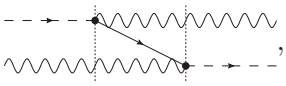 , (B.6)

which is exactly the form as in Sec. 3.3.2.

C TWO-EXCITATION SCATTERING MATRIX

In this Appendix, we provide the details of the calculation of the two-excitation scattering matrix for the case of a linear dispersion relation. The two-excitation S-Matrix is given by Eqs. (3.72) and (3.75). With the help of Eqs. (3.41) and (3.70), we can write this S-Matrix as

$$S_{k_i p_i, k_f p_f} = S^0_{k_i p_i, k_f p_f} + S^1_{k_i p_i, k_f p_f} + S^2_{k_i p_i, k_f p_f}, \tag{C.1}$$

$$S^0_{k_i p_i, k_f p_f} = \delta_{k_i, k_f}\delta_{p_i, p_f} + \delta_{p_i, k_f}\delta_{k_i, p_f}, \tag{C.2}$$

$$\begin{aligned} S^1_{k_i p_i, k_f p_f} =& - i\delta(\epsilon(k_i) + \epsilon(p_i) - \epsilon(k_f) - \epsilon(p_f)) \\ & \times U^2 \Big({}_2G^{\mathrm{r}}_{\mathrm{e}}(k_i;\omega)\delta_{k_i,k_f} + \{\mathrm{perm}\}\Big)\Big|_{os}, \end{aligned} \tag{C.3}$$

$$\begin{aligned} S^2_{k_i p_i, k_f p_f} =& - i\delta(\epsilon(k_i) + \epsilon(p_i) - \epsilon(k_f) - \epsilon(p_f)) \\ & \times \frac{U^4}{2\pi} \Big({}_2G^{\mathrm{r}}_{\mathrm{e}}(k_i)\, {}_2G_{\mathrm{w},0}(k_i, k_f)\, {}_2G^{\mathrm{r}}_{\mathrm{e}}(k_f) \\ & + \{\mathrm{perm}\}\Big)\Big|_{os}, \end{aligned} \tag{C.4}$$

where $\{\mathrm{perm}\}$ represents terms where the momenta have been permuted according to Eq. (3.41). Furthermore, we suppress the chirality indices, thus (initially) treating all (incoming and outgoing) photons as right-movers. The case of different chiralities will be discussed at the end of this appendix.

In order to calculate $S^1_{k_i p_i, k_f p_f}$, we rewrite the energy conserving δ-function by the help of the dispersion relation $\epsilon(k) = vk$

$$\delta(\epsilon(k_i) + \epsilon(p_i) - \epsilon(k_f) - \epsilon(p_f)) = \frac{\delta_{k_i + p_i, k_f + p_f}}{v}. \tag{C.5}$$

Bearing in mind that we have shifted $\omega \to \omega - \Omega/2$, using Eq. (3.35), and setting $\omega = vk_i + vp_i$, we find after tedious but straightforward calculation

$$\begin{aligned} S^1_{k_i p_i, k_f p_f} &= \delta_{p_i, p_f}\delta_{k_i, k_f} \frac{-iU^2/v}{vp_i - \Omega + iU^2/v} + \{\mathrm{perm}\} \\ &= r_{k_i}\left(\delta_{p_i,p_f}\delta_{k_i,k_f} + \delta_{p_i,k_f}\delta_{k_i,p_f}\right) \\ &\quad + r_{p_i}\left(\delta_{p_i,p_f}\delta_{k_i,k_f} + \delta_{p_i,k_f}\delta_{k_i,p_f}\right). \end{aligned} \tag{C.6}$$

Here, r_k is the single-excitation reflection amplitude as specified in Eq. (3.64).

In very much the same manner, we find

$$\begin{aligned} S^2_{k_i p_i, k_f p_f} =& \delta_{k_i+p_i, k_f+p_f} \frac{-iU^4}{2\pi v} \frac{1}{vk_i - \Omega + iU^2/v} \\ & \times \frac{1}{vk_f - vp_i + i0} \frac{1}{vp_f - \Omega + iU^2/v} + \{\text{perm}\}. \end{aligned} \tag{C.7}$$

Upon replacing the inner free Green's function by an application of the Dirac identity

$$\frac{1}{x + i0} = \mathcal{P}\left(\frac{1}{x}\right) - i\pi\delta(x), \tag{C.8}$$

the scattering matrix decomposes into two terms

$$S^2_{k_i p_i, k_f p_f} = S^{2,\text{P.V.}}_{k_i p_i, k_f p_f} + S^{2,\delta}_{k_i p_i, k_f p_f}, \tag{C.9}$$

where the term that results from the δ-function in the Dirac identity, $S^{2,\delta}_{k_i p_i, k_f p_f}$, reduces to

$$\begin{aligned} S^{2,\delta}_{k_i p_i, k_f p_f} =& \frac{1}{2} \delta_{p_i, p_f} \delta_{k_i, k_f} \frac{-iU^2/v}{vk_i - \Omega + iU^2/v} \\ & \times \frac{-iU^2/v}{vp_f - \Omega + iU^2/v} + \{\text{perm}\} \\ =& r_{k_1} r_{p_1} \left(\delta_{p_1, p_2} \delta_{k_1, k_2} + \delta_{k_1, p_2} \delta_{p_1, k_2} \right). \end{aligned} \tag{C.10}$$

This term is due to all two-particle scattering events that can composed out of single-particle scattering events. The term of the scattering matrix that originates from the principal value in the Dirac identity is given by

$$\begin{aligned} S^{2,\text{P.V.}}_{k_i p_i, k_f p_f} =& \frac{i}{2\pi} \delta_{k_i+p_i, k_f+p_f} r_{k_i} r_{p_f} \mathcal{P} \frac{1}{k_i - k_f} + \{\text{perm}\} \\ =& \frac{i}{2\pi} \delta_{k_i+p_i, k_f+p_f} \Bigg[\mathcal{P} \frac{1}{k_i - k_f} \left(r_{k_i} r_{p_f} - r_{p_i} r_{k_f} \right) \\ & + \mathcal{P} \frac{1}{k_i - p_f} \left(r_{k_i} r_{k_f} - r_{p_i} r_{p_f} \right) \Bigg]. \end{aligned} \tag{C.11}$$

Here, we have used energy conservation to facilitate certain simplifications. Using energy conservation another time, we find

$$\begin{aligned} & r_{k_i} r_{p_f} - r_{p_i} r_{k_f} \\ & = \frac{U^4}{v} \frac{(k_i - k_f) \left(E - 2\Omega + iU^2/v \right)}{(vp_i - \Omega + iU^2/v)(vk_i - \Omega + iU^2/v)} \\ & \quad \times \frac{1}{(vp_f - \Omega + iU^2/v)(vk_f - \Omega + iU^2/v)} \end{aligned} \tag{C.12}$$

and the same expression with interchanged momenta, $k_f \leftrightarrow p_f$, for $r_{k_i} r_{k_f} - r_{p_i} r_{p_f}$. Exploiting the fact that (this can easily be seen by remembering that this is an distributional identity which has to be integrated against an appropriate test function. Under the integral sign we then can just use $x \times 1/x = 1$)

$$\Big(k_i - k_f\Big)\,\mathcal{P}\frac{1}{k_i - k_f} = 1 \tag{C.13}$$

and combining the above expressions, we find

$$\begin{aligned} S^{2,\mathrm{P.V.}}_{k_i p_i, k_f p_f} =& \frac{iU^4}{\pi v}\delta_{k_i+p_i,k_f+p_f} \\ &\times \frac{\Big(k_i + p_i - 2\Omega + iU^2/v\Big)}{(vp_i - \Omega + iU^2/v)(vk_i - \Omega + iU^2/v)} \\ &\times \frac{1}{(vp_f - \Omega + iU^2/v)(vk_f - \Omega + iU^2/v)}. \end{aligned} \tag{C.14}$$

As a matter of fact this is the part of the scattering matrix responsible for photon-photon interactions and therefore can not be decomposed into a product of single particle scattering events.

Upon inserting Eq. (C.2), (C.6), and (C.10) in (C.1), we finally find

$$\begin{aligned} S^{RR,RR}_{k_i p_i, k_f p_f} =& t_{k_i} t_{p_i} \Big(\delta_{k_i,k_f}\delta_{p_i,p_f} + \delta_{k_i,p_f}\delta_{p_i,k_f}\Big) \\ &+ S^{2,\mathrm{P.V.}}_{k_i p_i, k_f p_f}, \end{aligned} \tag{C.15}$$

where $t_k = 1 + r_k$. As a matter of fact, the above expression is exactly the scattering matrix given in Ref. [72].

We now turn to the effects of chirality. First, the momenta are renormalized $k \to \mu k$, which controls the sign of the momenta. Second, chirality is conserved upon free propagation, which adds two chirality conserving δ-functions to $S^0_{k_i p_i, k_f p_f}$ and one to $S^1_{k_i p_i, k_f p_f}$. Combining all the relevant expressions, the S-matrix in the other chirality sectors calculates to

- $k_i^R p_i^R \to k_f^R p_f^L$

$$\begin{aligned} S^{RR,RL}_{k_i p_i, k_f p_f} =& t_{k_i} r_{p_i} \delta_{k_i,k_f}\delta_{p_i,-p_f} + r_{k_i} t_{p_i} \delta_{k_i,-p_f}\delta_{p_i,k_f} \\ &+ S^{2,\mathrm{P.V.}}_{k_i p_i, k_f p_f}, \end{aligned} \tag{C.16}$$

- $k_i^R p_i^R \to k_f^L p_f^L$

$$\begin{aligned} S^{RR,LL}_{k_i p_i, k_f p_f} =& r_{k_i} r_{p_i} \Big(\delta_{k_i,-k_f}\delta_{p_i,-p_f} + \delta_{k_i,-p_f}\delta_{p_i,-k_f}\Big) \\ &+ S^{2,\mathrm{P.V.}}_{k_i p_i, k_f p_f}, \end{aligned} \tag{C.17}$$

where the superscripts of k_j^μ indicate the values of chirality.

D PROOF OF THE GELL-MANN LOW THEOREM

The proof relies on the equation of motion in the interaction picture (we drop the I subscript for the rest of the subsection)

$$\partial_{t_j} V(t_j) = i[V(t_j), H_0] \tag{D.1}$$

and the mathematical identity

$$\sum_{i=1}^{n} \partial_{t_i} \Theta(t_{\pi(1)} - t_{\pi(2)}) \Theta(t_{\pi(2)} - t_{\pi(3)}) ... \Theta(t_{\pi(n-1)} - t_{\pi(n)}) = 0 \tag{D.2}$$

where $\pi(i)$ is any permutation of the $n-$ indices. This identity is crucial to move the time derivatives out of the time ordering symbol. [1]
Now let us look at the quantity $(E_0 - H_0)|\psi_H\rangle = [H_0, U_\lambda]|\phi_0\rangle$ and use (2.12,D.1,D.2). We obtain

$$\begin{aligned} &(E_0 - H_0)|\psi_H\rangle = \\ &\sum_{n=0}^{\infty} \frac{(-i)^{n-1}}{n!} \int_{t_i}^{t_f} dt_1 ... \int_{t_i}^{t_f} dt_n \\ &e^{-\lambda \sum_{j=1}^{n} |t_j|} \sum_{j=1}^{n} \partial_{t_j} (T[V(t_1) \cdot ... \cdot V(t_n)])|\psi_0\rangle \end{aligned} \tag{D.3}$$

We note that every time derivative will give the same contribution. This follows from the fact that we can relabel the dummy variables as we like. We can therefore eliminate the inner sum resulting in a factor of n in any order of perturbation theory

$$\begin{aligned} &(E_0 - H_0)|\psi_H\rangle = \\ &\sum_{n=0}^{\infty} \frac{(-i)^{n-1}}{(n-1)!} \int_{t_i}^{t_f} dt_1 ... \int_{t_i}^{t_f} dt_n \\ &e^{-\lambda \sum_{j=1}^{n} |t_j|} \partial_{t_1} (T[V(t_1) \cdot ... \cdot V(t_n)])|\psi_0\rangle \end{aligned} \tag{D.4}$$

[1] For a proof in the case $n = 2$ we calculate$(\partial_{t_1} + \partial_{t_2})\Theta(t_1 - t_2) = \delta(t_1 - t_2) - \delta(t_1 - t_2) = 0$, which is obviously also true if we exchange t_1 and t_2. The generalization to arbitrary n goes along the same line)

Now we assume that V is proportional to some small parameter, $V \equiv gV$. This trick is used to reproduce the perturbation series for U_λ (2.12) after performing an integration by parts. Using $\frac{g^n}{(n-1)!} = g\partial_g \frac{g^n}{n!}$, we obtain

$$(H_0 - E_0)|\psi_I(0)\rangle = -V|\psi_I(0)\rangle + i\lambda g\partial_g|\psi_I(0)\rangle \tag{D.5}$$

and it follows that

$$(H - E_0)|\psi_I(0)\rangle = \lambda g\partial_g|\psi_I(0)\rangle \tag{D.6}$$

Multiplying from the left with $\frac{\langle\psi_0|}{\langle\psi_0|\psi_H\rangle}$ we may conclude

$$E - E_0 = i\lambda\partial_g \log(\langle\phi_0|\psi_H\rangle) = \frac{\langle\phi_0|V|\psi_H\rangle}{\langle\phi_0|\psi_H\rangle} \tag{D.7}$$

which proves the theorem (There are some technical manipulations hidden in this step, the essence is that $\partial_g \log(\langle\phi_0|\psi_H\rangle)$ has to be proportional to $1/\lambda$ to make the above expression finite. This is in accordance with our earlier remark, that neither the numerator nor the denominator of (2.14) stays finite, instead a non-trivial cancellations of infinities occurs. This is a typical feature of QFT and will show up again in the development of diagrammatics).

E ASYMPTOTICS FOR THE TWO SCATTERER PROBLEM

In this appendix we give derivations for the various approximate solutions used throughout the main text. The idea of this pertubative analysis is the following: We know two limiting cases of our system very well: At $R = \infty$ we have two non-interacting TLS and at $R = 0$ we have a degenerate $V-$system. Let's call the corresponding Θ values Θ_0 and Θ_∞. We now take Θ at one of these special points and look what happens if we add a finite R correction, assuming that the that this correction is small (the meaning of "small" has to specified in every case separately) $\Theta(R) = \Theta_{0/\infty} + \delta_{0/\infty}(R)$.
Furthermore we can identify another important regime, namely the region of $R \approx R_{c\pm}$ where one of the energy eigenvalues slips out of the band. This regime can also treated perturbativly because we have $\Theta \approx 0$ in this case, so one can expand $\Theta \approx \delta(R - R_{c\pm})$ assuming again that the R-dependent correction is small. In a last step we apply all the expansions above to get asymptotic expressions for the occupation numbers which are functions of R as well as of $\Theta(R)$. This parts are much more complicated especially because we are confronted with the fact that in the large distance limit, we have to take care of the effects induced by the degenerate energy levels. We show that these effects are responsible for the cancellations of the whole lowest order asymptotics of the Förster energy, which in the end makes it necessary to perform a higher order expansion to obtain finite results for this quantity. To get optimal results, we take this analysis up to third order in the small parameter $e^{-\Theta_\infty R}$. Note that in principle every result we give in this appendix is equal up to a given order and should in principle contain a Landau symbol to indicate the less relevant terms but we decided to spare them to straighten the formulas a little bit.

E.1 Energies

We perform all calculations for the case where we are above the band (the results below the band can be easily obtained by a change of variable $R \to -R, \Omega \to -\Omega$ together with an appropriate choice of the limiting values for $\Theta_{\infty,0}$). Therefore the equation of interest is

$$\sinh(2\Theta) - \Omega \sinh(\Theta) = \frac{U^2}{2}(1 \pm e^{-\Theta R}) \tag{E.1}$$

For later convenience, we define $f(\Theta) = \sinh(2\Theta) - \Omega \sinh(\Theta) - \frac{U^2}{2}$ to be the explicitly R independent part of this equation.

E.1.1 Energies at small distances

Looking at our central equation (E.1) it is quite clear that we can expand the exponential in a Taylor series (this holds as long as $\Theta_0 R$ is small enough). We may note that depending on the system parameters the equation with the minus sign may not support a solution in this limit but we assume here that it has one ($\Omega > 2$). We set $\Theta_\pm(R) = \Theta_{0,\pm} + \delta_{0,\pm}(R)$ and use $e^{-\Theta_\pm R} \approx 1 - \Theta_\pm R$ to get

$$\delta_{0,\pm}(R)(2\cosh(2\Theta_{0,\pm}) - 2\Omega\cosh(\Theta_{0,\pm})) = -\text{sign}(\pm)\frac{U^2}{2}(\Theta_{0,\pm}R) \tag{E.2}$$

where we have used equation (E.1) at $R = 0$. Furthermore we have neglected terms of order $\delta(R)R$ because they turn out to be of order $\mathcal{O}(R^2)$, which can be checked self consistently by putting the result below (E.3) back into (E.2). Therefore we find to $\mathcal{O}(\Theta_{0,\pm}R)$ that

$$\delta_{0,\pm}(R) = -\text{sign}(\pm)\frac{U^2 R\Theta_{0,\pm}}{2f'(\Theta_{0,\pm})} \tag{E.3}$$

From here on, primes always denote derivatives with respect to Θ. The corresponding energy eigenvalues are then given by $\omega = 2\cosh(\Theta_{0,\pm} + \delta_{0,\pm}(R))$ expanded up to first order.

$$\omega_\pm = 2\cosh(\Theta_{0,\pm}) + \text{sign}(\pm)\frac{\sinh(\Theta_{0,\pm})U^2 R}{f'(\Theta_{0,\pm})} \tag{E.4}$$

Because for the typical sets of parameters ($\Omega \sim U \sim \mathcal{O}(1)$) we used in this thesis $\Theta_0 \sim \mathcal{O}(1)$ one can't expect that the above results to be good for R much bigger then 10^{-1}. To boost this a little bit, we perform the same analysis setting $\Theta_\pm(R) = \Theta_{0,\pm} + \delta_{0,\pm}(R) + \delta^{(2)}_{0,\pm}(R)$ and assume that terms of $\mathcal{O}(\delta_{0,\pm}(R)R)$ can be neglected and that $\delta_{0,\pm}(R) \gg \delta^{(2)}_{0,\pm}(R)$ holds. Both statements can be checked again self consistently in the end of the calculations. After a straightforward but tedious calculation one obtains

$$\delta^{(2)}_{0,\pm}(R) = -\frac{U^4 R^2}{2f'(\Theta_{0,\pm})^2}\left(\frac{f''(\Theta_{0,\pm})\Theta^2_{0,\pm}}{2} - \text{sign}(\pm)\Theta_{0,\pm}\right) \tag{E.5}$$

Surprisingly this yields good agreements with the numerics for values of R which are nearly a magnitude larger than the first order approximation. One might think this expansions are rather bad if the derivative in the denominator gets small, but this is prohibited as long as we stay away from Θ_0 very close to zero (It is bounded from below by $2 - \Omega$ yielding always a finite result, as long as we don't let $\Omega \to 2$. This case will be considered below).

E.1.2 Energies at R_c

In this section we want to discuss what happens if one of our energy eigenvalues slips out of the band for some R_{c+} The behaviour near $\Delta R = R - R_c$ is now much trickier to extract then our calculations in the last subsection. First observe that an expansion of the form $\Theta = \Theta_{R_{c+}} + \delta$ vanishes up to all orders. The reason for this strange behavior is the fact that $\delta \gg \Theta_{0,R_{c+}} = 0$ which makes a perturbative expansion of this type quite senseless. To do better, we use Θ itself

as small (and therefore ΘR because we evolve smoothly into a small neighborhood of ΔR). We obain

$$\Theta R_c + \Theta^3 \frac{2}{3!U^2}\left(2^3 - \Omega\right) = \Theta R - \frac{(\Theta R)^2}{2} + \frac{(\Theta R)^3}{3!} \tag{E.6}$$

We can get rid off an Θ and keeping in mind that $R = R_c + \Delta R$ we see that the first term on the left is canceled out. This means that in lowest order in Θ the perturbative independent do not yields any relevant information so we are forced to take into account higher order terms. Reformulating a little bit, we obtain:

$$\frac{2\Theta^2}{3U^2}\left(8 - \Omega\right) = \Delta R - \Theta\frac{R^2}{2} + \Theta^2\frac{R^3}{3!} \tag{E.7}$$

We want to add that possible issues for $\Omega \geq 8$ are irrelevant because such values are excluded by the condition for the existence of R_{c+}. Solving this equation we get one (physical) solution which has the following "nice" form

$$\Theta = \frac{3U^2\left(R_c + \Delta R\right)^2 - \sqrt{3}\sqrt{3U^4\left(R_c + \Delta R\right)^4 - 8\Delta R U^4\left(R_c + \Delta R\right)^3 - 16\Delta R U^2\Omega + 128\Delta R U^2}}{2\left(U^2\left(R_c + \Delta R\right)^3 + 2\Omega - 16\right)} \tag{E.8}$$

The other solution yields Θ values which are not small as we make R_c small which is a contradiction.

Now we assume that $1 \approx R_c \gg \Delta R$. Then we can safely use ΔR as the correct expansion parameter. We obtain

$$\Theta = \frac{2\Delta R}{R_c^2} \tag{E.9}$$

One may now ask why we do not use just the lower order approximation to (E.7) because this yields already the above (correct) result. The answer is, that in this order we do not obtain the correct behavior if $R_c \to 0$ [1]. To get this limit correctly one has to be very careful because the perturbation problem gets singular([132]) in the limit $R_c \to 0, \Delta R \to 0$ (this means that possible solutions just disappear to ∞). It turns out that one has to expand (E.8) first in ΔR and afterwards in R_c to get a sensitive limit (the intermediate algebra is quite messy and was done in Mathematica). The result is:

$$\Theta = \frac{U\sqrt{3\Delta R}}{\sqrt{8 - \Omega}} \tag{E.10}$$

Note that the occurrence of the square root is very typical in singular perturbation theory ([132]).

[1] Instead we would get $\Theta \sim 1/R$ which can't be correct as it becomes big as $R \to 0$ which contradicts the assumption that this quantity has to be small

E.1.3 Eigenvalues at infinity

Now we turn our attention to the case where R is very big. First of all we notice that the natural relevant small parameter to perform our asymptotic analysis is $a = \frac{U^2}{2} e^{-R\Theta}$. The reason for this is clear: If $R\Theta \gg 1$ the distance dependent part of (E.1) is small and we can threat it as a small perturbation. In principle we could follow a route very similar to the case $R \ll 1$: Setting $\Theta = \Theta_\infty + \delta_{\infty,\pm} + \delta^{(2)}_{\infty,\pm} + ...$ and solving order by order but as a matter of fact due to reasons which become clear in the next section we will need contributions as small as $\mathcal{O}(e^{-3\Theta_\infty R})$. Going to orders high as that, it turns out that this straightforward approach is overwhelmingly confusing because it becomes quite difficult to consistently keep track of all relevant terms. For this reason we take another way which closely resembles the one of the last subsection. We expand first in $\Theta_\infty + \delta_\pm$ up to the relevant order in $\delta_\pm$, solve the corresponding equation and expand afterwards consistently in powers of a. This works well up to order a^2 because the equations in $\delta_\pm$ are just of second order and therefore quite easy to solve (and to expand). Serious problems are showing up if we go to $\mathcal{O}(\delta^3_\pm)$ (which is necessary to stay consistent) because we then have to solve a cubic equation which is in principle possible by Cardano's method but the following expansions gets way too complicated. We, therefore, perform an additional trick. Namely because any additional correction will be very small we split the equation into two parts: The part which contains only terms up to second order and a second part containing the terms of order three. This last part can now be interpreted as a small perturbation which again can be checked self-consistently at the end of the calculations. This allows us to replace every term of $\mathcal{O}(\delta^3_\pm)$ by the solution (denoted by $\delta^{(0)}_{\infty,\pm}$) of the unperturbed second order equation.[2] Our equation of interest now reads

$$\left(f'(\Theta_\infty)\delta_{\infty,\pm} + \frac{f''(\Theta_\infty)}{2}\delta^2_{\infty,\pm} \right) + \frac{f'''(\Theta_\infty)}{3!}\delta^{(0)3}_{\infty,\pm} = (\pm)a\left(1 + \delta_{\infty,\pm} + \frac{1}{2}\delta^2_{\infty,\pm}\right) + \frac{a}{3!}\delta^{(0)3}_{\infty,\pm} \tag{E.11}$$

Now we have again to solve for δ and expand afterwards in third order in a. As a matter of fact, this part of the calculations is rather cumbersome (but straightforward) so we spare it here just giving the result which is the same as quoted in the main text:

[2] Indeed this procedure is quite well known, see [132]. For example let us look at $\epsilon x^2 - 2x + 1 = 0$ where $\epsilon \to 0$. Following the procedure outlined in the main text $x^2 \to x_0^2$ where $x_0 = \frac{1}{2}$ solves $2x - 1 = 0$ and we find $x \approx \frac{1}{2} + \frac{1}{8}\epsilon$. Comparing this with one of the full solutions $x_- = \frac{1-\sqrt{1-\epsilon}}{\epsilon}$ we see that we have found exactly the leading order behavior we were looking for (as a matter of fact the second solution is not obtainable by this method, this would again be a problem of singular perturbation theory but luckily this is not relevant to our problem at hand)

$$\Theta_\pm = \Theta_\infty \pm \frac{U^2 e^{-\Theta_\infty R}}{f'_\infty}\left(1 \mp \frac{U^2 e^{-\Theta_\infty R}(2Rf'_\infty + f''_\infty)}{2f'^2_\infty} \pm \frac{U^4 e^{-2\Theta_\infty R}\left(\pm 3Rf'_\infty f''_\infty + 3R^2 f'^2_\infty + f''^2_\infty\right)}{2f'^4_\infty} - \frac{U^4 e^{-2\Theta_\infty R} f'''_\infty}{6f'^3_\infty}\right) \tag{E.12}$$

where we have replaced $f^{(n)}(\Theta_\infty) \to f^{(n)}_\infty$ for the sake of a better readability.
It is interesting to note that additionally to terms which are just of exponential type there are also contributions which are of the form $Re^{-\Theta_\infty R}$ which dominates terms that are of the same exponential order but without the R in front. To give some justification that the above formula is indeed true, let's check the result up to $\mathcal{O}(e^{-\Theta_\infty R})$. Equation E.1 reads

$$f'(\Theta_\infty)\delta = (\mp)U^2 e^{-\Theta_\infty R}(1+\delta) \tag{E.13}$$

and therefore

$$f'(\Theta_\infty)\delta - (\mp)U^2 e^{-\Theta_\infty R}\delta = (\mp)U^2 e^{-\Theta_\infty R} \tag{E.14}$$

this gives us (using $(1-x)^{-1} \approx 1 + x$ for $x \ll 1$)

$$\delta = \frac{-(\mp)U^2 e^{-\Theta_\infty R}/f'(\Theta_\infty)}{1-(\mp)e^{-\Theta_\infty R}/f'(\Theta_\infty)} \approx \frac{\pm U^2 e^{-\Theta_\infty R}}{f'(\Theta_\infty)} \tag{E.15}$$

which is obviously consistent with (E.12).

E.2 Residues

In this section we want to discuss how we can extract the approximate analytic values for the residues discussed in 4.6.3. It turns out that in the cases $R \ll 1$ and $R \approx R_c$ are rather straightforward expansions but the case $R \gg 1$ turns out to be much more complicated so will be mainly concerned with this one.

E.2.1 Residues at infinity

To see why this case is quite non-trivial let's have a look at the formula for residue corresponding to the eigenvalue Θ_- (this problem also occurs for Θ_+) . Because we are dealing with simple poles we can calculate it according to $\alpha^- = \mathrm{Res}(\mathcal{G}_{11}(\Theta), \Theta = \Theta_-) = \frac{M_{11}(\Theta_-)}{f_+(\Theta_-)}\frac{1}{f'_-(\Theta_-)}$ where $M_{11}(\Theta_-)/f_-(\Theta_-)$ and $1/f'_+(\Theta_-)$ are the analytic and the pole part of 4.20, respectively. We get

$$\alpha^- = \frac{4\sinh^2(\Theta)2\sinh(\Theta)\left((2\cosh(\Theta)-\Omega)-U^2\right)}{\left(2\sinh(\Theta)(2\cosh(\Theta)-\Omega)-U^2e^{-\Theta R}-U^2\right)\left(4\cosh(2\Theta)-2\Omega\cosh(\Theta)-RU^2e^{-\Theta R)}\right)} \tag{E.16}$$

We define from here on $\Theta_- = \Theta$ for the remainder of this subsection to straighten the notation a little bit We can rewrite the above formula in terms of $f(\Theta)$ which also corresponds again to the equation which determines the eigenvalues for $R = \infty$ and therefore $f(\Theta_\infty) = 0$. We obtain the more compact form:

$$\alpha^- = \frac{4\sinh^2(\Theta) f(\Theta}{\left(f(\Theta) - U^2 e^{-\Theta R}\right)\left(f'(\Theta) - RU^2 e^{-\Theta R)}\right)} \tag{E.17}$$

We now have the following problem: Setting $\Theta_\infty = \Theta, R = \infty$ (or even close to that values if we are calculating numbers) naively this will yield a nonsensical result (0/0), which is clearly undefined. The reason behind this is the degeneracy of (E.1) at $R \to \infty$ which essentially renders the prefactor into another pole at the same position as the one we are originally interested in. This is no longer true for finite distances because the degeneracy is lifted but because we are expanding around this singular point we have to take care to define this limit properly. Because $\sinh^2(\Theta)$ and the part of the denominator containing $f'(\Theta)$ stay finite and cause no major problems for the moment we concentrate first on (S stands for singular piece)

$$S^- = \frac{f(\Theta)}{\left(f(\Theta) - U^2 e^{-\Theta R}\right)} \tag{E.18}$$

Please note, that taking the limit $R \to \infty$ first would give us a finite result ($= 1$). But this turns out out to be not correct, because this would correspond to count the pole we are interested in as well as the one which appears because of the degeneracies yielding an over-counting by a factor of 2. Instead we rewrite

$$S^- = \frac{1}{1 - \frac{U^2 e^{-\Theta R}}{f(\Theta)}} \tag{E.19}$$

We see immediately that for having a finite non zero limit we need to have $f(\Theta) \sim e^{-\Theta_\infty R}$, as $R \to \infty$. Performing an straightforward expansion we find that indeed $f(\Theta(R)) \sim -U^2 e^{-\Theta_\infty R} + \mathcal{O}(e^{-2\Theta_\infty R})$ which renders the result indeed finite

$$S^- = \frac{1}{1 - (-1 + \mathcal{O}(e^{-\Theta_\infty R}))} = \frac{1}{2 + \mathcal{O}(e^{-\Theta_\infty R})} \tag{E.20}$$

This means that the limit just $\frac{1}{2}$ which agrees with numerical calculations. Note we did not set $R = \infty$ in some brute force way but rather observe a very subtle cancellation which we think is the reason that everything is working out that fine. Carrying on our asymptotic analysis in the next order we obtain

$$\begin{aligned} &\frac{U^2 e^{-\Theta R}}{f(\Theta)} \approx \frac{U^2 e^{-\Theta_\infty R} + \frac{RU^4}{f'(\Theta_\infty)} e^{-2\Theta_\infty R}}{-U^2 e^{-\Theta_\infty R} - \frac{RU^4}{f'(\Theta_\infty)} e^{-2\Theta_\infty R}} = \\ &\frac{1 + \frac{RU^2}{f'(\Theta_\infty)} e^{-\Theta_\infty R}}{-1 + \frac{RU^2}{f'(\Theta_\infty)} e^{-\Theta_\infty R}} \approx -1 + \mathcal{O}(e^{-2\Theta_\infty R}) \end{aligned} \tag{E.21}$$

and

$$S^- = \frac{1}{2} + \mathcal{O}(e^{-2\Theta_\infty R}) \tag{E.22}$$

which shows again the corrections coming from this part of (E.16) are extremely small and we will need to expand its single components up to third order to catch them (which will be indeed necessary but we postpone this calculations until later).

Next we have to take care of the two other contributions to E.16), $\mathcal{R}$ (= Regular) and P (= it stems from the pole that we want to consider) $A = S \cdot \mathcal{R} \cdot P$.
We start with $\mathcal{R}$ which is easy because everything stays finite and we can perform a straightforward expansion.

$$\mathcal{R} = 4\sinh^2(\Theta) \approx 4\left(\sinh^2(\Theta_\infty) + \frac{U^2\sinh(2\Theta_\infty)}{f'(\Theta_\infty)}e^{-\Theta_\infty R}\right) \tag{E.23}$$

Now let's look at P

$$P^- = \frac{1}{f'(\Theta) - RU^2e^{-\Theta R}} \tag{E.24}$$

Because this term also stays finite in the limit which caused the trouble above, we may also proceed quite directly using $f'(\Theta) \sim f'(\Theta_\infty) - U^2\frac{f''(\Theta_\infty)}{f'(\Theta_\infty)}e^{-R\Theta_\infty}, \quad e^{-R\Theta} \sim e^{-R\Theta_\infty}$ We might write

$$\begin{aligned} P^- &\approx \frac{1}{f'(\Theta_\infty) - U^2\frac{f''(\Theta_\infty)}{f'(\Theta_\infty)}e^{-R\Theta_\infty} - RU^2e^{-\Theta_\infty R}} \approx \\ &\frac{1}{f'(\Theta_\infty)}\frac{1}{1 - \frac{RU^2e^{-\Theta_\infty R}}{f'(\Theta_\infty)}} \end{aligned} \tag{E.25}$$

where we again neglected terms of $\mathcal{O}(e^{-\Theta_\infty R})$ because they are asymptotically small compared to $Re^{-\Theta_\infty R}$
Now all what remain is to collect terms

$$\begin{aligned} \alpha^- =& S \cdot R \cdot P = \left(\frac{1}{2} + \mathcal{O}(e^{-2\Theta_\infty R})\right) \cdot 4\left(\sinh^2(\Theta_\infty) + \mathcal{O}(e^{-\Theta_\infty R})\right) \\ &\cdot \frac{1}{f'(\Theta_\infty)}\left(1 + \frac{RU^2e^{-\Theta_\infty R}}{f'(\Theta_\infty)} + \mathcal{O}(e^{-\Theta_\infty R})\right) \end{aligned} \tag{E.26}$$

Which yields after a few simplifications

$$\alpha^- = \frac{2\sinh^2(\Theta_\infty)}{f'(\Theta_\infty)}\left(1 + \frac{RU^2e^{-\Theta_\infty R}}{f'(\Theta_\infty)}\right) + \mathcal{O}(e^{-\Theta_\infty R}) \tag{E.27}$$

Carrying out the same analysis for the uppermost eigenvalue, we get

$$\alpha^{+} = \frac{2\sinh^2(\Theta_\infty)}{f'(\Theta_\infty)}\left(1 - \frac{RU^2 e^{-\Theta_\infty R}}{f'(\Theta_\infty)}\right) + \mathcal{O}(e^{-\Theta_\infty R}) \tag{E.28}$$

As it turns out, this level of approximation yields already quite good qualitative results for a large range of R if we where interested in the occupation numbers only. Furthermore it gives us good results for important quantities as the position of the extreme values of $\alpha_{\Psi,i}$ even if the approximation for the amplitudes itself start to deviate a bit from the exact numerics. To summarize we should be happy and satisfied with what we have reached so far.
But as most of the times there is a big pitfall here, namely what we said is indeed true for the occupation numbers but not for the quantity we are mainly interested in, namely the Förster energy. To see that we recall that it is given by

$$\phi_{\uparrow\downarrow} = \sum_i \alpha_{\uparrow\downarrow,i}\omega_i \tag{E.29}$$

Let us concentrate on the contributions from which comes from above (denoted by a superscript (a)) the band (the arguments for the other case are the same)

$$\phi^{(a)}_{\uparrow\downarrow} = \omega^{(a)}_{-}\alpha^{(a)}_{\uparrow\downarrow,-} + \omega^{(a)}_{+}\alpha^{(a)}_{\uparrow\downarrow,+} \tag{E.30}$$

we might now observe that in leading order we can replace $\omega^{(a)}_{\pm}(R) \to \omega^{(a)}_{\infty}$ because it contains no terms of order $Re^{-\Theta_\infty R}$. Furthermore let's write $\alpha^{(a)}_{\uparrow\downarrow,\pm}(R) = \alpha^{(a)}_{\uparrow\downarrow,\infty} \pm f^{(a)}(R)$ where $f^{(a)}(R)$ contains all informations on the distance dependence. We obtain

$$\begin{aligned}\phi^{(a)}_{\uparrow\downarrow} =& \phi_{\uparrow\downarrow,\infty} + \omega^{(a)}_{\infty}(f^{(a)}(R) - f^{(a)}(R)) + \mathcal{O}(e^{-\Theta_\infty R}) \\ =& \phi_{\uparrow\downarrow,\infty} + \mathcal{O}(e^{-\Theta_\infty R})\end{aligned} \tag{E.31}$$

where we defined $\phi^{(a)}_{\uparrow\downarrow,\infty} = 2\omega^{(a)}_{\infty}\alpha^{(a)}_{\uparrow\downarrow,\infty}$

So we see that to this order in perturbation theory the $R-$dependent contributions get canceled which is a consequence of the initial degeneracy of the two atoms. This is bad news because this means we have to push our calculations to the next order. This means that we have to include terms $\sim e^{-\Theta R}$ into $S \cdot \mathcal{R}$. We already have them for the $\mathcal{R}$ part, so the only thing which is left is to include them into P. From (E.2.1) we get

$$P^{\pm} = \frac{1}{f'(\Theta_\infty)}\left(1 \pm \frac{RU^2 e^{-\Theta_\infty R}}{f'(\Theta_\infty)} - \frac{U^2 f''(\Theta_\infty)e^{-\Theta_\infty R}}{f'^2(\Theta_\infty)}\right) \tag{E.32}$$

which allows us to write

$$\alpha^{\pm} = \frac{2\sinh^2(\Theta_\infty)}{f'(\Theta_\infty)}\left(1 \pm \frac{RU^2 e^{-\Theta_\infty R}}{f'(\Theta_\infty)}\right) - \frac{2\sinh^2(\Theta_\infty)}{f'(\Theta_\infty)}\left(\frac{U^2 f''(\Theta_\infty)e^{-\Theta_\infty R}}{f'^2(\Theta_\infty)} \mp \frac{U^2\sinh(2\Theta_\infty)e^{-\Theta_\infty R}}{f'(\Theta_\infty)}\right) + \tag{E.33}$$

By inspecting the above formula we see that one of the terms is not alternating, which means that it will yield a finite contribution to the potential.
To get even better results we also performed an perturbative analysis to order $\mathcal{O}(e^{-2\Theta_\infty R})$. This is a task which is involved but with the knowledge obtained so far rather straightforward, we therefore only state some intermediate which combined appropriately give the correct end result. We start with the different sub pieces from which $S, \mathcal{R}, P$ are build up from. For S, we need[3]. To straighten notation a little bit, we define $f'_\infty \equiv f'(\Theta_\infty)$,$f''_\infty \equiv f''(\Theta_\infty)$ and $f'''_\infty \equiv f'''(\Theta_\infty)$.

$$e^{-R\Theta^{\pm}} = e^{-R\Theta_\infty} \mp \frac{U^2 R e^{-2R\Theta_\infty}}{f'_\infty} + \frac{U^2 R(f''_\infty + 3f'_\infty U^2 R)e^{-3R\Theta_\infty}}{2f'^3_\infty} \tag{E.34}$$

and

$$f(\Theta^{\pm}) = \pm e^{-R\Theta_\infty} - \frac{U^4 R e^{-2R\Theta_\infty}}{f'_\infty} \pm \frac{U^4 e^{-3R\Theta_\infty}\left(2f'^3_\infty + 3f'_\infty R^2 + 6R\sinh\left(2\Theta_\infty\right)\right)}{2f'^3_\infty} \tag{E.35}$$

Note that we included terms like $\mathcal{O}(e^{-3R\Theta_\infty})$ and $\mathcal{O}(Re^{-3R\Theta_\infty})$ despite the fact that they are much smaller asymptotically then everything $\mathcal{O}(R^2 e^{-3R\Theta_\infty})$ for two reasons. First we get them for free and second we want to be sure that later when we start calculating potentials we pick up something which survives the summation. Using (E.35) we obtain

$$\frac{e^{-R\Theta^{\pm}}}{f(\Theta^{\pm})} = \pm 1 \pm \frac{U^2 R e^{-2R\Theta_\infty}\left(f''_\infty - 6\sinh\left(2\Theta_\infty\right) - 1\right)}{2f'^3_\infty} + \frac{U^4 R^2 e^{-3R\Theta_\infty}\left(f''_\infty - 6\sinh\left(2\Theta_\infty\right) - 1\right)}{2f'^4_\infty} \tag{E.36}$$

from which we may conclude that

$$S^{\pm} = \frac{1}{2} + \frac{U^2 R e^{-2R\Theta_\infty}\left(-f''_\infty + 6\sinh\left(2\Theta_\infty\right) + 1\right)}{8f'^3_\infty} \pm \frac{U^4 R^2 e^{-3R\Theta_\infty}\left(-f''_\infty + 6\sinh\left(2\Theta_\infty\right) + 1\right)}{8f'^4_\infty} \tag{E.37}$$

[3]For all the formulas which we list below this point in the main text we only plug in (E.12) into the defining equation for the particular quantity of interest and expand afterwards into the appropriate order

For $\mathcal{R}^{\pm}$ we need just one term

$$\frac{\mathcal{R}^{\pm}}{4} = \sinh^2\left(\Theta_\infty\right) \pm \frac{U^2 \sinh\left(2\Theta_\infty\right) e^{-R\Theta_\infty}}{f'_\infty} + \\ \frac{U^4 e^{-2R\Theta_\infty}\left(2f'_\infty \cosh\left(2\Theta_\infty\right) - \left(f''_\infty + 2f'_\infty R\right)\sinh\left(2\Theta_\infty\right)\right)}{2f'^3_\infty} \tag{E.38}$$

Last but not least, to obtain P we need additionally to (E.34) the following quantity

$$f'(\Theta^{\pm}) = f'_\infty \pm \frac{U^2 f''_\infty e^{-R\Theta_\infty}}{f'_\infty} - \frac{U^4 e^{-2R\Theta_\infty}\left(f''^2_\infty + 2f''_\infty f'_\infty R - f'^2_\infty - 12 f'_\infty \cosh\left(2\Theta_\infty\right)\right)}{2f'^3_\infty} \tag{E.39}$$

and therefore

$$P^{\pm} = \frac{1}{f'_\infty} + \frac{U^2 e^{-\Theta_\infty R}\left(\mp R f'_\infty + f''_\infty\right)}{f'^3_\infty} + \\ \frac{U^4 e^{-2\Theta_\infty R}\left(-12\cosh(2\Theta_\infty) f'_\infty \mp 2R f'_\infty f''_\infty - f'^2_\infty + 3f''^2_\infty\right)}{2f'^5_\infty} \tag{E.40}$$

Interestingly the term $\sim R^2 e^{-R\Theta_\infty}$ one would expect has canceled, leaving us with contributions $\sim R e^{-2R\Theta_\infty}$ as dominant contributions in this order of perturbation theory. We could now write the full expression for the occupations, because this would become even more lengthy then the above formulas we just state that we again have to calculate $\alpha = S \cdot \mathcal{R} \cdot P$ but now keeping all terms at least to order $\mathcal{O}(Re^{-2R\Theta_\infty})$

E.2.2 Residues at small distances and at R_c

We may are also interested in the behavior of the residues around $R = 0$. The calculation is much more straightforward then the one we gave above because we do not have any more degeneracies. Starting point is again (E.16) where we put in (E.5)) and expand in second order in $(\Theta_{0,\pm}R)^2$ which is what we used to generate FIG. 4.15 and FIG. 4.14 in the main text. The resulting formulas are quite long and yield no particularly new insight compared to the results in linear order, so we will not state them here and restrict our self to the lowest order approximation. It is given by

$$\alpha^{\pm} = \alpha_{0,\pm} - \chi_{\pm}(U^2\Theta_{0,\pm}R) + \mathcal{O}(U^4\Theta_{0,\pm}R) \tag{E.41}$$

with $\alpha_{0,\pm} = 4\frac{\sinh^2(\Theta_{0,\pm})}{f'_{0,\pm}}$ and $\chi_{\pm} = 2\frac{\sinh(2\Theta_{0,\pm})}{f'^2_{0,\pm}}$ we want to point out, that the prefactor of the $R-$ dependent term is a (at least for the parameters we are interested in) a monotonically

decreasing function of $\Theta_{0,\pm}$ with $\chi(0) = 0$. Furthermore the value of $\Theta_{0,\pm}$ is increasing if we increase the coupling strength U which means that the amount of change of the occupation numbers gets stronger for bigger coupling strengths.
The case $R \approx R_c$ can be tackled in the same straightforward manner then the last one (again we give only leading order contributions and spare the full expansion which was used to generate the plots in the main text), with the little difference that we observe a crossover behavior corresponding to the two limiting behaviors of the eigenvalues E.9 and E.10. We obtain

$$\alpha_{R_{cr}} = \chi_{cr,1}\Delta R \quad \text{if } R_c \sim \mathcal{O}(1) \tag{E.42}$$

with $\chi_{cr,1} = \frac{8}{R_c^4}$ and

$$\alpha_{R_c} = \chi_{cr,2}\sqrt{\Delta R} \quad \text{if } R_c \to 0 \tag{E.43}$$

with $\chi_{cr,2} = \sqrt{\frac{3}{8-\Omega}}$

PUBLICATIONS

1. T. Sproll and S. Carr "Conductance and shot noise in strongly correlated 1D systems with a spin gap", submitted to Phys. Rev. B

2. M. P. Schneider, T. Sproll, C. Stawiarski, P. Schmitteckert and K. Busch, "Green's Function Formalism for Waveguide QED Applications", Phys. Rev. A **93** 013828

3. T. Sproll, C. Martens, M. P. Schneider, F. Intravaia and K. Busch, "Förster Resonace Energy Transfer in WQED", in preparation

4. T. Sproll, C. Martens, M. P. Schneider, F. Intravaia and K. Busch, "Diagrammatic approach to the two scatterer problem in WQED", in preparation

5. M. P. Schneider, T. Sproll, C. Martens and K. Busch, "Tunability of a one-dimensional waveguide with an embedded two-level system subjected to few photon wavepackets", in preparation

6. M. P. Schneider, C. Martens, T. Sproll and K. Busch, "Decay properties of an atom coupled to a disordered waveguide", submitted to Phys. Rev. Lett.

7. C. Martens, T. Sproll, M. P. Schneider, F. Intravaia and K. Busch, "Decay properties of two atoms coupled to an 1D waveguide and the influence of bound states in the continuum ", to be submitted

Bibliography

[1] Moore G. (1965) Electronics **38**, 114

[2] Zutic, I., Fabian, J. and Da Sarma, S. (2004), Rev. Mod. Phys. **76**, 323

[3] Zhao, W. and Prenat G. (2015) *Spintronics-based Computation*, 1. Edition, Spinger, 2

[4] Flatté, E. and Awschalom D. (2007), Nature Physics **3**, 153

[5] Schwierz, F. (2010), Nature Nanotechnology **5**, 487

[6] Radisavljevic, B. et al (2011), Nature Nanotechnology **6**, 147

[7] Miller, D. (2010) Nature photonics **4**, 3

[8] Simonite, T. , MIT Technology review, Aug 4th 2010

[9] IBM Press release, May 12th 2015

[10] Feynman, R. (1981) Int. J. of Theo. Phys. **21**, 466

[11] Lloyd, S. (1996), Science **273** 1073

[12] Da Sarma, S., Freedman, M. and Nayak, C. (2015) npj Quantum Information **1**, 15001

[13] Flatte, M. and Tifrea I. (2007) *Manipulating Quantum Coherence in Solid State Systems*,Springer ,1

[14] Devoret M. and Schoelkopf R. (2013) Science, **339**, 1169

[15] Knill, E., Laflamme R. and Milburn G.J. (2001) Nature **409**,46

[16] Adhikari P., Hafezi M. and Taylor J. (2013) Phys. Ref. Lett **110**, 60503

[17] Zheng, H. Daniel Gauthier J. and Baranger H. (2013) Phys. Rev. Lett. **111**, 90502

[18] Gonzalez-Ballestero C., Moreno E. and Garcia-Vidal F. Phys. Rev. A. **89**, 42328

[19] Kimble, J. Nature **453**, 1023

[20] Born, M., Heisenberg, W., Jordan, P. (1926), Zur Quantenmechanik II, Zeitschrift für Physik **35** (8–9), 557–615

[21] Fermi, E. (1934), Versuch einer Theorie der -Strahlen, Z. Phys. **88** , 161-177

[22] Dyson ,F. (1949), The S Matrix in Quantum Electrodynamic,. Phys. Rev. **75**, 1736

[23] Schwinger,J. (1951), On Green's functions of quantized fields I + II, PNAS **37**, 452–459

[24] Feynman, R. (1949), The Theory of Positrons, Phys. Rev. **76**, 749

[25] Glashow S. (1961) ,Partial-symmetries of weak interactions, Nuclear Physics **4** , 589-588

[26] , Weinberg, S. (1967), A Model of Leptons, Phys. Rev. Lett. **19** , 1264–1266.

[27] Altland, S., Simmons. B, (2010),*Condensed Matter Field Theory*, Cambrige University Press

[28] McCoy (1994), The connection between statistical mechanics and quantum field theory ,arXiv:hep-th/9403084

[29] Prykarpatsky ,A ., Taneri, U., Bogoliubov, N. (2002),*Quantum Field Theory with Application to Quantum Nonlinear Optics* , World Scientific

[30] Tong, D. (2006), *Quantum Field Theory* , http://www.damtp.cam.ac.uk/user/tong/qft/qft.pdf ,124-130

[31] Weinberg, S. (2005), *The Quantum Theory of Fields II*, Cambrige University Press

[32] Sakurai, JJ. (1994), *Modern Quantum Mechanics*, Addison-Wesley

[33] Astapenko, V. (2013), *Interaction of Ultrashort Electromagnetic Pulses with Matter*, Springer

[34] Petrov, A., *Slow Light Photonic Crystal Line-defect Waveguides*, Cuvillier Verlag

[35] Le Kien, F. , Hakuta, K. , Reitz, D. et. al. (2013) , Quantum dynamics of an atom orbiting around an optical nanofiber, Phys. Rev. A **87**, 063607

[36] Poon, J., Scheuer, J. , Mookherjea, S. et al. (2004), Matrix analysis of microring coupled-resonator optical waveguides, Opt. Express **12**, 90-103

[37] Tolmachev , V.A. , Petrova, T.S. , Moore, R.A. et al (2006) Experimental evidence of photonic band gap extension for disordered 1D photonic crystals based on Si, Opt. Comm. **1** , 104-106

[38] Goban, A. (2014), Atom light interactions in photonic crystals, Nat. Comm. **5**

[39] Mizuochi, N., Makino, T., Kato, H. et al. (2006), Electrically driven single-photon source at room temperature in diamond , Nature **6**, 299-303

[40] Castelletto, S., Johnson, B. C., V. Ivády et al. (2014) , A silicon carbide room-temperature single-photon source, Nat. Mat. **13** ,151-156

[41] Kako, S., Santori, C., Hoshino, K. et al. (2006) A gallium nitride singlephoton source operating at 200K Nat. Mat. **5**, 887

[42] Balanis, C., Holzman, E. (2005), Circular Waveguides (*Encyclopedia of RF and Microwave Engineering*), Wiley and Sons

[43] Mookherjea, S. (2005), Dispersion characteristics of coupled-resonator optical waveguides, Opt. Letters **30** 2406-2408

[44] Fetter, A., Walecka, J. (2003), *Quantum Theory of Many-Particle Systems*, Dover

[45] Gell-Mann, M., Low, F. (1951),Phys. Rev. **84**, 350

[46] Brouder, C., Panati, G., Stoltz, G. (2010) Annales Henri Poincaré **10**, 1285

[47] Sproll, S., Diploma thesis (2011), unpublished

[48] Peskin, D., Schroeder, M. (1995) *An introduction to quantum field theory* . Westview Press Reading

[49] Kleinert, H., Schulte-Frohlinde, V. (2001) *Critical Properties of ϕ^4-Theories*, World-Scientific

[50] Borcherds, D., Barnard, A. (2001), *Quantum Field Theory* , http://arxiv.org/abs/math-ph/0204014

[51] Molinari, G. *Notes on quasi particles*, http://pcteserver.mi.infn.it/ molinari/NOTES/quasiparticle.pdf

[52] Giamarchi, T. (2003) *Quantum Physics in One Dimension*, Oxford University Press

[53] H. Lehmann, K. Symanzik and W. Zimmermann(1955), Il Nuovo Cimento 1, 205

[54] Schneider, M., Sproll, T et al. (2015) Phys. Rev. A **93** 013828

[55] O'Brien, J. L.; Furusawa, A. and Vučković, J. (2009) Nature Photonics **11** 687

[56] Benson, O. (2011) Natuen **480** 193

[57] Schell, A. W.; Kaschke, J.; Fischer, J.; Henze, R.; Wolters, J.; Wegener, M. and Benson, O. (2013) Sci. Rep. **3** 1577

[58] You, J. Q. and Nori, F. (2011) Nature **474** 589

[59] Devoret, M. H. and Schoelkopf, J. R. (2013) Science **339** 1169

[60] Mitsch, R., Sayrin C. and Albrecht, B. (2014) Phys. Rev. A.**5** 5713

[61] Shields, A. J. (2007) Nat. Phot. **1**, 215

[62] Claudon, J.; Bleuse, J.; Malik, N. S.; Bazin, M.; Jaffrennou, P.; Gregersen, N.; Sauvan, C.; Lalanne, P. and Gerard, J.-M (Nat. Phot. **4** 174

[63] Laucht, A.; Pütz, S.; Günthner, T.; Hauke, N.; Saive, R.; Frédérick, S.; Bichler, M.; Amann, M.-C.; Holleitner, A. W.; Kaniber, M. and Finley, J. J. (2012) Phys. Rev. X **2** 11014

[64] Fattahpoor, S.; Hoang, T. B.; Midolo, L.; Dietrich, C. P.; Li, L. H.; Linfield, E. H.; Schouwenberg, J. F. P.; Xia, T.; Pagliano, F. M.; van Otten, F. M. W. and Fiore, A. (2013) Appl. Phys. Lett. **102** 131105

[65] Hadfield, R. H. (2009) Nat. Phot. **3** 696

[66] Pernice, W. H. P.; Schuck, C.; Minaeva, O.; Li, M.; Goltsman, G. N.; Sergienko, A. V. and Tang, H. X. (2012) Nat. Comm. **3** 1325

[67] Sahin, D.; Gaggero, A.; Zhou, Z.; Jahanmirinejad, S.; Mattioli, F.; Leoni, R.; Beetz, J.; Lermer, M.; Kamp, M.; Höfling, S. and Fiore, A. (2013) Appl. Phys. Lett. **103** 111116

[68] Najafi, F.; Mowver, J.; Harris, N. C.; Bellei, F.; Dane, A.; Lee, C.; Hu, X.; Kharel, P.; Marsili, F.; Assefa, S.; Berggren, K. K. and Englund, D. (2015) Nat. Comm. **6** 5873

[69] Chang, D. E.; Vuletić, V. and Lukin, M. D. (2014) Nat. Phot. **8** 685

[70] Volz, J.; Scheucher, M.; Junge, C. and Rauschenbeutel, A. (2014) Nat. Phot. **8** 965

[71] Lodahl, P.; Mahmoodian, S. and Stobbe, S. (2015) Rev. Mod. Phys **87** 347

[72] Shen, J.-T. and Fan, S. (2007) Phys. Rev. A **2** 76, 62709

[73] Shi, T. and Sun, C. P. (2019) Phys. Rev. B **79** 205111

[74] Fan, S.; Kocabaş, S. E. and Shen, J.-T. (2010) Phys. Rev. A **82** 63821

[75] Pletyukhov, M. and Gritsev, V. (2012) New Journal of Physics **14** 95028

[76] Zheng, H.; Gauthier, D. J. and Baranger, H. U. (2010) Phys. Rev. A **82** 63816

[77] Zheng, H.; Gauthier, D. J. and Baranger, H. U. (2011) Phys. Rev. Lett. **107** 223601

[78] Zheng, H.; Gauthier, D. J. and Baranger, H. U. (2012) Phys. Rev. A **85** 43832

[79] Longo, P.; Schmitteckert, P. and Busch, K. (2009) J. Opt. A **11** 114009

[80] Longo, P.; Schmitteckert, P. and Busch, K (2010) Phys. Rev. Lett. **104** 23602

[81] Auerbach, A.(1994) *Interacting Electrons and Quantum Magnetism*, Springer

[82] Nysteen, A.; McCutcheon, D. P. S. and Mork, J. (2015) New J. Phys **15** 23030

[83] Schneider, M., Sproll, T. Busch, K. (2015) to be published

[84] Sanchez-Burillo, E.; Zueco, D.; Garcia-Ripoll, J. J. and Martin-Moreno, L. (2014) Phys. Rev. Lett. **113** 263604

[85] Notomi, M.; Kuramochi, E. and Tanabe, T. (2008) Nat. Photon. **2** 741

[86] Takesue, H.; Matsuda, N.; Kuramochi, E.; Munro, W. J. and Notomi, M. (2013) Nat. Commun **4** 2725

[87] Schell, A. W.; Takashima, H.; Kamioka, S.; Oe, Y.; Fujiwara, M.; O., B. and Takeuchi, S. (2015) Scientific Reports **5** 9619

[88] Jaynes, E. and Cummings, F. W. Proceedings of the IEEE **51** 89

[89] Dicke, R. (1954) Phys. Rev **93** 99

[90] Anderson, P. W. (1961) Phys. Rev **124** 41

[91] Rammer, J. (2007) *Quantum Field Theory of Non-equilibrium States* Cambridge University Press

[92] Rammer, J. (2004) *Quantum Transport Theory* Westview Press

[93] Boudjedaa, T.; Bounames, A.; Nouicer, K.; Chetouani, L. and Hammann, T. F. (1996) Physica Scripta **54** 225

[94] Fujimoto T.and Atsushi, I. *Plasma Polarization Spectroscopy*(2008) Springer

[95] Moeferdt, M.; Schmitteckert, P. and Busch, K. (2013) Opt. Lett. **38** 3693

[96] Borda, L.; Fritz, L.; Andrei, N. and Zaránd, G. (2007) Phys. Rev. B **75** 235112

[97] Zhou, L.; Gong, Z. R.; Liu, Y.-x.; Sun, C. P. and Nori, F (2008) Phys. Rev. Lett. **101** 100501

[98] Miroshnichenko, A.; Flach, S. and Kivshar, Y. (2013) Rev. Mod. Phys. **82** 2257

[99] Braun, A. and Schmitteckert, P. (2014) Phys. Rev. B **90** 165112

[100] Shen, J.-T. and Fan, S. (2007) Phys. Rev. Lett **98** 153003

[101] Kocabaş, Ş. E. (2015) arXiv:1510.03069

[102] Zheng, H.; Gauthier, D. J. and Baranger, H. U. (2013) Phys. Rev. Lett. **110** 113601

[103] C. Gonzalez-Ballestero, Esteban Moreno and F. J. Garcia-Vidal (2014) Phys. Rev. A **89** 42328

[104] Wang, Y. Koo,I. (1974), Opt. Comm. **11** 323

[105] Warren, W. (1994) *Advances in Magnetic and Optical Resonance, Volume 18* Academic Press

[106] Yang H., Yang L. and Zheng T. Y. arXiv: 1402.5574

[107] Zelevinsky, V. (2011), *Quantum Physics: Volume 1: From Basics to Symmetries and Perturbations*, Wiley, 254

[108] von Neumann, J.,Wigner, E. (1929), Phys. Zeitschrift **30** 465

[109] Stilliger, D., Herrick D., (1975), Phys. Rev. A **11** 446

[110] Ordonez, G., Na, K., Kim, S. (2006), Phys. Rev. A **74** 2213

[111] Kristensen, P., Ge, R. and Hughes, D.(2015), Phys. Rev. A **92** 53810

[112] Corless, R. et al (1996), in *Advances in Computational Mathematics* **5**, 329

[113] Martens C., Longo, P., Busch, K. (2013) New Journal of Physics **15** 83019

[114] Few-photon transport in low-dimensional systems
Longo, P., Schmitteckert, P., Busch, K. (2011) Phys. Rev. A **83** 63828

[115] Casimir, H. and Polder D. (1948), Phys. Rev. **73**, 360

[116] Dzyaloshinskii E., Lifshitz E. and Pitaevskii L. (1959) J. exp. theor. Phys **36** 1797

[117] Milloni,P., Dalvit,D. and Rogers, D. *Casimir Physics*, Springer

[118] Martens, C. (2016)
Wellenleiterquantenelektrodynamik mit Mehrniveausystemen, PhD Thesis
http://edoc.hu-berlin.de/docviews/abstract.php?id=42401

[119] Capasso, F. et al (2007), Journal of Selected Topics in Quantum Electronics **13**, 400

[120] Zwischenmolekulare Energiewanderung und Fluoreszenz
Förster, Th. Annalen der Physik **437**, 55 (1948)

[121] Using {GFP} in FRET-based applications
Pollok, Br., Heim Ro., Trends in Cell Biology **9**, 57 (1999).

[122] The use of FRET imaging microscopy to detect protein–protein interactions and protein conformational changes in vivo
Truong, Ke., Ikura, Mi., Current Opinion in Structural Biology**11**, 573 (2001).

[123] *Nano/Micro Biotechnology, Endo, Is., Nagamune, Te.* {*Eds.*}, chapter 3
Ni, Q., Zhang, J., Springer(2010).

[124] Sekar, R. and Periasamy, A. (2003) J Cell Biol. 2003 **5**,629

[125] Stöhr, R. et al (2012) ACS Nano **10**,9175

[126] Fluorescence Energy Transfer in One Dimension: Frequency-Domain Fluorescence Study of DNA-Fluorophore Complexes (1995)
Maliwal, Ba., Kuśba, Jó.,Jakovicz, Jo. R. Biopolymers **35**, 245.

[127] Quantum electrodynamics of resonant energy transfer in condensed matter (1995), Juzeliūnas, Ge., and Andrews, Da. L., Phys. Rev. B **49** 8571.

[128] Caffarri S.(2009), The EMBO Journal **28**, 3052

[129] Bauer G. and Giessen H. (2013), Opt. Express **21**, 363

[130] Flensberg, B., Bruus, H. (2004), *Many-Body Quantum Theory in Condensed Matter Physics* 1. Edition, Oxford,128

[131] Kim, D. (2010), *Introductory Quantum Mechanics for Semiconductor Nanotechnology* 1. Edition, Wiley, 72

[132] Bender,C. and Orzag, S. (1999) *Advanced Mathematical Methods for Scientists and Engineers: Asymptotic Methods and Perturbation Theory* Springer, 9th edition, 324

[133] Many-Particle Physics (2000) Springer

[134] Longo P., Cole JH. and Busch K. (2012) Opt. Express **11**, 12326